2012

Aqueous Oxidation of Methanol by Vanadium Containing Biocatalysts and Biocatalyst Mimics

Julie Elizabeth Molinari
Lehigh University

Aqueous Oxidation of Methanol

by Vanadium Containing Biocatalysts and Biocatalyst Mimics

by

Julie E. Molinari

A Dissertation

Presented to the Graduate and Research Committee

of Lehigh University

in Candidacy for the Degree of

Doctor of Philosophy

in

Chemical Engineering

Lehigh University

May 2012

Approved and recommended for acceptance as a dissertation in partial fulfillment of the requirements for the degree of Doctor of Philosophy.

_____

Date

_____

Professor Israel E. Wachs
Dissertation Advisor

_____

Accepted Date

Committee Members:

_____

Bryan Berger, Ph.D.
Professor, Lehigh University

_____

Anand Jagota, Ph.D.
Professor, Lehigh University

_____

James Hsu, Ph.D.
Professor, Lehigh University

_____

Imara Charles, Ph.D.
Director of Project Management
Laureate Biopharmaceutical Services

Acknowledgements

I would like to sincerely thank Professor Israel Wachs for helping me embark on this difficult and unique biocatalysis project. This research project was new and unchartered territory, especially for our laboratory. I have learned a great deal from Professor Wachs about the drive, commitment, and creativity which is involved in the pursuit of knowledge in a brand new field. Additionally, I would like to sincerely thank Professor Wachs for providing the amazing opportunity for me to travel to Italy, Turkey, and Japan for conferences and research experiences. I would also like acknowledge my fellow lab coworkers who were always willing to help and provide insight during my research. I would especially like to thank Mike Ford for performing the first read-through of my dissertation and providing a great deal of insight.

Most of all, I would like to extend a heartfelt thanks to my friends and family. My parents Lauren and Chris Molinari, my brother Stephen Molinari, my boyfriend Chris Erwin, my grandparents Betty and George Duff and Joan and Ignatius Molinari, my great aunts Frederica, Joan, and Janet, great grandmother Pietrina Naples, my aunts and uncles, and cousins, and friends for making me who I am today, and for your love, support, encouragement, and for believing in me. Thank you from the bottom of my heart. I would not have made it this far without you all.

Table of Contents

List of Figures

Chapter 1

Chapter 2

Chapter 3

Chapter 4

Chapter 5

Chapter 6

Abstract

Despite significant structural differences between the active sites of supported vanadium oxide catalysts such as supported VO_4/SiO_2, and vanadium bromoperoxidase enzyme mimics such as the vanadium peroxo-oxo compound chelated with N-(2-hydroxyethyl)iminodiacetic acid (heida) or $K[VO(O_2)(heida)]$, both catalysts are capable of conducting similar partial oxidation reactions. The $K[VO(O_2)(heida)]_{(aq)}$ vanadium enzyme mimic contains a vanadium peroxo-oxo structure, $O=VO_2$, that is not present for vanadia supported on inorganic oxides such as silica. Vanadia dispersed on silica is present as a trigonal pyramidal surface VO_4 species possessing one terminal V=O bond and three bridging V-O-Si bonds under dehydrated conditions. The first objective of the studies included in this dissertation was to compare the aqueous methanol oxidation mechanism of $K[VO(O_2)(heida)]_{(aq)}$ with that of the vapor-solid methanol oxidation by supported VO_4/SiO_2. The second objective was then to extend this to the study of Vanadium Haloperoxidases (VHPOs), thereby beginning to bridge the gap between heterogeneous and enzyme catalysis. In this study, we have used *in situ* Raman, UV-vis and ATR-IR spectroscopy during methanol oxidation to examine the nature of the active sites, most abundant reaction intermediates, rate-determining-step, and oxidation mechanisms of the $K[VO(O_2)(heida)]_{(aq)}$ mimic compound and inorganic supported vanadia catalyst. In both catalytic systems, methanol chemisorbs at the bridging V-O-ligand and V-O-Si sites. The use of methanol as a molecular probe was employed to provide important information on the active site and mechanism of oxidation by $K[VO(O_2)(heida)]_{(aq)}$. This study elucidates the $K[VO(O_2)(heida)]_{(aq)}$ active site, most abundant reaction intermediates, the rate-determining-step, and the

important role of the vanadium peroxo structure for aqueous methanol oxidation, bridging the gap between inorganic and protein based vanadate oxidation catalysts. These results were then used as a benchmark for the study of Vanadium Haloperoxidase enzymes.

Chapter 1: Introduction

Selective oxidation of methanol to formaldehyde over supported vanadium oxide catalysts has emerged as the model system for oxidation reactions over metal oxide catalysts in recent years because the structure-activity relationship for this catalytic system is becoming fairly well understood. This is due to recent extensive fundamental characterization studies (EXAFS [1, 2], ^{51}V NMR [3], Raman[4], IR[5], UV-vis [6, 7] and DFT calculations[8, 9]). The supported vanadium oxide catalysts contain isolated and polymeric surface VO_4 species below monolayer coverage. Only isolated surface VO_4 sites are present below ~20% of monolayer coverage and mostly polymeric surface VO_4 species are present at monolayer coverage. Crystalline V_2O_5 nanoparticles form if monolayer coverage is exceeded. The surface VO_4 species possess one terminal oxo V=O bond and three bridging V-O-Support/V-O-V bonds with the V-O-V bonds only present for the polymeric species. The oxidation of methanol to formaldehyde over an isolated surface VO_4 site proceeds via CH_3OH chemisorption on the bridging V-O-Support bond to form surface methoxy (CH_3O*) and hydroxyl species as seen below in equation (1.1). [8-10]

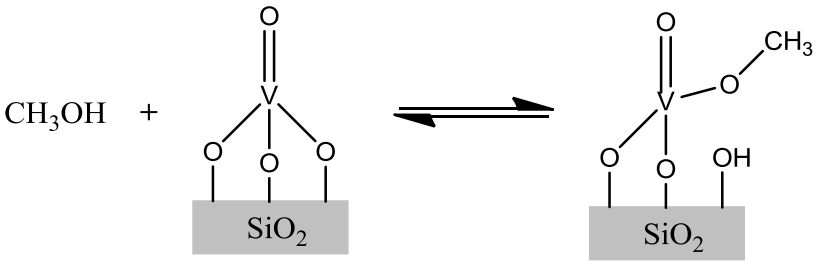

(1.1)

The surface methoxy intermediate subsequently transfers one of its hydrogen atoms to the terminal V=O bond, which irreversibly forms the departing formaldehyde reaction product, shown below in equation 1.2.[8, 9]

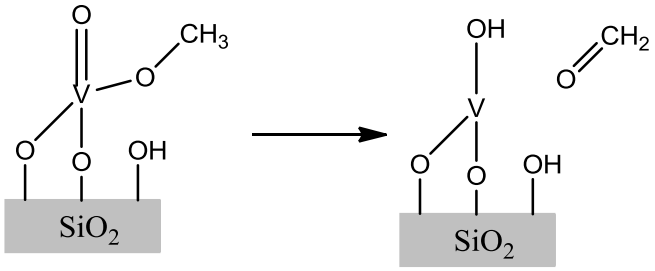

(1.2)

The reduced surface VOx species can further react with the adjacent surface hydroxyl to form H_2O via the reaction (see equation 1.3):

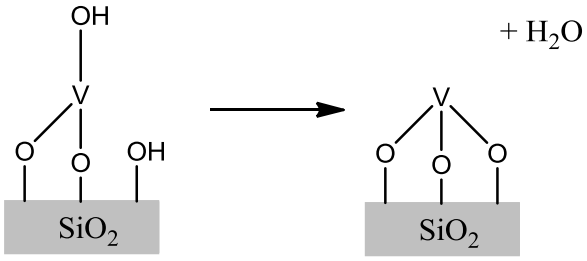

(1.3)

It should be noted that the exact molecular structures of the reduced surface VOx species have still not been determined in the heterogeneous catalysis literature, although during reduction, the loss of the V=O stretching vibration can be observed using *in situ* Raman and IR spectroscopy. In order to complete the catalytic cycle, the reduced surface VOx species is reoxidized back to V^{+5} by either gas phase molecular O_2 or oxygen donated from the bulk. If the oxidation reaction involves chemisorbed oxygen species (e..g., superoxide, peroxide or atomic oxygen species), the reaction is

referred to as proceeding via a Langmuir-Hinshelwood mechanism. If the oxidation reaction involves oxygen supplied by the surface VOx species or the catalyst bulk lattice, the reaction is referred to proceeding via a Mars-van Krevelen mechanism.[11]

Supported vanadium oxide catalysts are frequently used in gas phase chemical processes. However, in pharmaceuticals, fine chemicals, and other industries where aqueous phase chemistry is prominent, aqueous vanadium complexes using functional ligands as supports can be employed as oxidation catalysts in aqueous and non-aqueous liquid media. Additionally, bioinspired catalysts are also beginning making their debut in the world of traditional heterogeneous catalysis.[12-16] Drug discovery laboratories have already embraced such an approach to research. Rather than designing a pharmaceutical compound *de novo*, researchers can modify a natural compound to produce a better analog.[17, 18]

Because of the great deal of knowledge that already exists on supported vanadium oxides, and considering the interest in vanadia biocatalysts and biocatalyst mimics, a unique research opportunity for the study of vanadium containing enzymes has presented itself. Unfortunately, the use of methanol oxidation as a model chemical reaction molecular probe has been ignored in biocatalysis research, but this is partially due to enzyme substrate specificity. Enzymes are typically oriented so that their catalytically active amino acids only accept the natural substrate, or at least a very similar substrate, or a substrate that passes through a similar transition state.[19, 20] An example of this is a serine protease. In serine proteases the catalytic active site is an amino acid triad. This makes the enzyme extremely selective. However,

metalloenzymes, including the vanadium haloperoxidase family of enzymes, are usually more likely to exhibit what has been dubbed "catalytic promiscuity" (accepting multiple different substrates) than strictly proteinaceous active site enzymes, due to their isolated metal cofactor.[19, 20]

The vanadium haloperoxidases (VHPOs) are a class of enzymes that contain a vanadium oxide cofactor in the center.[21] VHPOs are named for their ability to catalyze the two-electron oxidation of halide ions (Cl^-, Br^-, or I^-) in the presence of hydrogen peroxide to produce hypohalous acids (HOCl, HOBr, or HOI).[22]

$$H^+ + H_2O_2 + X^- \rightarrow HOX + H_2O \qquad (1.4)$$

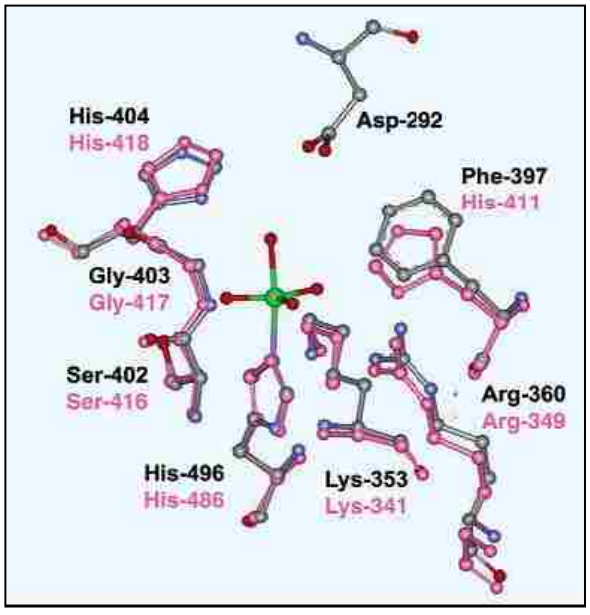

Figure 1.1 Superimposed active sites of the native form of vanadium chloroperoxidase from *C. inaequalis* (displayed in CPK color) and vanadium bromoperoxidase from *A. nodosum* (displayed in pink color). Figure adapted from Pooransingh-Margolis *et al.* [38]

The VHPOs are named according to the most electronegative halide ion they are able to oxidize. For example, a vanadium bromoperoxidase (VBrPO) can catalyze the oxidation of both Br^- and I^-, but not Cl^-.[23] The chloroperoxidase form can be extracted from fungus such as *Curvularia inaequalis*, the bromoperoxidase form of the enzyme can be extracted from brown and red algae such as *Corallina officinalis* and *Ascophyllum nodosum*,

and the iodoperoxidase enzyme can be found in green algae such as *Acrosiphonia sonderi*.[2-4] The molecular mass and number of amino acid residues for each type of VHPO varies from species to species. However, on average, the molecular mass of a vanadium haloperoxidase monomer is approximately 73.4 kDa. A halide ion is not required for enzymatic activity despite the implication of the enzyme's name. In the native form, VHPOs maintain a trigonal bipyramidal vanadium configuration represented in Figure 1.1.[24-26] In the presence of H_2O_2, the vanadium cofactor is activated, and the vanadate cofactor is transformed. This transformation turns the vanadate cofactor into a side-bound vanadium peroxo group, a double bond oxo group, two long V-O bonds ligated to supporting amino acids, and a direct long V-N bond to a distal histidine residue. The peroxo-oxo structure of VHPOs is referred to as the "active form."

VHPOs and vanadium mimic compounds have many functions both in nature and in research. VHPOs exist naturally in some types of algae and fungi and are thought to catalyze the oxidation of a halide to the hypohalous acid as a defense mechanism against microbes and other potentially destructive organisms.[21, 27, 28] VHPOs are being studied not only as halide oxidant, but also as a catalyst for other reactions such as sulfoxidations, and alcohol oxidations.[22, 29-31] In addition, VHPOs are gaining interest in medical research since vanadium appears to have therapeutic effects on diseases such as diabetes mellitus and osteosarcomas.[32-34] Vanadium and vanadium enzymes are an essential component for many different species, including humans, although there is less than 0.1 mg of vanadium in an adult human.[35] Vanadium is believed to act as an alkaline phosphotase inhibitor in the human body and in other

species. Also, recent research has shown that some aqueous vanadate complexes have an insulin enhancing effect.[36] It is still not entirely clear, however, why vanadium is useful for humans.

Studies on the structure and function of vanadium haloperoxidases are well documented with respect to the signature oxidation of a halide in the presence of hydrogen peroxide.[24, 25, 37-39] Although X-ray crystallographic structural studies of VHPOs are well established,[24, 37] there have not been many spectroscopic characterization studies during reaction. X-ray absorption spectroscopy (XANES/EXAFS) studies of VHPOs have been reported, but were found to be of limited value because EXAFS yields an average V-O bond length for the multiple oxygen ligands and requires somewhat high aqueous VHPO concentrations for measurement (mM concentrations).[39-41] Solid-state MAS ^{51}V NMR studies of the V^{+5} VHPO enzymes have also been successfully reported in the μmol range and are in agreement with crystallographic findings.[42] Furthermore, EPR spectroscopy has been employed to measure the inactive reduced form of VHPO enzymes with the V^{+4} cation.[43] The most interesting spectroscopic study to date was reported with *in situ* UV-vis spectroscopy during HCl oxidation by vanadium chloroperoxidase (VCPO) and H_2O_2.[44] This study demonstrates that μM concentrations of the aqueous VCPO could be monitored with time-resolved UV-vis spectroscopy and that the oxidation reaction required several minutes to completion. To the best of our knowledge, no Raman or ATR-IR studies have been reported of aqueous VHPO and its oxidation reactions.

Furthermore, literature studies have primarily focused on halide oxidation by VHPO, not sulfoxidation or alcohol oxidation.

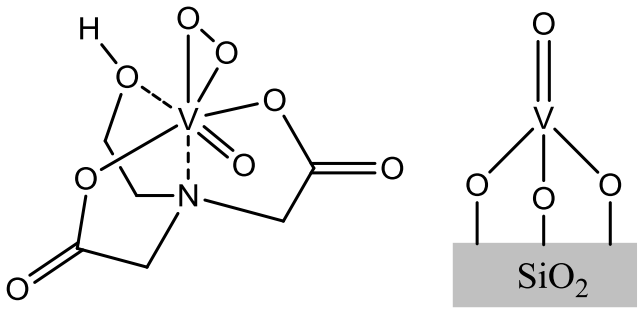

Figure 1.2 a. Structure of K[VO(O_2)(heida)] mimic of VHPO showing peroxo and oxo groups **b.** Structure of dehydrated supported vanadia species on silica possessing the trigonal pyramid structure.

Several research groups have designed metal-organic compounds that mimic the structure and function of the active peroxidated form of VHPOs.[45-47] Enzyme mimic compounds are advantageous since the synthesis procedure is significantly simpler than the synthesis or extraction and purification procedure for the actual enzyme. The most studied of these VHPO mimic compounds is K[VO(O_2)(heida)], a vanadium peroxo-oxo compound chelated with N-(2-hydroxyethyl) iminodiacetic acid (heida), depicted in Figure 1.2 a.[45] The K[VO(O_2)(heida)] complex is a structural and functional mimic of vanadium bromoperoxidase which is able to catalyze bromide and iodide oxidation, asymmetric sulfoxidation, and also (as will be demonstrated in this study) aqueous methanol oxidation in the presence of hydrogen peroxide.[45, 48] Bromide oxidation by the K[VO(O_2)(heida)] complex appears frequently in the literature, and is reported to occur via nucleophilic attack of the incoming halide on the peroxo group.[45] The proposed mechanism for anaerobic oxidation of 2-propanol by aqueous vanadium peroxo compounds occurs via propanol adsorption at the vanadium center, followed by hydrogen abstraction by the peroxo group, passing through a short-lived radical

species.[49] However, this mechanism is only a putative mechanism, and until now, direct experimental evidence for this type of alcohol oxidation mechanism has been lacking.

This proposed alcohol oxidation mechanism[49] is fairly similar to that of gas phase alcohol oxidations over supported vanadium oxide heterogenous catalysts. However, there are significant structural and reactivity differences between the active site of supported vanadium oxide catalysts and the $K[VO(O_2)(heida)]_{(aq)}$ complex. The vanadium peroxo-oxo structure present for the $K[VO(O_2)(heida)]$ mimic is not present for vanadia supported on inorganic oxides such as silica.[50] The dehydrated supported vanadia species on silica at low coverage are present as the trigonal pyramidal structure shown in Figure 1.2 b with the surface VO_4 species possessing one terminal V=O bond and three bridging V-O-Si bonds. Details regarding the structural differences between these two systems will be discussed further in Chapter 2.

The intent to study VHPOs and VHPO mimics was preceded by several studies to develop experimental techniques required for studying vanadium containing clusters in both solid and aqueous form. We have demonstrated our laboratory capabilities for examining vanadium containing clusters in two recent publications.[51, 52] In these publications, we have examined two different families of $W_{12-x}V_xO_{40}$ and $W_{12-x}V_xO_{40}$ Keggin clusters. The Keggin structure is shown in Figure 1.3. We have investigated the influence of introducing VO_x sites into the primary, bulk structure of polyoxometalates $H_{3+x}PM_{12-x}V_xO_{40}$ (x = 0, 1, 2, 3 and M=W or Mo) and the secondary, surface structure of supported $VO_x/H_3PM_{12}O_{40}$ Keggins. This was done in order to establish their structure-reactivity/selectivity relationships.[51, 52] VO_x deposited onto the

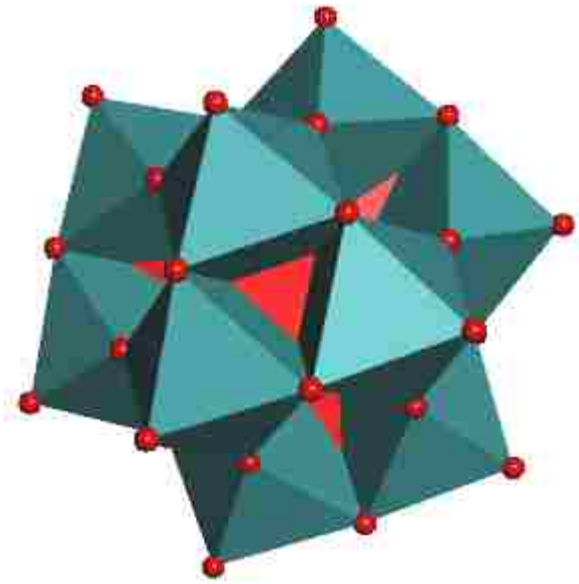

Figure 1.3 Keggin Structure representing the overall structure of molybdophosphoric ($H_3PMo_{12}O_{40}$) and tungstophosphoric ($H_3PW_{12}O_{40}$) acid clusters

secondary surface of the Keggin is depicted in Figure 1.4 for the purpose of better visualization.

The addition of vanadium centers to molybdophosphoric ($H_3PMo_{12}O_{40}$) and tungstophosphoric ($H_3PW_{12}O_{40}$) acid clusters is beneficial for redox catalysis. This shifts reactivity primarily from acidic character to redox character as evidenced by a shift in selectivity of methanol oxidation from production of dimethyl ether to formaldehyde, respectively.[53] Vanadium-containing molybdophosphoric acid (MPA) clusters, $H_{3+x}PMo_{12-x}V_xO_{40}$ (x = 0, 1, 2, 3) are particularly interesting because of their exceptionally dynamic character in both the solid and aqueous phase. These vanadium

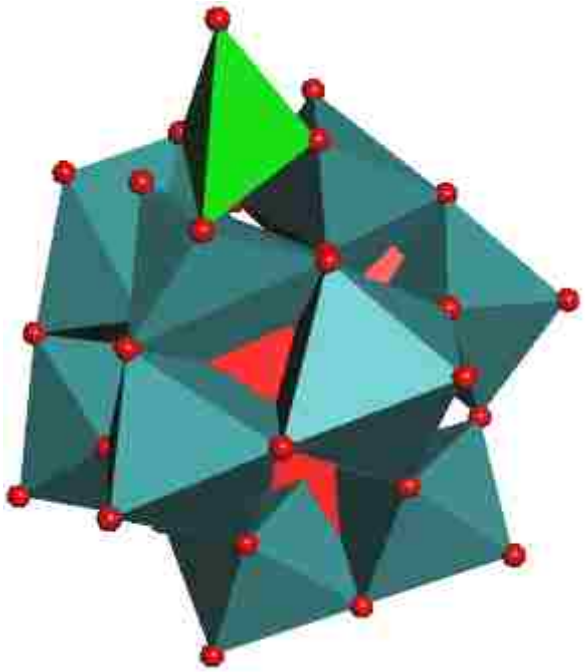

Figure 1.4 VOx deposited onto the secondary surface of a Keggin cluster.

containing MPA studies were important vanadium-containing cluster preliminary investigations. Here we learned the techniques and knowledge required to analyze dynamic vanadium-containing enzymes and enzyme mimics as seen in the following chapters.

Recent *in situ* solid state heterogeneous characterization studies by EPR, UV-vis, Raman, FTIR, and NMR during heat treatment up to 350^{o}C have revealed that the vanadium cation can be expelled from the vanadium containing MPA Keggin.[54-56] Even when the vanadium is located in the primary structure after synthesis, it can migrate outwards to sit on the secondary structure as a surface vanadyl group under reaction conditions.[57] *In situ* Raman spectroscopy experiments during thermal treatment and

under propylene oxidation conditions have revealed that the decomposition of the intact MPA Keggin begins with the expulsion of vanadyl and molybdenyl species. This expulsion causes defective Keggin structures to form, then the defective Keggin units disintegrate into intermediate MoO_x species before finally fully decomposing to MoO_3.[58] The appearance of a "multiplet" of Raman bands in the 900-1000 cm^{-1} spectral region appears to be indicative of the transformation of intact Keggin anions to the intermediate mixed MoO_x phase.[58]

We recognized the complexity of the vanadium-containing MPA catalysts and, also, the need for *in situ* characterization studies, especially *in situ* Raman characterization studies under reaction conditions because of the dynamic nature of such complex mixed oxide catalysts. Additionally, the complexity of these catalysts made them an ideal starting point for the development of Raman techniques for the study of vanadium-containing clusters such as $K[VO(O_2)(heida)]_{(aq)}$. Therefore, a series of vanadium incorporated MPA Keggins, with vanadium introduced into the primary and onto the secondary Keggin structure, was examined for the first time with *in situ* Raman spectroscopy to determine their molecular structural evolution under reaction and aqueous conditions. Additionally, the overall capability of Raman spectroscopy to monitor dynamic changes of vanadium containing clusters was evaluated.

These vanadium containing MPA studies have proven our ability to accurately characterize vanadium containing clusters under various conditions. We have observed dynamic changes in MPA and vanadium containing MPA structures in the solid state at

both ambient and dehydrated conditions, during reaction conditions, and in aqueous solution.

The research included in the remainder of this dissertation examines vanadium containing biocatalysts and biocatalyst mimics and compares each system to traditional vanadium oxide supported catalysts such as V_2O_5 supported on SiO_2. These studies utilize the same techniques developed during preliminary vanadium containing MPA studies. The studies in this dissertation bridge the gap between biocatalysis and traditional heterogeneous catalysis by (1) establishing effective characterization methods and approaches for the *in situ* study of vanadium biocatalysts and biocatalyst mimics in the aqueous phase, (2) extending the *in situ* spectroscopic characterization methodologies to VHPOs and $K[VO(O_2)(heida)]_{(aq)}$ in H_2O_2 and CH_3OH oxidation environments, (3) applying the advanced methodologies to study the VOx structure, oxidation state, catalytic active site, and mechanism of oxidation for VHPOs and $K[VO(O_2)(heida)]_{(aq)}$, and (4) investigating the kinetics of aqueous methanol oxidation by $K[VO(O_2)(heida)]_{(aq)}$.

References

(1) Tanaka, T.; Yamashita, H.; Tsuchitani, R.; Funabiki, T.; Yoshida, S. *J. Chem. Soc. , Faraday trans.* **1988**, *84*, 2987-2999.

(2) Swart, I.; Fielicke, A.; Redlich, B.; Meijer, G.; Weckhuysen, B. M.; De Groot, Frank M. F. *J. Am. Chem. Soc.* **2007**, *129*, 2516-2520.

(3) Eckert, H.; Wachs, I. E. *J. Phys. Chem.* **1989**, *93*, 6796-6805.

(4) Vuurman, M. A.; Wachs, I. E.; Hirt, A. M. *J. Phys. Chem.* **1991**, *95*, 9928.

(5) Cristiani, C.; Forzatti, P.; Busca, G. *J. Catal.* **1989**, *116*, 586-589.

(6) Gao, X.; Wachs, I. E. *J. Phys. Chem. B* **2000**, *104*, 1261-1268.

(7) Tian, H.; Ross, E. I.; Wachs, I. E. *J. Phys. Chem. B* **2006**, *110*, 9593-9600.

(8) Khaliullin, R. Z.; Bell, A. T. *J. Phys. Chem. B* **2002**, *106*, 7832-7838.

(9) Dobler, J.; Pritzsche, M.; Sauer, J. *J. Am. Chem. Soc.* **2005**, *127*, 10861-10868.

(10) Burcham, L. J.; Deo, G.; Gao, X.; Wachs, I. E. *Top. Catal.* **2000**, *11/12*, 85.

(11) Mars, P.; van Krevelen, D. W. *Spec. Suppl. Chem. Eng. Sci.* **1954**, *3*, 41-57.

(12) Brimblecombe, R.; Koo, A.; Dismukes, G. C.; Swiegers, G. F.; Spiccia, L. *J. Am. Chem. Soc.* **2010**, *132*, 2892-2894.

(13) Fontecave, M.; Artero, V. *Comptes Rendus Chimie , In Press, Corrected Proof*.

(14) Ruettinger, W.; Yagi, M.; Wolf, K.; Bernasek, S.; Dismukes, G. C. *J. Am. Chem. Soc.* **2000**, *122*, 10353-10357.

(15) Schmid, A.; Dordick, J. S.; Hauer, B.; Kiener, A.; Wubbolts, M.; Witholt, B. *Nature* **2001**, *409*, 258-268.

(16) Schneider, C. J.; Penner-Hahn, J.; Pecoraro, V. L. *J. Am. Chem. Soc.* **2008**, *130*, 2712-2713.

(17) Beghyn, T.; Deprez-Poulain, R.; Willand, N.; Folleas, B.; Deprez, B. *Chemical Biology & Drug Design* **2008**, *72*, 3-15.

(18) Paterson, I.; Anderson, E. A. *Science* **2005**, *310*, 451-453.

(19) Kazlauskas, R. J. *Curr. Opin. Chem. Biol.* **2005**, *9*, 195-201.

(20) Hult, K.; Berglund, P. *Trends Biotechnol.* **2007**, *25*, 231-238.

(21) Butler, A.; Walker, J. V. *Chem. Rev.* **1993**, *93*, 1937-1944.

(22) Butler, A. *Coordination Chemistry Reviews*, **1999**, *187*, 17-35.

(23) Zampella, G.; Fantucci, P.; Pecoraro, V. L.; De Gioia, L. *J. Am. Chem. Soc.* **2005**, *127*, 953-960.

(24) Messerschmidt, A.; Wever, R. *Proceedings of the National Academy of Sciences* **1996**, *93*, 392-396.

(25) Raugei, S.; Carloni, P. *J Phys Chem B* **2006**, *110*, 3747-3758.

(26) Simons, B. H.; Barnett, P.; Vollenbroek, E. G. M.; Dekker, H. L.; Muijsers, A. O.; Messerschmidt, A.; Wever, R. *European Journal of Biochemistry* **1995**, *229*, 566-574.

(27) Hansen, E. H.; Albertsen, L.; Schafer, T.; Johansen, C.; Frisvad, J. C.; Molin, S.; Gram, L. *Appl. Environ. Microbiol.* **2003**, *69*, 4611-4617.

(28) Renirie, R.; Dewilde, A.; Pierlot, C.; Wever, R.; Hober, D.; Aubry, J. M. *Journal of Applied Microbiology* **2008**, *105*, 264-270.

(29) Andersson, M.; Willetts, A.; Allenmark, S. *J. Org. Chem.* **1997**, *62*, 8455-8458.

(30) ten Brink, H. B.; Tuynman, A.; Dekker, H. L.; Hemrika, W.; Izumi, Y.; Oshiro, T.; Schoemaker, H. E.; Wever, R. *Inorg. Chem.* **1998**, *37*, 6780-6784.

(31) Butler, A.; Tschirret-Guth, R. A.; Simpson, M. T. *ACS Symp. Ser.* **1999**, *711*, 202-215.

(32) Rehder, D.; Bashirpoor, M.; Jantzen, S.; Schmidt, H.; Farahbakhsh, M.; Nekola, H. *ACS Symp. Ser.* **1999**, *711*, 60-70.

(33) Rehder, D. *Inorganic Chemistry Communications*, **2003**, *6*, 604-617.

(34) Mukherjee, B.; Patra, B.; Mahapatra, S.; Banerjee, P.; Tiwari, A.; Chatterjee, M. *Toxicol. Lett.* **2004**, *150*, 135-143.

(35) Greenwood, N. N. *Catalysis Today*, **2003**, *78*, 5-11.

(36) Meyerovitch, J.; Farfel, Z.; Sack, J.; Shechter, Y. *J. Biol. Chem.* **1987**, *262*, 6658-6662.

(37) Weyand, M.; Hecht, H. J.; Kieb, M.; Liaud, M. F.; Vilter, H.; Schomburg, D. *Journal of Molecular Biology*, **1999**, *293*, 595-611.

(38) Pooransingh-Margolis, N.; Renirie, R.; Hasan, Z.; Wever, R.; Vega, A. J.; Polenova, T. *J. Am. Chem. Soc.* **2006**, *128*, 5190-5208.

(39) Renirie, R.; Charnock, J. M.; Garner, C. D.; Wever, R. *J. Inorg. Biochem.* **2010**, *104*, 657-664.

(40) Arber, J. M.; de Boer, E.; Garner, C. D.; Hasnain, S. S.; Wever, R. *Physica B: Condensed Matter*, **1989**, *158*, 126-127.

(41) Hormes, J.; Kuetgens, U.; Chauvistre, R.; Schreiber, W.; Anders, N.; Vilter, H.; Rehder, D.; Weideman, C. *Biochim. Biophys. Acta* **1988**, *956*, 293-299.

(42) Tromp, M. G.; Olafsson, G. Krenn, B. E.; Wever, R. *Biochim. Biophys. Acta* **1990**, *1040*, 192-198.

(43) Van Schijndel, J. W. P. M.; Vollenbroek, E. G. M.; Wever, R. *Biochim. Biophys. Acta* **1993**, *1161*, 249-256.

(44) Renirie, R.; Hemrika, W.; Piersma, S. R.; Wever, R. *Biochemistry (N. Y.)* **2000**, *39*, 1133-1141.

(45) Colpas, G. J.; Hamstra, B. J.; Kampf, J. W.; Pecoraro, V. L. *J. Am. Chem. Soc.* **1996**, *118*, 3469-3478.

(46) de la Rosa, Roger I.; Clague, M. J.; Butler, A. *J. Am. Chem. Soc.* **1992**, *114*, 760.

(47) Butler, A.; Baldwin, A. H. In *Vanadium bromoperoxidase and functional mimics;* Hill, H., Sadler, P. and Thomson, A., Eds.; Metal Sites in Proteins and Models; Springer Berlin: Heidelberg, 1997; Vol. 89, pp 109-132.

(48) Smith, T. S.; Pecoraro, V. L. *Inorg. Chem.* **2002**, *41*, 6754-6760.

(49) Butler, A.; Clague, M. J.; Meister, G. E. *Chem. Rev.* **1994**, *94*, 625-638.

(50) Molinari, J. E.; Wachs, I. E. *J. Am. Chem. Soc.* **2010**, *132*, 12559-12561.

(51) Nakka, L.; Molinari, J. E.; Wachs, I. E. *J. Am. Chem. Soc.* **2009**, *131*, 15544-15554.

(52) Molinari, J. E.; Nakka, L.; Kim, T.; Wachs, I. E. *ACS Catal.* **2011**, *1*, 1536-1548.

(53) Bruckman, K.; Tatibouet, J. M.; Che, M.; Serwicka, E.; Haber, J. *Journal of Catalysis* **1993**, *139*, 455-467.

(54) Brückner, A.; Scholz, G.; Heidemann, D.; Schneider, M.; Herein, D.; Bentrup, U.; Kant, M. *Journal of Catalysis* **2007**, *245*, 369-380.

(55) Blouet-Crusson, E.; Rigole, M.; Fournier, M.; Aboukaïs, A.; Daubrege, F.; Hecquet, G.; Guelton, M. *Applied Catalysis A: General* **1999**, *178*, 69-83.

(56) Ilkenhans, T.; Herzog, B.; Braun, T.; Schlogl, R. *Journal of Catalysis* **1995**, *153*, 275-292.

(57) Fournier, M.; Louis, C.; Che, M.; Chaquin, P.; Masure, D. *Journal of Catalysis* **1989**, *119*, 400-414.

(58) Mestl, G.; Ilkenhans, T.; Spielbauer, D.; Dieterle, M.; Timpe, O.; Kröhnert, J.; Jentoft, F.; Knözinger, H.; Schlögl, R. *Applied Catalysis A: General* **2001**, *210*, 13-34.

(59) Busca, G. *J. Raman Spectroscopy* **2002**, *33*, 348-358.

(60) Caliman, E.; Dias, J. A.; Dias, S. C. L.; Prado, A. G. S. *Catalysis Today*, **2005**, *107-108*, 816-825.

(61) Kim, D. S.; Ostromecki, M.; Wachs, I. E. *Journal of Molecular Catalysis A: Chemical* **1996**, *106*, 93-102.

(62) Brown, G. M.; Noe-Spirlet, M. -.; Busing, W. R.; Levy, H. A. *Acta Crystallographica Section B* **1977**, *33*, 1038-1046.

(63) Hardcastle, F. D.; Wachs, I. E. *J. Phys. Chem.* **1991**, *95*, 5031-5041.

(64) Gao, X.; Jehng, J.; Wachs, I. E. *Journal of Catalysis* **2002**, *209*, 43-50.

(65) Rocchiccioli-Deltcheff, C.; Aouissi, A.; M. Bettahar, M.; Launay, S.; Fournier, M. *Journal of Catalysis* **1996**, *164*, 16-27.

(66) Wang, C.; Cai, Y.; Wachs, I. E. *Langmuir* **1999**, *15*, 1223-1235.

(67) Burcham, L. J.; Briand, L. E.; Wachs, I. E. *Langmuir* **2001**, *17*, 6164-6174.

(68) Pope, M. T. In *Heteropoly and Isopoly Oxometalates;* Inorganic Chemistry Concepts; Springer-Verlag Berlin, Heidelberg: New York, 1983; Vol. 8, .

(69) Briand, L. E.; Valle, G. M.; Thomas, H. J. *J. Mater. Chem.* **2002**, *12*, 299-304.

Chapter 2: $K[VO(O_2)(heida)]_{(aq)}$, A Vanadium Bromoperoxidase Mimic

The $K[VO(O_2)(heida)]_{(aq)}$ metal-organic vanadium bromoperoxidase mimic compound was designed by the Pecoraro laboratory group at University of Michigan.[1] Various other mimic compounds have been designed by the Pecoraro group and other research groups.[1-3] Many of these soluble VOx hybrid complexes, have been employed as oxidation catalysts in many different types of media such as, ionic liquids, aqueous and non-aqueous soutions.[1, 2, 4, 5] These other mimic complexes may contain ligands such as nitrilotriacetic acid (nta), N-(2-amidomethyl) iminodiacetic acid (ada), N,N-bis(2-pyridylmethyl) glycine (BPG), and N,N,N-tris(2-pyridylmethyl) amine (TPA). The structures of these ligands are shown in Figure 2.1 in addition to the N-(2-hydroxyethyl)iminodiacetic acid ligand (Figure 2.1 B), commonly abbreviated as "heida."[1] A literature search reveals that the most studied, and most effective of these ligands for mimicking the structure and function of the active form of VHPOs is the

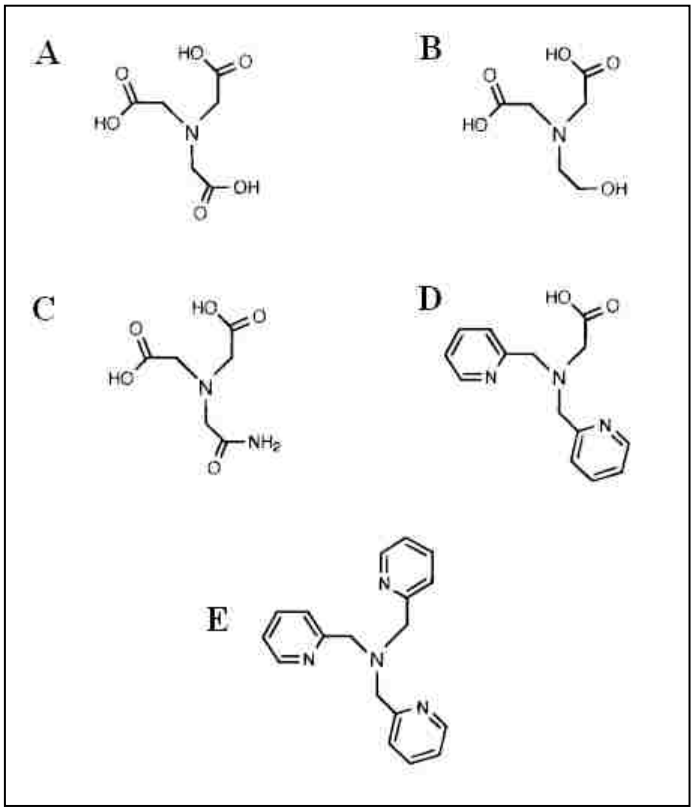

Figure 2.1 Edited figure published by Colpas et al.[1] **A.** nitrilotriacetic acid, **B.** N-(2-hydroxyethyl) iminodiacetic acid, **C.** N-(2-amidomethyl) iminodiacetic acid, **D.** N,N-bis(2-pyridylmethyl) glycine, and **E.** N,N,N-tris(2-pyridylmethyl) amine.

heida ligand. Every form of VHPO contains a vanadate cofactor which is covalently bound to the imidazole nitrogen of a histidine residue. The central nitrogen atom in the heida compound serves as a mimic for the conserved histidine residue which is present in the first coordination sphere of all forms of vanadium haloperoxidase, bromo-, chloro-, and iodoperoxidases alike.[1, 3, 6, 7]

$K[VO(O_2)(heida)]$ is actually a mimic of the active form of vanadium bromoperoxidase (VBPO). It is a vanadium bromoperoxidase mimic specifically because it is able to oxidize bromide and iodide, but not chloride. It is an active form (and not native form) mimic because it contains a vanadium peroxo-oxo structure (which will be examined and characterized further in this chapter) much like all VHPOs when they are activated by exposure to H_2O_2. Prior to activation by exposure to H_2O_2, VHPOs do not contain a vanadium peroxo group, but are present in the native form as what appears to be a vanadium dioxo resonant structure.[6] Likewise, a native form mimic of VBPO is obtainable prior to addition of H_2O_2. The dioxo structure, $K[VO(O)(heida)]$ a mimic of the native form of VBPO, will also be examined later in this chapter, since the dioxo form is crucial to the full oxidation mechanism of methanol by $K[VO(O_2)(heida)]$.

The first section of this chapter focuses on the characterization of the peroxo-oxo active form mimic compound $K[VO(O_2)(heida)]$. The second section focuses on the characterization of the dioxo native form mimic, $K[VO(O)(heida)]$. The third section of this chapter presents a comparison between the peroxo-oxo $K[VO(O_2)(heida)]_{(aq)}$ structure and the heterogeneous case of VO_4/SiO_2.

Section 1: Spectroscopic Characterization of $K[VO(O_2)(heida)]_{(aq)}$

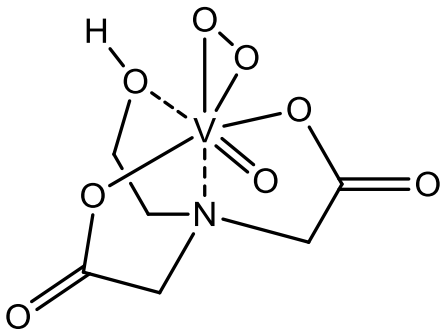

Figure 2.2 Structure of $K[VO(O_2)(heida)]_{(aq)}$ showing peroxo and oxo groups

Few research groups have reported on characterization of $K[VO(O_2)(heida)]$ (shown in Figure 2.2) by vibrational spectroscopic methods. Raman and FTIR characterization have been performed on the solid state crystalline form of $K[VO(O_2)(heida)]$[1], and Raman and ATR-IR spectra of $K[VO(O_2)(heida)]$ in organic solvents such as acetonitrile have been collected with less than perfect results (although vibrational spectroscopy was not the focus of this referenced study).[8] Since $K[VO(O_2)(heida)]$ is only marginally soluble in acetonitrile, lower signal to noise ratios were obtained than if $K[VO(O_2)(heida)]$ were solubilized in water, and some of the $K[VO(O_2)(heida)]$ bands of interest are masked by the acetonitrile signal. Additionally, it appears that the vanadium peroxo $V\text{-}O_2$ stretching vibration was mis-identified as the asymmetric stretch, and not the symmetric stretch in acetonitrile solution. However it is important to note that in this referenced study, the focus was density functional theory (DFT), and not the identification of Raman bands.[8] The excellent results of the DFT portion of this referenced study will be revisited in Chapter 3.[8]

UV-vis and ^{51}V-NMR[1] have been used to identify the presence of a vanadium peroxo-oxo chelated structure and to investigate the coordination of vanadate to the ligand. To the best of our knowledge, high quality, high signal-to-noise ratio, high

resolution aqueous vibrational spectroscopy characterization of the K[VO(O_2)(heida)] complex specifically in aqueous media has not been reported. Characeterization of the peroxo-oxo form of K[VO(O_2)(heida)] in aqueous media by vibrational spectroscopy is important, since the active form of all VHPOs are proposed to possess a vanadium peroxo-oxo cofactor. In this chapter, K[VO(O_2)(heida)] is synthesized, assayed by ^{51}V-NMR and UV-vis, and then is fully characterized in aqueous solution by Raman and ATR-IR spectroscopy. The K[VO(O_2)(heida)]$_{(aq)}$ mimic is then compared to the heterogeneous model catalyst, supported VO_4/SiO_2.

Experimental

K[VO(O_2)(heida)] Synthesis

The K[VO(O_2)(heida)] mimic was synthesized according to the method published by Colpas *et al*[1]. 30 mL of deionized water was cooled to approximately 0^{o}C with stirring, and 5 mmol of KVO_3 (Alfa Aesar, 99.9% pur.) was added and stirred until dissolved. Special care was taken so that there was no excess KVO_3. The solution was filtered and 5 mmol of N-(2-hydroxyethyl)iminodiacetic acid (TCI America, min. 98% pur.) was added and stirred until completely dissolved. Then, 2 mL of 30% H_2O_2 was added dropwise to yield a dark red solution and buffered to pH 4 $\pm$ 0.2 with potassium hydroxide or hydrochloric acid if needed, but buffering was typically not required. The mixture was stirred overnight, and then refrigerated at 2-8^{o}C for at least 24 hours. Chelation of vanadate and formation of the peroxo-oxo group is highlighted in Scheme 2.1. K[VO(O_2)(heida)]$_{(s)}$ was isolated by crystallization. To facilitate nucleation of

Scheme 2.1 Synthesis of $K[VO(O_2)(heida)]_{(aq)}$

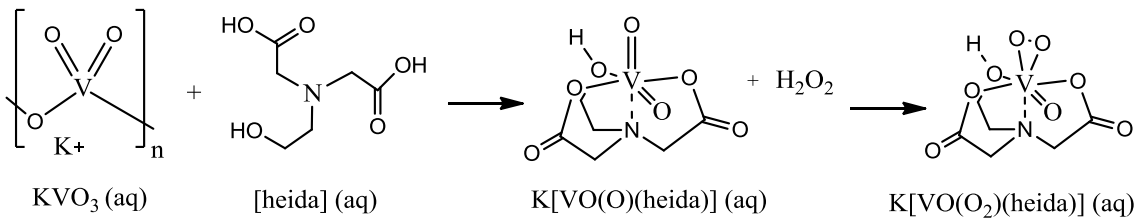

the $K[VO(O_2)(heida)]$ crystals, approximately 30 mL of 200 proof cold ethanol at 2-8 ^{o}C was added slowly. The suspension was returned to the refrigerator for at least another 24 hours until rod shaped, dark red crystals formed. The crystals were collected by filtration, washed with cold 200-proof ethanol and allowed to air dry. The $K[VO(O_2)(heida)]_{(s)}$ crystals were redissolved in deionized water for the aqueous experiments.

K[VO($^{18}O_2$)(heida)] and K[V^{18}O(O_2)(heida)] Synthesis with Isotopic ^{18}O

Isotopic $H_2{}^{18}O_2$ at 90 atom % was purchased from ICON Isotopes. Isotopically labelled $K[VO(^{18}O_2)(heida)]$ was synthesized as described above according to the procedure designed by Colpas *et al*[1] and modified from experiments in acetonitrile from Schneider[8] using isotopically labeled $H_2{}^{18}O_2$ in the vanadium peroxo formation step. This isotopic synthesis procedure was designed so that only the two oxygen atoms in the vanadium peroxo position were isotopically labeled. The V=O bond was not affected in this particular experiment.

The vanadyl V=O bond was exchanged with ^{18}O by dissolving $K[VO(O_2)(heida)]$ in $H_2{}^{18}O$ and incubating at 2-4^{o}C for a few days. The vanadium

peroxo group was unaffected by this exchange method. The $H_2{}^{18}O$ at 95 atom % was purchased from Isotec via Sigma-Aldrich.

UV-vis Transmission and Liquid Phase ^{51}V-NMR Spectroscopy

^{51}V-NMR spectroscopy and transmission UV-vis and were used to check the integrity of the synthesized K[VO(O_2)(heida)].

Aqueous phase ^{51}V-NMR was performed using a Bruker Avance 500 MHz NMR under ambient conditions. Aqueous K[VO(O_2)(heida)] was compared to a neat $VOCl_3$ reference standard.

Aqueous K[VO(O_2)(heida)] was examined using a Varian Cary 5E UV-vis spectrophotometer. First, a deionized water baseline spectrum was prepared over the range of 200-800 nm under ambient conditions, and the spectrum of each aqueous catalyst sample was collected from 200-800 nm under ambient conditions. The UV-vis spectra were analyzed using the Kubelka-Munk function $F(R_\infty)$ in order to better visualize broad bands.[9]

Raman Spectroscopy

Raman spectra of K[VO(O_2)(heida)] and supported V_2O_5/SiO_2 catalysts were collected with a Horiba-Jobin Yvon LabRam-HR spectrometer equipped with a confocal microscope, 2400/900 grooves/mm gratings, and a notch filter. The visible laser excitation at 532 nm (green) was supplied by a Yag doubled diode pumped laser (20 mW). The scattered photons were directed and focused onto a single-stage

monochromator and measured with a UV-sensitive liquid nitrogen-cooled CCD detector (Horiba-Jobin Yvon CCD-3000V). For the collection of ambient aqueous spectra, a single droplet was placed on a glass or CaF_2 slide and the laser was focused just slightly below the droplet surface in order to accommodate droplet spreading. The Raman signal using the 532 nm laser was significantly stronger than the signal obtained using the 442 or 325 nm lasers and, consequently, only results with the 532 nm laser will be presented.

ATR-IR Spectroscopy

The solid K[VO(O_2)(heida)] crystals were dissolved in deionized water and the IR spectrum was recorded using a Thermo Nicolet 8700 IR spectrometer equipped with a liquid nitrogen cooled DTGS detector and Harrick Horizon ATR attachment on a zinc selenide crystal. The spectrum was collected in the 400-4000 cm^{-1} range with 72 scans, and the deionized water spectrum was background subtracted.

Results

The ^{51}V NMR spectrum of aqueous K[VO(O_2)(heida)] is shown in Figure 2.3. Aqueous K[VO(O_2)(heida)] exhibits a sharp ^{51}V NMR band at -593 ppm, which is consistent with that of a ligated aqueous vanadium peroxo-oxo species with solvation effects.[1] This indicates that the compound synthesized is indeed K[VO(O_2)(heida)] and not other forms of aqueous vanadate species.

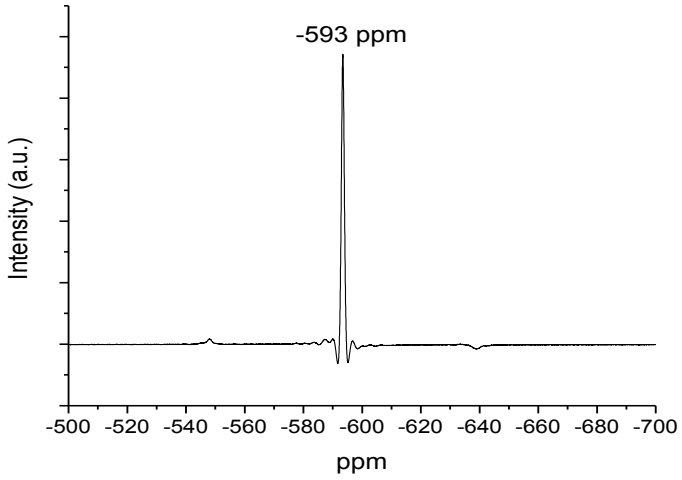

Figure 2.3 ^{51}V-NMR spectrum of K[VO(O_2)heida] (aq) confirming identity of peroxo-oxo structure.

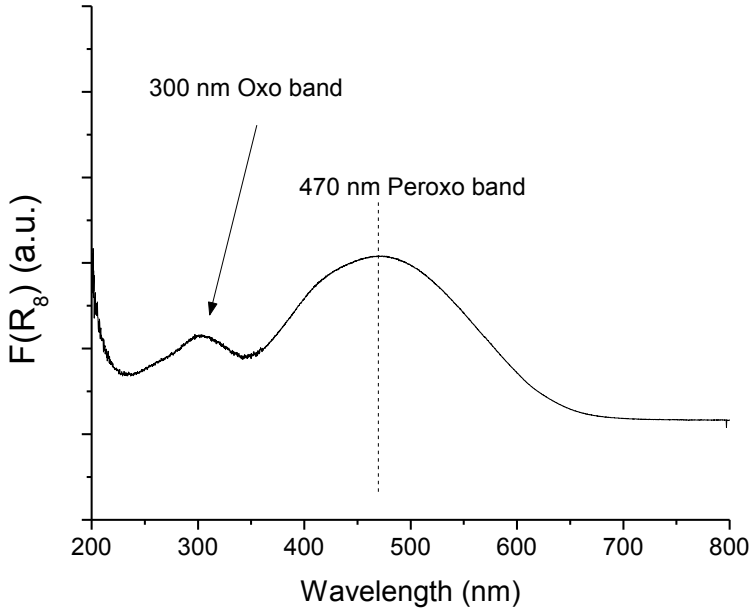

Figure 2.4 UV-vis Absorbance spectrum of K[VO(O_2)(heida)]$_{(aq)}$ enzyme mimic showing peroxo band at 470 nm and oxo band below 300 nm.

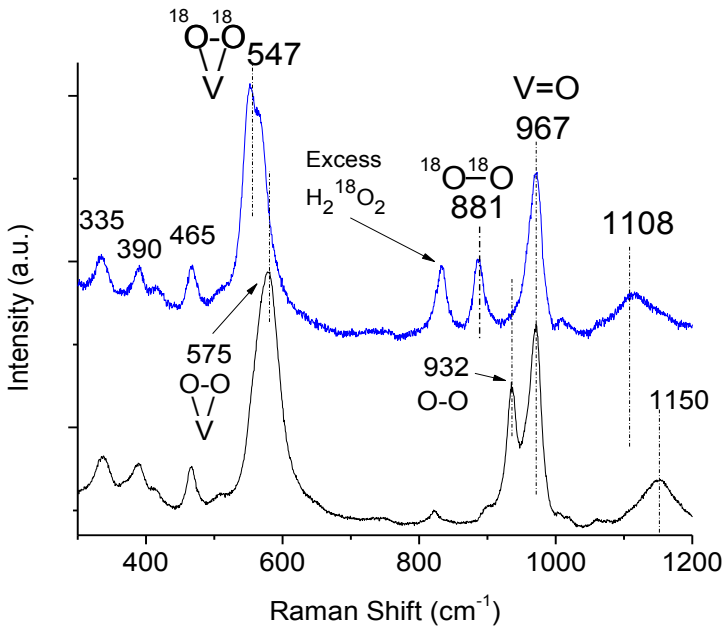

Figure 2.5 Raman Spectrum of $K[VO(O_2)heida]_{(aq)}$, black line, and isotopic $K[VO(^{18}O_2)heida]_{(aq)}$, blue line, demonstrating the vibrational assignment of the peroxo bands at 575 and 932 cm^{-1} and overtone of the 575 cm^{-1} band at 1150 cm^{-1}.

The Kubelka-Munk function $F(R_\infty)$ transformed absorbance spectrum of aqueous $K[VO(O_2)(heida)]$ is presented in Figure 2.4 and highlights the 470 nm band of the vanadium peroxo group and the 300 nm oxo group.[1] The UV-vis spectrum is a clear indicator of the ligand to metal charge transition (LMCT) from vanadium to a peroxo group at 470 nm, and from vanadium to an oxo group at 300 nm.

Assignment of the Raman bands for aqueous $K[VO(O_2)(heida)]$ was achieved with the aid of isotopic oxygen labeling studies. In order to selectively investigate the vibrational positions of the peroxo bands, isotopic $H_2{}^{18}O_2$ was used during synthesis. The Raman spectra of $K[VO(^{16}O_2)(heida)]_{(aq)}$ and $K[VO(^{18}O_2)(heida)]_{(aq)}$ are presented in Figure 2.5. The addition of $H_2{}^{18}O_2$ during $K[VO(O_2)(heida)]$ synthesis elicits a red

shift in the peroxo vibrations due to the heavier mass of $^{18}O_2$ in the vanadium O-O stretch (932 → 881 cm^{-1}), V-O_2 stretch (575 → 547 cm^{-1}) and its V-O_2 overtone (1150 → 1108 cm^{-1}) indicating that these are peroxo related vibrations. In contrast, the Raman band at 967 cm^{-1} is not perturbed indicating that this band is not peroxo related.

The Raman spectra of K[$V^{16}O(O_2)$(heida)] and K[$V^{18}O(O_2)$(heida)] are shown in Figure 2.6. Incubation with $H_2{}^{18}O$ initiates the selective exchange of the oxygen atom of the oxo V=^{16}O to V=^{18}O. The exchange using $H_2{}^{18}O$, does not perturb the K[$VO(O_2)$(heida)] peroxo bands at 1150, 575 or 932 cm^{-1}, but only leads to a red shift of the 967 cm^{-1} band to 932 cm^{-1}. This indicates that the 967 cm^{-1} band must be associated with the vanadyl V=O oxo stretch. Dissolution of K[$VO(O_2)$(heida)] in deuterated water yielded

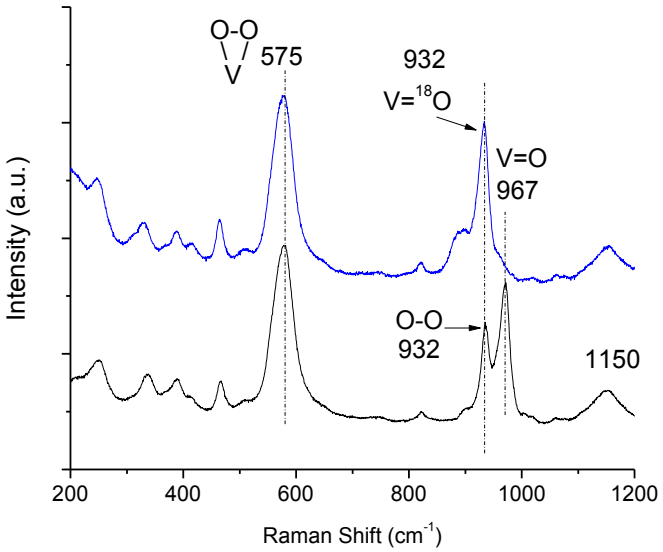

Figure 2.6 Raman Spectrum of K[$VO(O_2)$heida](aq), black line, and isotopic K[$V^{18}O(O_2)$heida], blue line, demonstrating the assignment of the vanadyl V=O oxo band at 967 cm^{-1}.

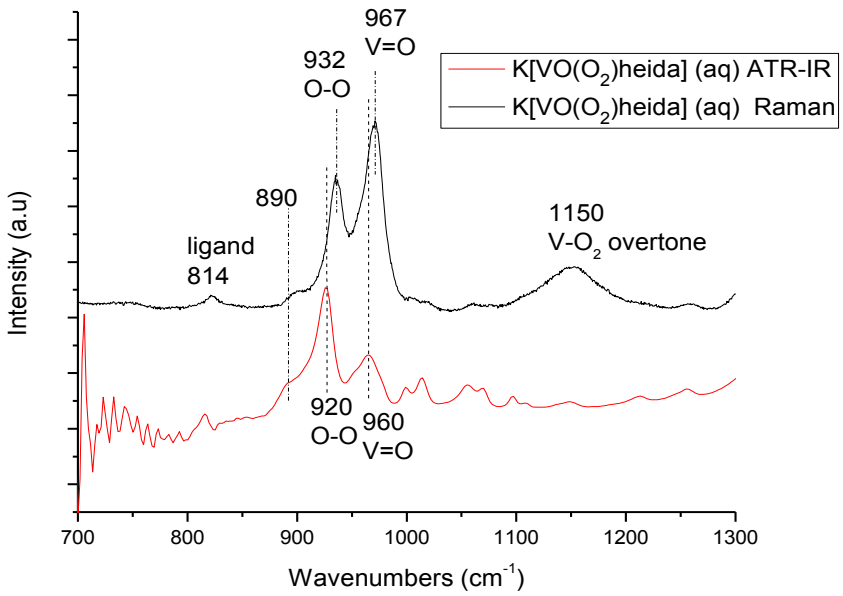

Figure 2.7 Comparison of ATR-IR and Raman spectra of K[VO(O_2)heida] (aq).

no change in the Raman spectra, indicating neither the peroxo nor the oxo groups are affected by solvent hydrogen bonding or protonation in aqueous solution.

The Raman and ATR-IR spectra of K[VO(O_2)(heida)]$_{(aq)}$ are compared in Figure 2.7. The O-O and V=O stretching vibrations observed in the ATR-IR spectrum are consistent with the vibrations observed in Raman indicating that these are symmetric vibrations.[10]

Discussion

We have successfully synthesized characterized K[VO(O_2)(heida)] in aqueous solution. 51V NMR reveals a sharp single band at -593 ppm, which is consistent with literature findings indicating that K[VO(O_2)(heida)] is a peroxo-oxo compound

correctly chelated to the heida ligand with water solvation effects.[1] UV-vis reveals both the vanadium-oxo band at 300 nm, and a vanadium-peroxo ligand-to-metal charger transfer band at 470 nm. Additionally, the K[VO(O_2)(heida)] mimic is very soluble in water, so high molar concentrations of K[VO(O_2)(heida)]$_{(aq)}$ which yield better Raman and ATR-IR spectra, can be achieved, unlike organic solutions like acidified acetonitrile, where K[VO(O_2)(heida)] is only marginally soluble.

The peroxo-oxo active K[VO(O_2)(heida)]$_{(aq)}$ enzyme mimic catalyst contains three distinct oxygen functionalities: a peroxo V-O_2 group, an oxo V=O group, and bridging V-O-C coordinating ligand bonds. The peroxo and oxo groups of K[VO(O_2)(heida)]$_{(aq)}$ are easily observed by Raman and ATR-IR spectroscopy in aqueous solution. This is a significant departure from previous Raman studies in acetonitrile, in which only the V=O and O-O stretching vibrations of K[VO(O_2)(heida)] were able to be resolved, albeit weakly, with interfering bands from the acetonitrile solvent.[8] For the first time, (Figure 2.5) the symmetric "breathing" mode vibration of V-O_2 is sharply resolved by Raman spectroscopy in aqueous solution for K[VO($^{16}O_2$)(heida)]$_{(aq)}$ at 575 cm^{-1}, and for isotopic K[VO($^{18}O_2$)(heida)]$_{(aq)}$ at 547 cm^{-1}. The identification of the symmetric V-O_2 Raman overtone at 1150 cm^{-1} is also important since it is too weak to resolve in the ATR-IR spectrum shown in Figure 2.7. The stronger 575 cm^{-1} band and 1150 cm^{-1} overtone band in the Raman spectrum, and weak, nearly unresolvable nature of any overtone band in the ATR-IR spectrum confirms that the 575 cm^{-1} band and 1150 cm^{-1} overtone are indeed symmetric vibrations, and not asymmetric vibrations as previously assigned.[8] This is because Raman spectroscopy detects symmetric vibrations more strongly than ATR-IR

spectsrocopy, and ATR-IR spectroscopy detects asymmetric vibrations more strongly than Raman spectroscopy.

Raman spectroscopy has precisely identified the V=O oxo stretch for the $K[VO(O_2)(heida)]_{(aq)}$ mimic for the first time (Figure 2.6). The red shift of the 967 cm^{-1} symmetric V=O stretch to 932 cm^{-1} upon isotopic exchange with $V=^{18}O$ clearly confirms this assignment. In addition, these assignments agree with previously reported IR results for $K[VO(O_2)(heida)]$ in both the solid crystalline state and in organic media[8].

Conclusions

The $K[VO(O_2)(heida)]_{(aq)}$ mimic has been fully characterized using Raman and ATR-IR spectroscopy. The signature vanadium peroxo and oxo vibrations have been identified using isotopic oxygen-18 studies. This study demonstrates the powerful capabilities of vibrational spectroscopy. Vanadium peroxo and vanadium oxo bands in aqueous solution are sharp and easy to resolve, indicating that Raman and ATR-IR spectroscopy are ideal tools for future studies of $K[VO(O_2)(heida)]$ and vanadium haloperoxidases.

Section 2: K[VO(O)(heida)] dioxo characterization

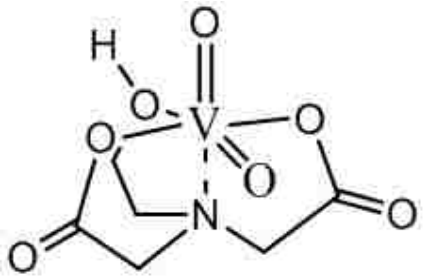

Figure 2.8 Structure of dioxo $K[VO(O)(heida)]_{(aq)}$ compound

The parent compound for the synthesis of $K[VO(O_2)(heida)]_{(aq)}$, before addition of H_2O_2 is presumed to be the dioxo compound, K[VO(O)(heida)], (see Scheme 2.1). The presumed dioxo compound K[VO(O)(heida)] is pictured in Figure 2.8. The true identity of this dioxo compound in aqueous solution, and the precise identification of the Raman bands corresponding to this compound is not trivial, since oxidations involving the peroxo-oxo $K[VO(O_2)(heida)]$ must cycle through the dioxo K[VO(O)(heida)] before being reoxidized by H_2O_2 back to the peroxo-oxo form. This is similar to the way VHPOs, during oxidation reactions, cycle back to the native dioxo form of the vanadium cofactor before being reactivated by H_2O_2 to regenerate the peroxo-oxo active form of the vanadium cofactor.[11, 12] In the next chapter, the mechanism of methanol oxidation by $K[VO(O_2)(heida)]_{(aq)}$ is examined with Raman and ATR-IR spectroscopy, therefore is it is critical to identify the Raman and ATR-IR fingerprint of the parent compound, K[VO(O)(heida)].

A similar dioxo compound, $Na[VO(O)(heida)]_{(s)}$, has been characterized by XRD crystallography, confirming the dioxo nature of this compound in pure crystalline form.[13] However, no aqueous vibrational spectroscopy characterization literature has been found on the $K[VO(O)(heida)]_{(aq)}$ dioxo compound prior to this study. In this

section, the $K[VO(O)(heida)]_{(aq)}$ dioxo compound is fully characterized by Raman and ATR-IR spectroscopy.

Experimental

K[VO(O)(heida)] Dioxo compound Synthesis

Dioxo $K[VO(O)(heida)]_{(aq)}$ was synthesized using a modified version of the method published by Colpas *et al* which was truncated prior to any addition of H_2O_2[1]. 30 mL of deionized water was cooled to approximately 0^oC while stirring, and 5 mmol of KVO_3 (Alfa Aesar, 99.9% pur.) was added and stirred until dissolved. Special care was taken so that there was no excess KVO_3. The solution was filtered and 5 mmol of N-(2-hydroxyethyl)iminodiacetic acid (TCI America, min. 98% pur.) was added and stirred until completely dissolved, forming the dioxo structure as shown in Scheme 2.2.

Aquesous, unchelated KVO_3 and the heida ligand alone were also examined by Raman spectroscopy in order to assist in the assignment of free aqueous vanadate species.

Scheme 2.2 Synthesis of dioxo $K[VO(O)(heida)]_{(aq)}$

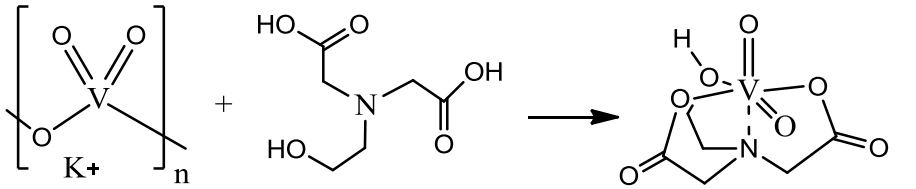

KVO_3 (aq) [heida] (aq) K[VO(O)(heida)] (aq)

Isotopic K[$V^{18}O(^{18}O)$(heida)] Synthesis

The isotopic dioxo K[$V^{18}O(^{18}O)$(heida)] structure was synthesized as described above using $H_2{}^{18}O$ as a solvent (Isotec via Sigma-Aldrich; 95 atom % $H_2{}^{18}O$ isotopic enrichment) and stopping before any addition of H_2O_2. The dioxo $^{16}O=V=^{16}O$ group was found to convert to $^{18}O=V=^{18}O$ almost immediately at room temperature.

Results

The Raman spectrum of the dioxo compound $K[VO(O)(heida)]_{(aq)}$, formed by chelation of KVO_3 to the heida ligand, is shown in Figure 2.9 (black line). The Raman

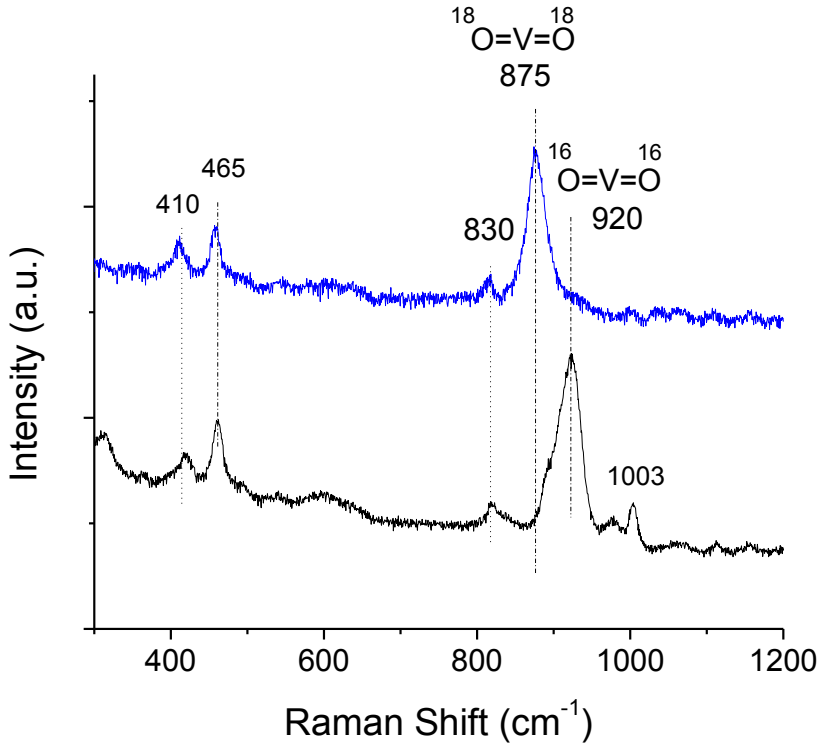

Figure 2.9 Raman spectra of the dioxo $K[V^{16}O(^{16}O)(heida)]_{(aq)}$ enzyme mimic in $H_2{}^{16}O$, black line, and its isotopically labeled $K[V^{18}O(^{18}O)(heida)]_{(aq)}$ enzyme mimic in $H_2{}^{18}O$, blue line, confirming the dioxo $^{16}O=V=^{16}O$ vibrational modes at 920 (ν_s) and ~900 (ν_{as}) cm^{-1}.

spectrum of the dioxo compound does not possess the vanadium peroxo-oxo bands at 575, 932 and 967 cm^{-1}. Instead, a large broad band at approximately 920 cm^{-1} with a weak shoulder at ~895 cm^{-1} is present, plus two smaller bands at 975 and 1003 cm^{-1}. The Raman spectrum of the isotopic dioxo $K[V^{18}O(^{18}O)(heida)]_{(aq)}$ compound is also shown in Figure 2.9 (blue line). The large broad band at 920 cm^{-1} is red shifted approximately 45 cm^{-1} due to the heavier mass of $^{18}O_2$ in the vanadium dioxo ν_s(O=V=O) stretch (920 → 875 cm^{-1}).

A complementary ATR-IR spectrum was also collected to assist in distinguishing between asymmetric and symmetric stretching vibrational assignments for the 895, 920, 975 and 1003 cm^{-1} bands (see Figure 2.10). The 920 cm^{-1} band corresponds to the symmetric dioxo ν_s(O=V=O) stretching mode and is accompanied by the weak dioxo ν_{as}(O=V=O) stretching mode at 895 cm^{-1}.

Since different vanadate species are present at different pH values in aqueous solution, aqueous KVO_3 standards were examined and compared to the spectrum of $K[VO(O)(heida)]_{(aq)}$. Figure 2.11 shows 5mmol KVO_3 in 30 mL of deionized water at a pH value of 7 (black line). Under these conditions, KVO_3 is present as a dioxo polymeric vanadate species[14] which produces a broad symmetric symmetric dioxo ν_s(O=V=O) stretching mode at 948 cm^{-1}. As the pH is dropped using HCl to pH 4 (the working pH during $K[VO(O_2)(heida)]_{(aq)}$ synthesis), the dioxo species is converted to decavandate clusters.[14] The decavanadate clusters at pH 4 (blue line) exhibit decavanadate $[V_{10}O_{28}]^{6-}$ vibrations near 997 and 970 cm^{-1}.

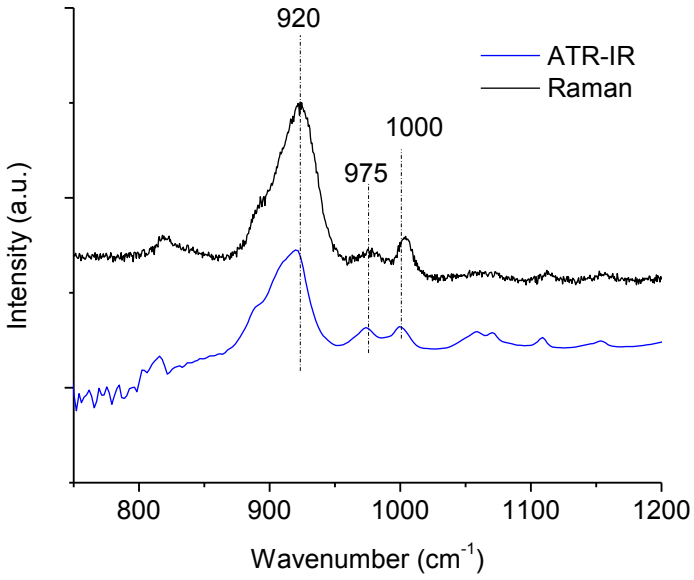

Figure 2.10 Comparison of Raman spectrum (black line) and ATR-IR spectrum (blue line) of K[VO(O)(heida)] (aq) dioxo structure.

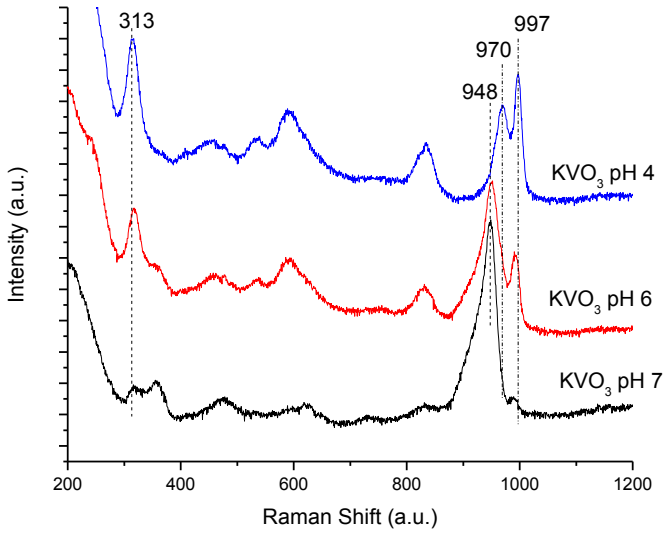

Figure 2.11 Raman spectra of aqueous vanadate species at different pH values.

The effect of chelation of the decavanadate $[V_{10}O_{28}]^{6-}$ solution by the heida ligand is shown in Figure 2.12. A highly concentrated spectrum of the heida ligand alone is also included (red line) for comparison. When 5 mmol of heida is added to the decavanadate solution (blue line), some of the vanadate is chelated to form $K[VO(O)(heida)]_{(aq)}$ and some remain as decavanadates. This solution containing both $K[VO(O)(heida)]_{(aq)}$ and decavanadates can be seen in Figure 2.12 (green line).

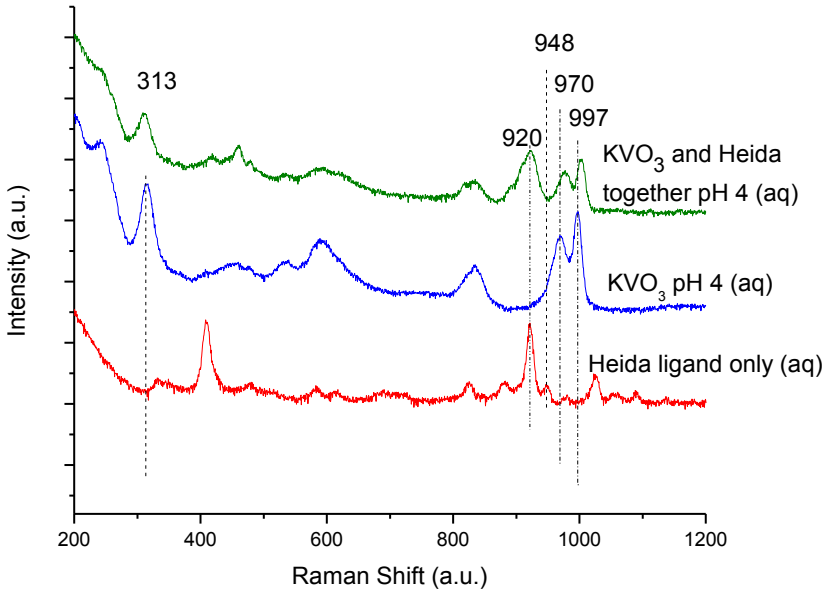

Figure 2.12 Raman spectra showing chelation of decavanadate KVO3 solution at pH 4 with the heida ligand. A highly concentrated heida solution is shown in red for comparison. No strong heida bands are observed in the chelated spectrum.

The presence of the $K[VO(O)(heida)]_{(aq)}$ compound causes the broad band at 920 cm^{-1} to form which is the symmetric dioxo $\nu_s(O=V=O)$ stretching mode.

An additional batch of the dioxo $K[VO(O)(heida)]_{(aq)}$ was synthesized in D_2O in order to determine the effect of hydrogen bonding, and to eliminate the possibility of

the 920 cm^{-1} band actually being a V-OH vibration. The Raman spectra of K[VO(O)(heida)] in both water and D_2O solution are shown in Figure 2.13. Unlike the peroxo-oxo $K[VO(O_2)(heida)]_{(aq)}$ compound, the dioxo K[VO(O)(heida)](aq) is affected by hydrogen bonding. The tall 920 cm^{-1} symmetric vanadium dioxo ν_s(O=V=O) stretching mode is slightly perturbed by the presence of deuterated water. The small bands at 975 and 1003 cm^{-1} are also slightly red shifted in the presence of D_2O.

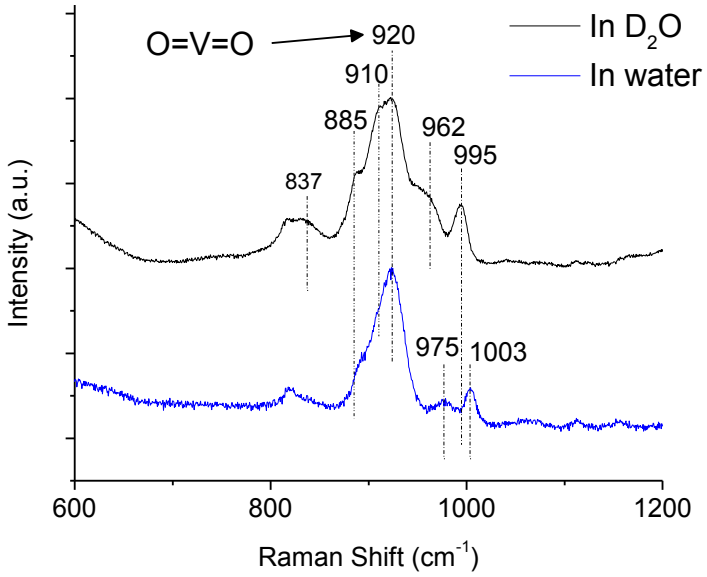

Figure 2.13 K[VO(O)(heida)] (aq) dioxo structure in water (blue line) and deuterated water (black line).

Discussion

The crystal structure of a similar vanadium dioxo compound, $Na[VO(O)(heida)]_{(s)}$, features the two V=O dioxo bond lengths of 1.663 Å and 1.624 Å.[13] The correlation of V=O bond length to the Raman band position reported by

Hardcastle *et al*. indicates that the dioxo 895 and 920 cm^{-1} Raman bands are located in the range consistent with the reported V=O bond lengths.[15] Furthermore, dioxo $F_2V(=O)_2^-$ (970/962 cm^{-1}) vibrates much lower than mono-oxo $F_3V=O$ (1058 cm^{-1}) and reflects the significant vibrational difference between dioxo and mono-oxo vanadyl structures.[10] The V=O and O=V=O vibrations of the aqueous peroxo-oxo $K[VO(O_2)(heida)]_{(aq)}$ (967 cm^{-1}) and dioxo $K[VO(O)(heida)]_{(aq)}$ (920/895 cm^{-1}) enzyme mimics, respectively, occur at lower wavenumbers than the corresponding gas phase complexes because hydrogen bonding by H_2O elongates their V-O bonds.

The 975 and 1003 cm^{-1} bands also present in the Raman spectrum of the dioxo $K[VO(O)(heida)]_{(aq)}$ correspond to decavanadate $[V_{10}O_{28}]^{6-}$ vibrations resulting from dissociation of dioxo-vanadate from the heida ligand and conversion to decavanadates in the acidic pH. The weak Raman bands at ~410 and 830 cm^{-1} correspond to heida ligand vibrations that are present in the Raman spectra of both the peroxo-oxo $K[VO(O_2)(heida)]_{(aq)}$ and dioxo $K[VO(O)(heida)]_{(aq)}$ compounds. Therefore, the $K[VO(O)(heida)]_{(aq)}$ dioxo compound also appears to be in equilibrium with dissociated heida ligand and decavanadates $[V_{10}O_{28}]^{6-}$ as shown in Scheme 2.3. This equilibrium is also in agreement with what is found for solid supported vanadium oxide catalysts on acidic metal oxide supports such as Al_2O_3. At low coverage, solid V_2O_5 supported on Al_2O_3 is present as a dioxo structure, as observed by Raman spectroscopy. However, at high coverage, solid V_2O_5 supported on Al_2O_3 converts to decavanadate clusters.[16]

Scheme 2.2 Equilibrium solution of $K[VO(O)(heida)]_{(aq)}$ dioxo compound and decavanadates $[V_{10}O_{28}]^{6-}$ plus dissociated heida ligand

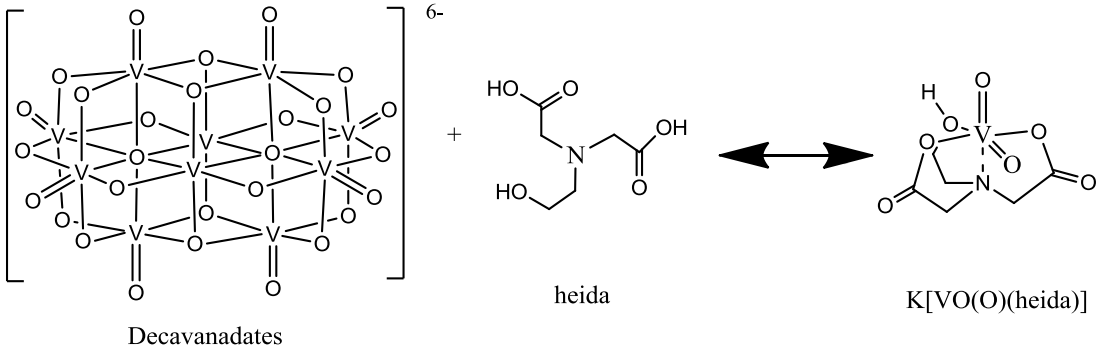

Conclusions

$K[VO(O)(heida)]_{(aq)}$ has been fully characterized using Raman and ATR-IR spectroscopy for the first time. The vanadium dioxo vibrations have been identified using isotopic oxygen studies. Raman spectroscopy on $K[VO(O)(heida)]_{(aq)}$ dissolved in deuterated water has revealed that $K[VO(O)(heida)]_{(aq)}$ is affected by hydrogen bonding, but there are no V-OH groups present for $K[VO(O)(heida)]_{(aq)}$. Additionally, and equilibrium exists between the dioxo compound and decavanadate clusters $[V_{10}O_{28}]^{6-}$ along with the dissociated heida ligand. These dioxo characterization studies will prove invaluable to methanol oxidation studies, as described in the next chapter, since oxidation by $K[VO(O_2)(heida)]_{(aq)}$ cycles through the $K[VO(O)(heida)]_{(aq)}$ dioxo compound before it is reactivated by H_2O_2.

Section 3: Structural Comparison to Supported Vanadium Oxide Catalysts

A vanadium peroxo-oxo structure has recently been proposed to be present on dehydrated supported vanadia catalysts, such as V_2O_5/SiO_2 (see Figure 2.15 c), where it has been dubbed the vanadium oxide "umbrella" structure. The umbrella structure proposal was based on a comparison between Density Functional Theory (DFT) results and a previously un-assigned Raman band at ~920 cm^{-1} present for supported vanadium oxide catalysts[17]. The proposed vanadium peroxo-oxo umbrella structure happens to be nearly identical to the active site structure present for $K[VO(O_2)(heida)]$ shown in Figure 2.14 a. There is no experimental evidence, however, for the existence of a stable, dehydrated surface vanadium oxide umbrella structure on an oxide support like silica. Multiple spectroscopic characterization studies have demonstrated that, at low coverage, the molecular structure of the dehydrated surface vanadium oxide species on oxide supports exists in its fully oxidized state as the VO_4 trigonal pyramidal structure with an apical V=O oxo and three bridging V-O-Support bonds shown in Figure 2.14 b. [18-25]

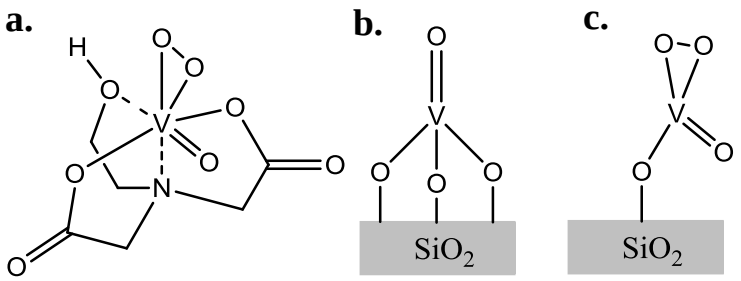

Figure 2.14 **a.** Structure of $K[VO(O_2)(heida)]$ mimic of VHPO showing peroxo and oxo groups **b.** Structure of dehydrated supported vanadia species on silica possessing the trigonal pyramid structure, and **c.** Proposed vanadium oxide "umbrella" structure supported on silica showing the proposed peroxo-oxo groups

Although the vanadium peroxo-oxo umbrella structure under dehydrated conditions has subsequently been revoked, it has been suggested that a hydrated version

of the umbrella structure is still possible where the peroxo O-O moiety would instead be present as two –OH groups.[26, 27] Furthermore, there are still research groups who continue to look for evidence of the dehydrated surface vanadium peroxo-oxo umbrella structure on oxide supports and seek to assign vibrational modes to the umbrella structure.[28] Recent published DFT results concluded that the full catalytic cycle for methanol oxidation over silica passes through a dehydrated vanadium peroxo-oxo umbrella structure upon reoxidation of the catalyst.[28]

The true surface structure of solid supported vanadium oxide catalysts like V_2O_5/SiO_2 is not trivial, since an important step of bridging the gap between heterogeneous catalysis and enzyme catalysis in this study, is comparing the structure and function of V_2O_5/SiO_2 to $K[VO(O_2)(heida)]_{(aq)}$. The mechanism and reactivity of these two systems will be examined thoroughly later in this dissertation to establish a solid basis for this comparison. Therefore, it is paramount to fully characterize and understand the structure of each system. This portion of the study determines whether or not the surface vanadium peroxo-oxo structure is truly present on oxide supports by comparing the vibrational spectrum of the true peroxo-oxo umbrella structure present in $K[VO(O_2)(heida)]$ to the vibrational spectrum of supported vanadium oxide species on a silica support.[18]

Experimental

Supported Catalyst Synthesis

The supported catalysts were synthesized according to the method published by Tian *et al*[25]. Supported V_2O_5/SiO_2 was prepared by incipient wetness impregnation under continuously flowing N_2 atmosphere in a glove box using 2-propanol solutions of vanadium isoproproxide and dried overnight under N_2. The supported V_2O_5/SiO_2 catalyst was then dried under flowing air (100 cc/min) at 120^oC for 1 hour, 300^oC for another hour, and calcined at 450^oC for 2 hours. The supported $K[VO(O_2)(heida)]/SiO_2$ was prepared by incipient wetness impregnation under ambient conditions using an aqueous solution of $K[VO(O_2)(heida)]$, since $K[VO(O_2)(heida)]$ is not sensitive to air. The supported $K[VO(O_2)(heida)]/SiO_2$ was then dried in ambient air for approximately 8 hours, and then dried at 100^oC in flowing air (100 cc/min) for 1 hour to avoid any thermal decomposition.

Raman Spectroscopy

Raman spectra of $K[VO(O_2)(heida)]$ and V_2O_5/SiO_2 were collected with a Horiba-Jobin Yvon LabRam-HR spectrometer as described in the previous section. For the collection of ambient solid spectra, solid samples were spread evenly onto a glass slide. Dehydrated spectra were taken using an environmental cell (Linkam T-1500) maintained below the confocal microscope and treating the samples at different temperatures representing typical reaction temperatures for each catalyst under flowing 10% O_2/ balance He.

Results

The Raman spectrum of aqueous $K[VO(O_2)(heida)]_{(aq)}$ exhibits four major bands at 575, 932, and 967 with an overtone of the 575 cm^{-1} band at 1150 cm^{-1}. These key bands are also present for $K[VO(O_2)(heida)]$ impregnated onto SiO_2 as seen in Figure 2.15. Silica-supported $K[VO(O_2)(heida)]$, however, was found decompose after approximately 24 hours, which reflects its poor stability on oxide supports. Additionally, silica-supported $K[VO(O_2)(heida)]$ was unable to tolerate dehydration temperatures of greater than 125°C, which further reflects the poor stability of a peroxo-oxo structure on oxide supports. The fully hydrated supported V_2O_5/SiO_2 catalysts exhibit broad Raman bands (not shown) at ~1020, ~704, ~652, 506−523,

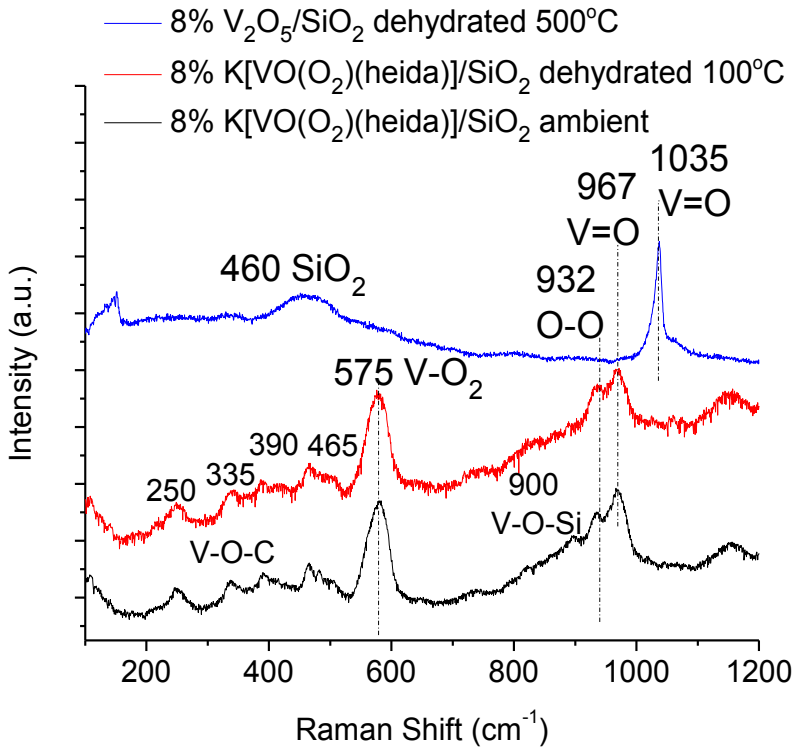

Figure 2.15 Raman spectra of supported $K[VO(O_2)heida]/SiO_2$ under ambient and dehydrated conditions and supported V_2O_5/SiO_2 under dehydrated conditions. The peroxo breathing mode at 575 cm^{-1} and O-O stretching at 932 cm^{-1} are observed for supported $K[VO(O_2)heida]/SiO_2$ but not for dehydrated supported V_2O_5/SiO_2.

264−274, and 155−164 cm^{-1} that do not match those of the silica supported K[VO(O_2)(heida)] complex[30]. The observed Raman bands for the dehydrated supported K[VO(O_2)(heida)]/SiO_2 are also quite different from those of dehydrated supported VO_4/SiO_2 (Figure 2.15) with the V=O vibration at 1035 cm^{-1}. The dehydrated supported VO_4/SiO_2 catalyst contains neither the O-O stretch at ~930 cm^{-1}, the V-O_2 stretch at ~575 cm^{-1} nor the UV-vis O-O transition at ~470 nm.

Discussion

Retention of the key bands of K[VO(O_2)(heida)] after impregnation onto SiO_2 as seen in Figure 2.15, clearly indicates that the peroxo-oxo molecular structure of K[VO(O_2)(heida)] is conserved when it is impregnated onto a silica support. However the peroxo-oxo structure of K[VO(O_2)(heida)]/SiO_2 begins decomposing after approximately 24 hours at room temperature, or almost immediately at temperatures of 125^oC. Therefore, it is extremely unlikely that a peroxo-oxo structure umbrella structure for V_2O_5/SiO_2 is stable at room temperature, let alone at typical reaction conditions of up to 500^oC.

The observed Raman bands for the both hydrated and dehydrated supported K[VO(O_2)(heida)]/SiO_2 are vastly different than those for hydrated (not shown) and dehydrated supported VO_4/SiO_2 in Figure 2.15. If the dehydrated surface umbrella structure on SiO_2 did indeed exist, then the V-O_2 stretch at ~575 cm^{-1}, overtone at 1150 cm^{-1}, the V-peroxo O-O stretch at ~930 cm^{-1} and the 470 nm transition would be easily detected with Raman and UV-vis spectroscopy, respectively.

Conclusions

It is, therefore, concluded that an umbrella-type vanadium peroxo-oxo structure does not exist for hydrated or dehydrated supported V_2O_5/SiO_2 catalysts. Examination of the Raman spectra for other supported vanadium oxide catalyst systems also reveals that the umbrella vanadium peroxo-oxo structures are not present. The umbrella-type vanadium peroxo-oxo structure, however, is a valid model in vanadium oxide biocatalyst systems including VHPOs and mimic compounds such as K[VO(O_2)(heida)]. Thus, although a protein or organic support stabilizes vanadium peroxo-oxo structures, oxide supports do not seem to stabilize the vanadium peroxo-oxo structures that have been suggested for supported vanadium oxide catalysts. Hence, comparisons between K[VO(O_2)(heida)] and $V2O_5/SiO_2$ should be made using, respectively, the peroxo-oxo and mono-oxo trigonal pyramid structures shown in Figure 2.15 a and Figure 2.15 b.

References

(1) Colpas, G. J.; Hamstra, B. J.; Kampf, J. W.; Pecoraro, V. L. *J. Am. Chem. Soc.* **1996**, *118*, 3469-3478.

(2) de la Rosa, Roger I.; Clague, M. J.; Butler, A. *J. Am. Chem. Soc.* **1992**, *114*, 760.

(3) Butler, A.; Baldwin, A. H. In *Vanadium bromoperoxidase and functional mimics;* Hill, H., Sadler, P. and Thomson, A., Eds.; Metal Sites in Proteins and Models; Springer Berlin: Heidelberg, 1997; Vol. 89, pp 109-132.

(4) Conte, V.; Floris, B. *Inorg. Chim. Acta* **2010**, *363*, 1935-1946.

(5) Butler, A.; Clague, M. J.; Meister, G. E. *Chem. Rev.* **1994**, *94*, 625-638.

(6) Wever, R.; Hemrika, W. In *Vanadium Haloperoxidases;* Messerschmidt, A., Huber, R., Poulos, T. and Wieghardt, K., Eds.; Handbook of Metalloproteins; Wiley: Chichester, 2001; pp 1417-1428.

(7) Butler, A. *Curr. Opin. Chem. Biol.* **1998**, *2*, 279-285.

(8) Schneider, C. J. Development of Asymmetric Sulfoxidation Catalysts Based on Functional Models for Vanadium-Dependent Haloperoxidases, University of Michigan, 2009.

(9) Kubelka, P.; Munk, R. *Z. Tech. Phys.* **1931**, *12*.

(10) Nakamoto, K. In *Infrared and Raman Spectra of Inorganic and Coordination Compounds;* Handbook of Vibrational Spectroscopy; John Wiley & Sons, Ltd: New York, 1986; pp 140-149 and references therein.

(11) Pooransingh-Margolis, N.; Renirie, R.; Hasan, Z.; Wever, R.; Vega, A. J.; Polenova, T. *J. Am. Chem. Soc.* **2006**, *128*, 5190-5208.

(12) Hemrika, W.; Renirie, R.; Macedo-Ribeiro, S.; Messerschmidt, A.; Wever, R. *J. Biol. Chem.* **1999**, *274*, 23820-23827.

(13) Mahroof-Tahir, M.; Keramidas, A. D.; Goldfarb, R. B.; Anderson, O. P.; Miller, M. M.; Crans, D. C. *Inorg. Chem.* **1997**, *36*, 1657-1668.

(14) Baes, C. F.; Mesmer, R. E. In *The hydrolysis of cations;* Wiley New York: 1976; Vol. 489.

(15) Hardcastle, F. D.; Wachs, I. E. *J. Phys. Chem.* **1991**, *95*, 5031-5041.

(16) Deo, G.; Wachs, I. E. *J. Phys. Chem.* **1991**, *95*, 5889-5895.

(17) Gijzeman, O. L. J.; van Lingen, J. N. J.; van Lenthe, J. H.; Tinnemans, S. J.; Keller, D. E.; Weckhuysen, B. M. *Chemical Physics Letters* **2004**, *397*, 277-281.

(18) Burcham, L. J.; Deo, G.; Gao, X.; Wachs, I. E. *Top. Catal.* **2000**, *11/12*, 85.

(19) Cristiani, C.; Forzatti, P.; Busca, G. *J. Catal.* **1989**, *116*, 586-589.

(20) Deo, G.; Eckert, H.; Wachs, I. E. In *In Molecular structure-reactivity relationships of supported vanadium oxide catalysts;* Symposium on Structure-Activity Relationships in Heterogeneous Catalysis - Presented before the Division of Petroleum Chemistry, ACS, Boston Meeting; Publ by ACS, Washington, DC, USA: Boston, MA, USA, 1990; Vol. 35, pp 16-21.

(21) Eckert, H.; Wachs, I. E. *J. Phys. Chem.* **1989**, *93*, 6796-6805.

(22) Gao, X.; Wachs, I. E. *J. Phys. Chem. B* **2000**, *104*, 1261-1268.

(23) Gao, X.; Bare, S. R.; Weckhuysen, B. M.; Wachs, I. E. *The Journal of Physical Chemistry B* **1998**, *102*, 10842-10852.

(24) Tanaka, T.; Yamashita, H.; Tsuchitani, R.; Funabiki, T.; Yoshida, S. *J. Chem. Soc. , Faraday trans.* **1988**, *84*, 2987-2999.

(25) Tian, H.; Ross, E. I.; Wachs, I. E. *J. Phys. Chem. B* **2006**, *110*, 9593-9600.

(26) van Lingen, J. N. J.; Gijzeman, O. L. J.; Weckhuysen, B. M.; van Lenthe, J. H. *Journal of Catalysis* **2006**, *239*, 34-41.

(27) Keller, D. E.; Visser, T.; Soulimani, F.; Koningsberger, D. C.; Weckhuysen, B. M. *Vibrational Spectroscopy* **2007**, *43*, 140-151.

(28) Ding, X.; Xue, W.; Ma, Y.; Zhao, Y.; Wu, X.; He, S. *The Journal of Physical Chemistry C* **2010**, *114*, 3161-3169.

Chapter 3: Oxidation Mechanism by $K[VO(O_2)(heida)]_{(aq)}$ and Comparison to Oxidation Mechanism by Supported Vanadium Oxide Catalysts

Despite the significant difference in the molecular surface structures between the $K[VO(O_2)(heida)]$ enzyme mimic and the supported VO_4/SiO_2 catalyst (see Chapter 2, Section 3), both are capable of oxidizing methanol to formaldehyde even under vastly different reaction conditions: $K[VO(O_2)(heida)]$ under aqueous conditions at mild temperatures, and VO_4/SiO_2 at the gas/solid interface at high temperatures. The $K[VO(O_2)(heida)]_{(aq)}$ enzyme mimic, contains a vanadium peroxo-oxo structure, $O=VO_2$, that is not present for supported vanadia catalysts on inorganic oxides such as silica. The dispersed vanadia on silica is present as a trigonal pyramidal surface VO_4 species possessing one terminal V=O bond and three bridging V-O-Si bonds under dehydrated conditions. However, given the different molecular structures of the catalytic active site in the enzyme mimic and supported catalyst, can we expect the methanol adsorption site, reaction intermediates, and mechanism for both catalysts to be the same? This chapter examines the similarities and differences between the $K[VO(O_2)(heida)]_{(aq)}$ enzyme mimic and the supported VO_4/SiO_2 catalyst for methanol oxidation to formaldehyde.

Section 1: Catalytic Active Sites, Reaction Intermediates, Reaction Mechanism and Kinetics of Aqueous Methanol Oxidation by $K[VO(O_2)(heida)]_{(aq)}$ *versus* Gas Phase Methanol Oxidation by Supported V_2O_5/SiO_2

The reactivity studies of the $K[VO(O_2)(heida)]$ enzyme mimic have mostly focused on bromide oxidation in acidified organic media.[1] Several studies have appeared on sulfoxidation reactions[2-4], and a few have touched on propanol and ethanol oxidation by similar vanadium peroxo-oxo compounds[5, 6] One very interesting recent study by Conte et al., has investigated the reactivity of vanadium mono oxo and vanadium peroxo-oxo compounds for bromide oxidation, sulfoxidation, epoxidation, and hydroxylations in two phase and ionic liquid systems[7]. No studies, however, have been reported for characterization of vanadium peroxo-oxo enzyme mimics during oxidation reactions that would allow for direct observation and molecular insights about the catalytic active sites, reaction intermediates and reaction mechanism.

The objective of this study is to compare the aqueous methanol oxidation reaction mechanism of $K[VO(O_2)(heida)]_{(aq)}$ with that of the well-established vapor-solid methanol oxidation by the supported VO_4/SiO_2 catalyst system. In this chapter, the $K[VO(O_2)(heida)]_{(aq)}$ enzyme mimic is monitored during methanol oxidation with cutting edge *in situ* Raman and ATR-IR spectroscopy. These *in situ* vibrational techniques, which are traditionally applied for the study of heterogeneous catalysts like VO_4/SiO_2 for vapor-solid catalysis, are also shown in the current investigation to be highly effective and informative in the study of homogenous reactions of aqueous enzyme mimics. The *in situ* vibrational spectroscopic measurements were able to identify the catalytic active site, reaction intermediate and reaction mechanism during methanol oxidation in aqueous media by the $K[VO(O_2)(heida)]_{(aq)}$ enzyme mimic.

Raman and IR spectroscopy revealed that CH_3OH chemisorbs at the bridging V-O-carbon bond forming the V-OCH_3 reaction intermediate that transfers its methyl hydrogen to the VO_2 peroxo functionality. Although the chemisorption sites are identical for the enzyme mimic and the supported vanadium systems, the methoxy methyl hydrogen rate-determining-step occurs at the terminal V=O bond for the supported vanadia catalyst while the methoxy methyl hydrogen is transferred to the peroxo functionality in the enzyme mimic. Thus, methanol oxidation follows different rate-determining-steps for enzyme mimics and vapor-solid catalysts due to the presence of different vanadium functionalities.

Experimental

Raman Spectroscopy

The Raman spectrum of $K[VO(O_2)(heida)]_{(aq)}$ was collected with a Horiba-Jobin Yvon LabRam-HR spectrometer as described in the previous chapter. For the collection of aqueous *in situ* Raman spectra, six stoichiometric molar equivalents of methanol and hydrogen peroxide were added to a vial of K[$VO(O_2)$(heida)] (aq) (0.2M), and the vial was placed in a water bath maintained at 50^{o}C. Negative controls using $K[VO(O_2)(heida)]_{(aq)}$ only and methanol and hydrogen peroxide only at 50^{o}C were run in parallel. The Raman spectra of aqueous formaldehyde, methanol, hydrogen peroxide, dimethyl ether, dimethoxy methane, and formic acid standards were used for comparison. Raman spectra were collected at 20-25 minute intervals. For the monitoring of the peroxo band using Raman spectroscopy, six stoichiometric equivalents of methanol only, but no H_2O_2, were added to a vial of

$K[VO(O_2)(heida)]_{(aq)}$, and the vial was placed in a water bath maintained at 50°C. Raman spectra were collected every 3-5 minutes once the rapid loss of the V-O_2 group was observed.

ATR-IR Spectroscopy

The $K[VO(O_2)(heida)]$ dissolved in deionized water was examined using a Thermo Nicolet 8700 IR spectrometer equipped with a DTGS detector cooled with liquid N_2 and Harrick Horizon ATR attachment on a zinc selenide crystal. The spectrum was collected in the 400-4000 cm^{-1} range with 72 scans and deionized water was background subtracted. For the collection of aqueous *in situ* ATR-IR spectra, six stoichiometric equivalents of methanol and hydrogen peroxide were added to a vial of 1M $K[VO(O_2)(heida)]_{(aq)}$, and the vial was placed in a water bath maintained at 50°C. $K[VO(O_2)(heida)]_{(aq)}$ was used at a higher concentration for the ATR-IR experiments in order to yield a better signal to noise ratio at the higher concentration. Negative controls at 50°C using $K[VO(O_2)(heida)]_{(aq)}$ only and methanol and hydrogen peroxide only were run in parallel. The ATR-IR spectra were collected at 20-25 minute intervals, and the $K[VO(O_2)(heida)]_{(aq)}$ negative control was background subtracted for better observation of reaction intermediate species. The ATR-IR spectra contained both information about the aqueous $K[VO(O_2)(heida)]$ structure, reaction intermediates (methoxy), and the dissolved oxygenated components (methanol and reaction products).

Rate Determining Step

The rate determining step for methanol oxidation with H_2O_2 by $K[VO(O_2)(heida)]_{(aq)}$ was investigated by performing an experiment using using CH_3OH and CD_3OH. Three identical vials were prepared containing 0.2 grams $K[VO(O_2)(heida)]$ in 20 mL deionized water. One vial was designated as the negative control, the others were designated as the positive sample reaction vials and labeled with either CH_3OH or CD_3OH. Each vial was placed into a 70^oC hot water bath for approximately 30 minutes before the reagents were added. 200 μL of CH_3OH or CD_3OH was added to the reaction vial, and 200 μL of deionized water was added to the negative control vial. Each vial was sampled every 20 minutes by removing 200 μL from the vial and assayed by the Purpald® method described in Chapter 4.

Results

Methanol Oxidation by $K[VO(O_2)(heida)]_{(aq)}$ Enzyme Mimic in the Absence of H_2O_2

Liquid phase oxidation of methanol at 50^oC by the $K[VO(O_2)(heida)]_{(aq)}$ enzyme mimic in the absence of H_2O_2 was monitored with time-resolved *in situ* Raman spectroscopy and the findings are presented in Figure 3.1 for the 200-1200 cm^{-1} spectral region. The time-resolved *in situ* Raman spectra during aqueous methanol oxidation by $K[VO(O_2)(heida)]_{(aq)}$ illustrate the consumption of the V-O_2 peroxo bands at 575, 932 and 1150 cm^{-1}. In the absence of the H_2O_2 oxidant, $K[VO(O_2)(heida)]_{(aq)}$ is transformed to dioxo $K[VO(O)(heida)]_{(aq)}$ (see Chapter 2, Section 2 for dioxo characterization)

because it is unable to regenerate the vanadium peroxo functionality via reoxidation and repeat the catalytic cycle. Consequently, the 575 cm^{-1} vanadium peroxo Raman band and its overtone at 1150 cm^{-1} progressively decrease as the reaction proceeds.

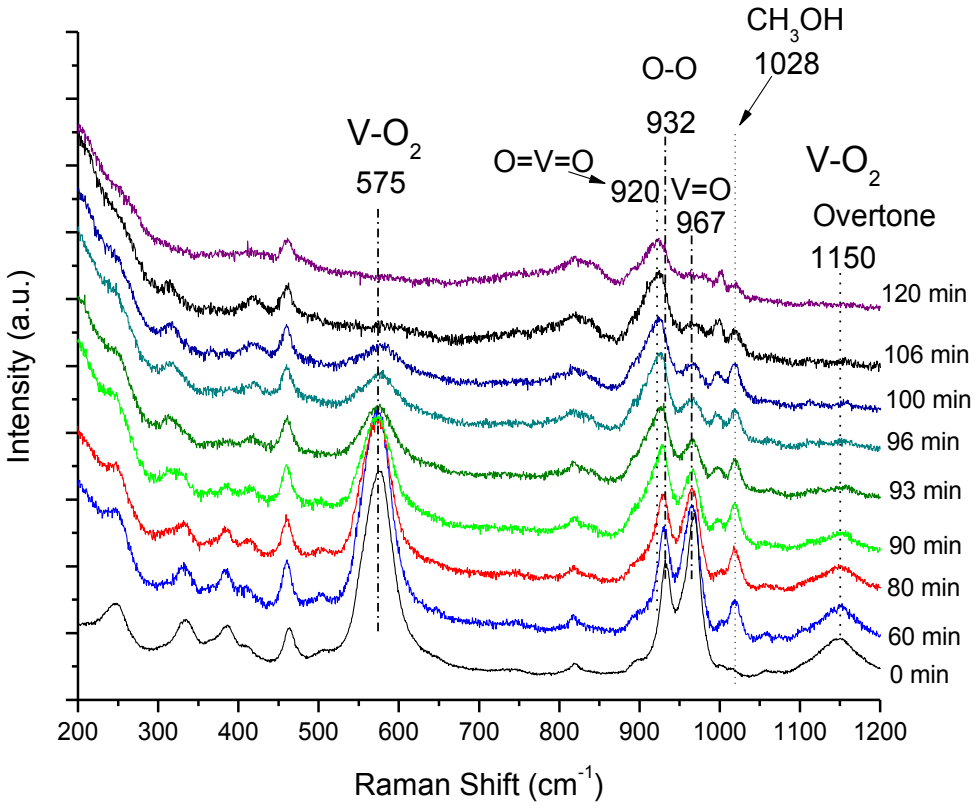

Figure 3.1 Time-resolved *in situ* Raman spectra of the 0.2M $K[VO(O_2)(heida)]_{(aq)}$ enzyme mimic in the presence of methanol and without H_2O_2 in the 200–1200 cm^{-1} spectral region. The Raman spectrum at the end of the reaction at the top of the figure matches the Raman spectrum for the dioxo $K[VO(O)(heida)]_{(aq)}$ enzyme mimic. (See Figure Chapter 2, Section 2 for the dioxo $K[VO(O)(heida)]_{(aq)}$ characterization).

Simultaneously, the vanadium peroxo ν_s(O-O) stretching vibration at 932 cm^{-1} becomes eclipsed by the broad ν_s(O=V=O) stretch at 920 cm^{-1} and the ν_{as}(O=V=O) stretch of the 895 cm^{-1} shoulder that are characteristic of the dioxo $K[VO(O)(heida)]_{(aq)}$ (which was characterized in Chapter 2) during the course of the methanol oxidation reaction. Note

that the vanadyl shift from 967 to 920 cm^{-1} is not related to the reduction in the oxidation state of the vanadium, since both the dioxo and oxo-peroxo are both V(V) compounds, and the vibrational shift is simply from the conversion of the mono-oxo V=O functionality into the dioxo O=V=O functionality. The small band which emerges at ~1003 cm^{-1} is due to the presence of decavanadates. The presence of decavanadates in equilibrium with the dioxo K[VO(O)(heida)] compound are described in Chapter 2, Section 2.

Methanol Oxidation by $K[VO(O_2)(heida)]_{(aq)}$ Enzyme Mimic in the Presence of H_2O_2

Liquid phase oxidation of methanol at 50°C by the $K[VO(O_2)(heida)]_{(aq)}$ enzyme mimic in the presence of H_2O_2 also was monitored with time-resolved *in situ* Raman spectroscopy and the findings are presented in Figure 3.2 for the 200-1200 cm^{-1} spectral region. The black curve is the Raman spectrum of 0.2 M $K[VO(O_2)(heida)]_{(aq)}$ prior to the addition of six molar equivalents of methanol and hydrogen peroxide. The blue curve is the spectrum taken immediately after the addition of six molar equivalents of methanol and hydrogen peroxide. The subsequent ascending spectra in Figure 3.2 were collected at 20–25 minute intervals as the reaction proceeded. Aqueous H_2O_2 gives rise to the strong 878 cm^{-1} band corresponding to the O-O stretch of H_2O_2 and $CH_3OH_{(aq)}$ gives rise to the strong 1028 cm^{-1} band related to the C-O stretch of CH_3OH.[8] Both bands decrease as these reactants are consumed during the course of the methanol oxidation reaction, and the new shoulder band at ~895 cm^{-1} from the dioxo ν_{as}(O=V=O) stretch of $K[VO(O)(heida)]_{(aq)}$ simultaneously increases in intensity with extent of

reaction, but the spectrum for aqueous free formaldehyde also has a strong band present at approximately 900 cm^{-1}, so band overlap may be a possibility.[9] Upon addition of CH_3OH and H_2O_2, the weak Raman bands in the 331-465 cm^{-1} region, corresponding to

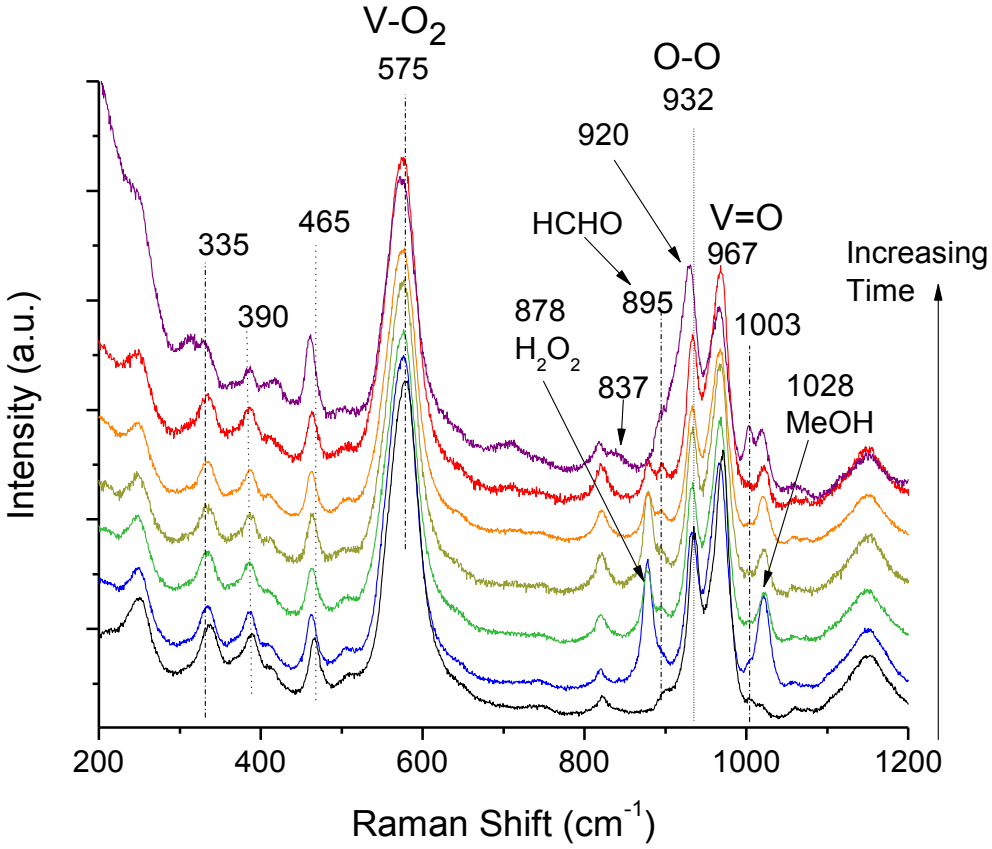

Figure 3.2 Time-resolved *in situ* Raman spectra during methanol oxidation with H_2O_2 at 50°C by the 0.2M $K[VO(O_2)(heida)]_{(aq)}$ enzyme mimic in the 200–1200 cm^{-1} spectral region. The black curve is the initial Raman spectrum for the $K[VO(O_2)(heida)]_{(aq)}$ enzyme mimic prior to addition of CH_3OH and H_2O_2. The subsequent Raman spectra are taken at 20–25 minute intervals following the addition of six molar equivalents of CH_3OH and H_2O_2.

V-O-C bending and V-N stretching vibrations,slightly downshift indicating a slight lengthening of these bonds from coordination of methanol to the vanadium oxide active site. Note that the peroxo V-O_2 vibrations at (932, 575 and 1150 cm^{-1}) and the V=O oxo vibration at (967 cm^{-1}) of the $K[VO(O_2)(heida)]_{(aq)}$ compound are unperturbed

during the course of the reaction while H_2O_2 is still present. This indicates that neither the peroxo nor the oxo groups function as the methanol adsorption site and suggests that the methanol adsorption site is the bridging V-O-C ligand bond.

Once H_2O_2 has been completely consumed, as indicated by the disappearance of the 878 cm^{-1} band, the $K[VO(O_2)(heida)]_{(aq)}$ peroxo Raman bands at 575 cm^{-1} and 1150 cm^{-1} begin to decrease in intensity. The intensity of the 932 cm^{-1} peroxo Raman band also decreases and becomes eclipsed by a larger broad band at ~920 cm^{-1}, which corresponds to the dioxo ν_s(O=V=O) stretch of $K[VO(O)(heida)]_{(aq)}$. The latter band overlaps the 932 cm^{-1} V-O_2 peroxo functionality of $K[VO(O_2)(heida)]_{(aq)}$ (see Figure 3.2). After complete consumption of H_2O_2, new Raman bands begin to appear at 1003 and 976 cm^{-1} that is associated with the ν_s(V=O) and ν_{as}(V=O) stretching modes, respectively, of decavanadate $[V_{10}O_{28}]_{(aq)}^{6-}$ clusters resulting from dissociation of the dioxo K[VO(O)(heida)] compound in the acid pH solution (see Chapter 2, section 2).

The corresponding time-resolved *in situ* Raman spectra during aqueous methanol oxidation by $K[VO(O_2)(heida)]_{(aq)}$ and H_2O_2 in the 1000-2000 cm^{-1} spectral region associated with the reactant and product oxygenates are presented in Figure 3.3. The black curve is the Raman spectrum of the $K[VO(O_2)(heida)]_{(aq)}$ enzyme mimic prior to the addition of methanol and hydrogen peroxide, and the blue curve is the spectrum taken immediately after addition of methanol and hydrogen peroxide. The subsequent ascending spectra were taken at 20–25 minute intervals. It is important to note that in low concentration aqueous solutions of formaldehyde, formaldehyde (HCHO) and formaldehyde monohydrate ($HOCH_2OH$) are in equilibrium, with the

monohydrate species predominating at concentrations up to 5 mol%.[9] Approximately 20-25 minutes into the reaction, a broad band appears at 1715 cm^{-1} characteristic of the carbonyl C=O stretching functionality of formic acid (HCOOH).[10] A formic acid

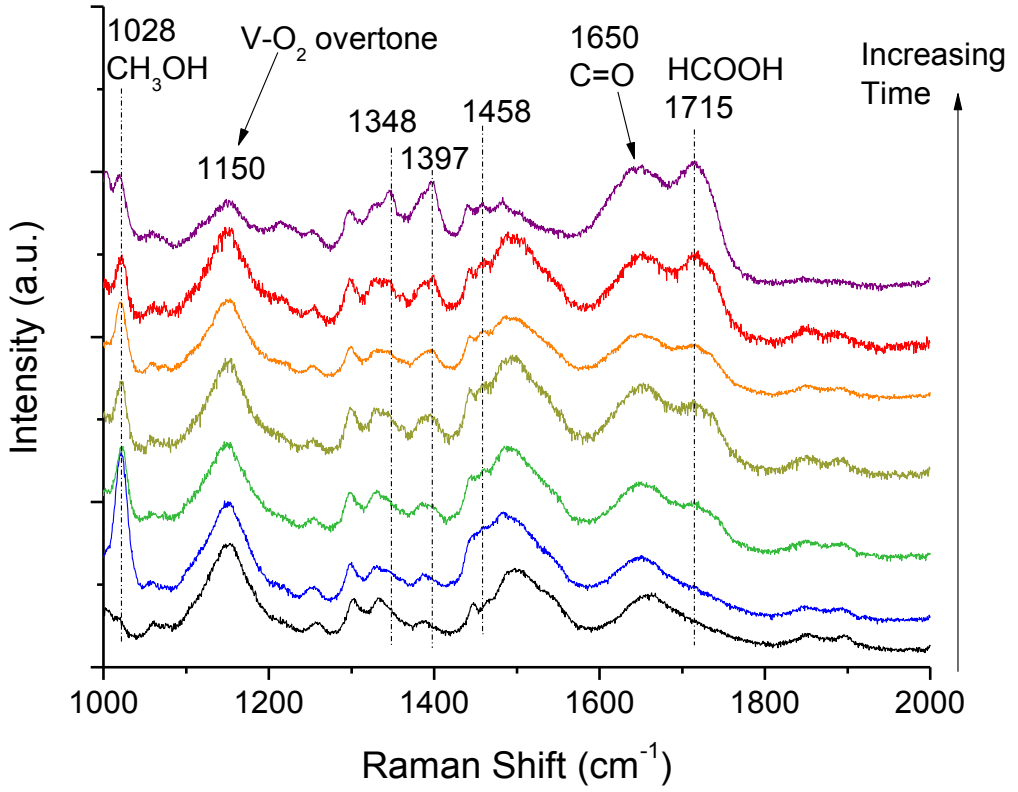

Figure 3.3 Time-resolved *in situ* Raman spectra during methanol oxidation with H_2O_2 at 50°C by the 0.2M $K[VO(O_2)(heida)]_{(aq)}$ enzyme mimic in the 1000-2000 cm^{-1} spectral region. The black curve is the initial Raman spectrum for $K[VO(O_2)(heida)]_{(aq)}$ prior to addition of CH_3OH and H_2O_2. The subsequent Raman spectra are taken at 20–25 minute intervals following the addition of six molar equivalents of CH_3OH and H_2O_2.

standard was examined by Raman spectroscopy to confirm the assignment (not shown). The 1715 cm^{-1} formic acid Raman band appears after formaldehyde is produced and is related to further oxidation of formaldehyde to formic acid by either $K[VO(O_2)(heida)]_{(aq)}$ or by excess H_2O_2.

Aqueous oxidation of methanol by $H_2O_{2(aq)}$ and $K[VO(O_2)(heida)]_{(aq)}$ at 50°C was also monitored with time-resolved *in situ* ATR-IR spectroscopy since vanadium methoxy vibrations are more easily detected by IR. This study was performed in order to observe the catalytic active site for methanol oxidation by $K[VO(O_2)(heida)]_{(aq)}$. The resulting IR spectra are presented in Figure 3.4 for the 2500-3100 cm^{-1} spectral region corresponding to the various oxygenated species. The red curve in Figure 3.4 represents the spectrum obtained for $K[VO(O_2)(heida)]_{(aq)}$, which possesses small IR bands in this region. Negative controls were run in parallel and a baseline negative

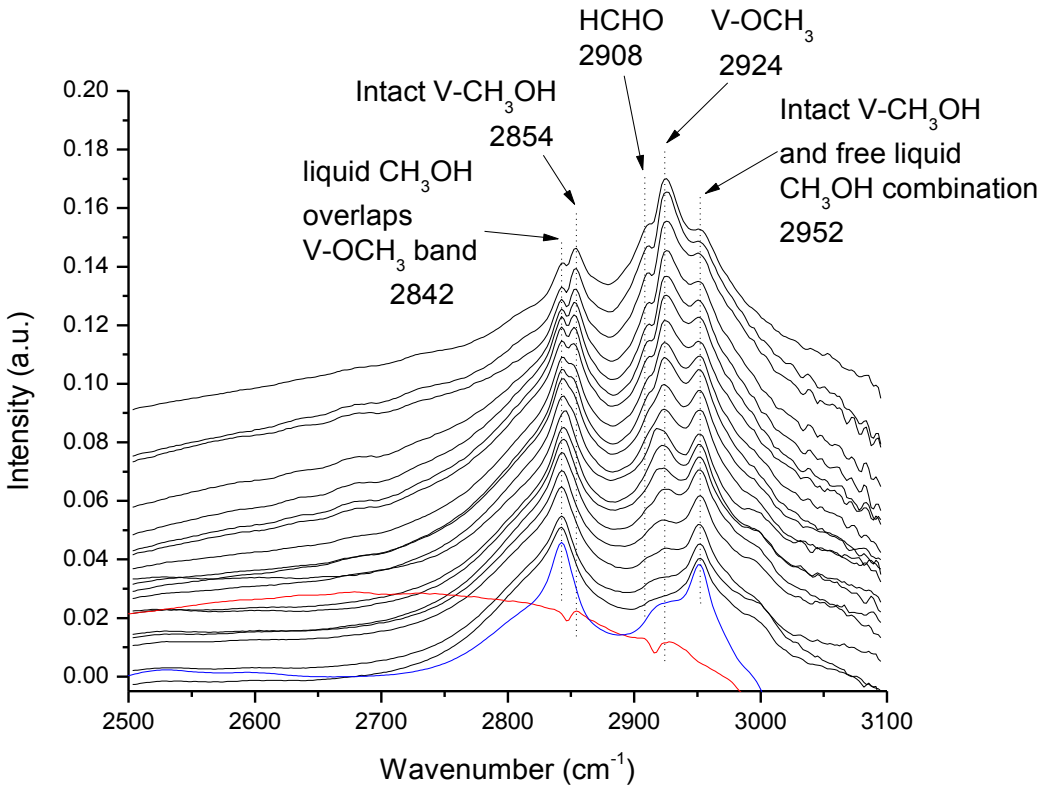

Figure 3.4 Time-resolved *in situ* ATR-IR spectra during $CH_3OH_{(aq)}$ oxidation by $H_2O_{2(aq)}$ and $K[VO(O_2)(heida)]_{(aq)}$ enzyme mimic in the 2500–3100 cm^{-1} spectral region. The red curve is for the 0.2M $K[VO(O_2)(heida)]_{(aq)}$ enzyme mimic prior to addition of six molar equivalents CH_3OH and H_2O_2 and was used as a baseline for the subsequent reaction spectra. The blue curve is the $CH_3OH_{(aq)}$ standard. The spectra were collected at 10 minute intervals following the addition of CH_3OH and H_2O_2.

control spectrum was subtracted from each sample spectrum in order to avoid any interference from $K[VO(O_2)(heida)]_{(aq)}$ IR bands. The blue curve in Figure 3.4 is the spectrum for an aqueous solution of $CH_3OH_{(aq)}$ (2854 and 2952 cm^{-1} with weak shoulder bands at ~2800 and 2900 cm^{-1}).[8] The ascending black spectra were taken at 5-10 minute intervals after the introduction of $CH_3OH_{(aq)}$ and $H_2O_{2(aq)}$. As CH_3OH adsorption proceeds, new bands begin to appear from intact CH_3OH bound to the vanadium active site ($2\delta_s(CH_3)$ at 2854 cm^{-1}), the V-OCH_3 reactive methoxy intermediate ($\nu_s(CH_3)$ at 2924 cm^{-1}) and the $HCHO_{(aq)}$ reaction product ($\nu_{as}CH_2$ at 2908 cm^{-1}).[11] Note that intensity of the IR bands for $CH_3OH_{(aq)}$ decrease while the intensity of the IR bands for V-$OCH_{3(aq)}$ and $HCHO_{(aq)}$ increase with extent of methanol oxidation. The aqueous methanol vibrational bands at 2842 and 2952 cm^{-1} overlap the methoxy V-OCH_3 $2\delta_s(CH_3)$ and intact methanol $\nu_s(CH_3)$ vibrations, respectively. Assignments for the methoxy and intact bound methanol IR band assignments were made by comparison to analogous vanadium oxide catalysts.[11]

Rate Determining Step

The kinetics of CH_3OH and CD_3OH oxidation by $K[VO(O_2)(heida)]_{(aq)}$ at 70°C in the presence of H_2O_2 is shown in Figure 3.5. It can be seen that the kinetic rate of oxidation of CD_3OH by $K[VO(O_2)(heida)]_{(aq)}$ to deuterated formaldehyde (DCDO) is slower than the kinetic rate of oxidation of CH_3OH to formaldehyde (HCHO). This indicates that the rate of C-D methoxy bond breaking is slowed down by the kinetic isotope effect. The rate of C-H methoxy bond breaking proceeds at a faster rate.

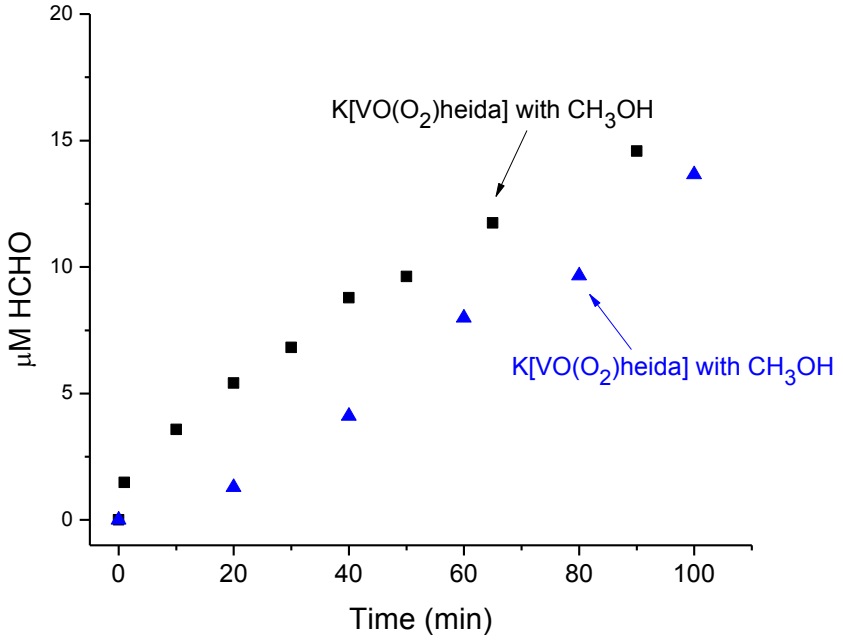

Figure 3.5 Kinetics of CH_3OH and CD_3OH oxidation by $K[VO(O_2)(heida)]_{(aq)}$ at 70°C in the presence of H_2O_2 showing kinetic isotope effect. The kinetic oxidation rate is slower for CD_3OH than for CH_3OH indicating that the C-H methoxy bond breaking step is rate determining.

Discussion

Active Structure for Aqueous Methanol Oxidation by the $K[VO(O_2)(heida)]_{(aq)}$ Enzyme Mimic

Two V-O-heida aqueous molecular complexes are present during methanol oxidation: the peroxo-oxo $K[VO(O_2)(heida)]_{(aq)}$ and the dioxo $K[VO(O)(heida)]_{(aq)}$, with the peroxo-oxo structure $K[VO(O_2)(heida)]_{(aq)}$ being the catalytic active form (see spectra in Figure 3.1).

Chemisorption

The active peroxo-oxo $K[VO(O_2)(heida)]_{(aq)}$ enzyme mimic contains three distinct oxygen functionalities: a peroxo V-O_2 group, an oxo V=O group, and bridging V-O-C coordinating ligand bonds. The appearance of the $\nu_s(CH_3)$ V-OCH_3 ATR-IR vibration (2924 cm^{-1}) upon chemisorption of CH_3OH on the $K[VO(O_2)(heida)]_{(aq)}$ enzyme mimic and the absence of perturbation of the peroxo V-O_2 and oxo V=O vanadyl vibrations (see Figures 3.4 and 3.2, respectively) implicates the bridging V-O-C(heida) bonds as being involved in dissociative chemisorption of methanol at the vanadium atom of the enzyme mimic to from V-OCH_3 and C-O-H. The current determination that methanol chemisorbs at the bridging V-O-C(ligand) site is in agreement with the proposal of Conte *et al*. that 2-propanol oxidation by an analogous vanadium-peroxo-tri-isoproproxide compound initiates with propanol complexation with the central vanadium atom.[5]

Most Abundant Reaction Intermediates

Two reaction intermediates are present during $CH_3OH_{(aq)}$ oxidation by the $K[VO(O_2)(heida)]_{(aq)}$ enzyme mimic: physisorbed intact V-CH_3OH and V-OCH_3 species (see Figure 3.4). As the CH_3OH oxidation reaction proceeds, the ATR-IR vibrational bands from intact CH_3OH bound to the vanadium active site ($2\delta_s(CH_3)$ at 2854 cm^{-1}) and the V-OCH_3 reactive methoxy intermediate ($\nu_s(CH_3)$ at 2924 cm^{-1}) both begin to increase in intensity, the latter with greater intensity. The preponderance of the

V-OCH_3 band indicates that V-OCH_3 is the most abundant reaction intermediate for the partial oxidation of methanol to formaldehyde by $K[VO(O_2)(heida)]_{(aq)}$.

Rate Determining Step

The kinetic isotope effect for CH_3OH and CD_3OH oxidation by $K[VO(O_2)(heida)]_{(aq)}$ at 70^oC in the presence of H_2O_2 can be clearly seen in Figure 3.5. When the methoxy hydrogen atoms (CH_3O-) are replaced by deuterium atoms, the heavier mass of the deuterium results in lower vibrational frequencies and therefore a lower zero point energy for CD_3O-. Therefore more energy is required to break a C-D bond than a C-H bond. This results in a lower kinetic rate of C-D bond breaking than C-H bond breaking.[12, 13] If the methoxy C-H bond breaking step was not rate limiting (for example if the rate determining step was adsorption or desorption), the rate for CD_3OH oxidation would not appear to be slower than CH_3OH oxidation. CD_3OH oxidation to DCDO by $K[VO(O_2)(heida)]_{(aq)}$ proceeds at a much slower rate than CH_3OH oxidation to HCHO as seen in Figure 3.5. This indicates that the rate determining step for methanol oxidation by $K[VO(O_2)(heida)]_{(aq)}$ is the methoxy C-H bond breaking step.

Catalytic Active Site

The peroxo V-O_2 functionality is the catalytic site where methanol oxidation takes place by performing the methyl C-H bond breaking step and losing one of the oxygen atoms from the peroxo group in the formation of the water byproduct. The remaining oxygen atom of the peroxo group forms the second vanadyl V=O bond of the

dioxo $K[VO(O)(heida)]_{(aq)}$ complex. This is directly observed during oxidation of methanol by the $K[VO(O_2)(heida)]_{(aq)}$ enzyme mimic in the absence of the H_2O_2 oxidant as consumption of the peroxo V-O_2 functionality (e.g., the strong peroxo Raman vibration at 575 cm^{-1} in Figure 3.1) during the oxidation reaction. The appearance of the broad Raman band at 920 cm^{-1}, characteristic of the dioxo $K[VO(O)(heida)]_{(aq)}$ compound, demonstrates that the second oxygen atom from the peroxo forms a second vanadyl group (see Chapter 2, section 2 for the dioxo spectrum). It, thus, appears that the oxo V=O vanadyl bond is not directly involved in the aqueous methanol oxidation reaction by the $K[VO(O_2)(heida)]_{(aq)}$ enzyme mimic and is retained to form the reduced dioxo $K[VO(O)(heida)]_{(aq)}$ complex.

Reaction Mechanism of Aqueous CH_3OH oxidation by $K[VO(O_2)(heida)]_{(aq)}$

The catalytic cycle for aqueous methanol oxidation by the $K[VO(O_2)(heida)]_{(aq)}$ enzyme mimic is schematically shown in Scheme 3.1. The first step involves the chemisorption of methanol at the bridging V-O-C(ligand) bond that results in scission of this bond and formation of V-OCH_3 and H-O-C(ligand) bonds. In the second step, the V-OCH_3 intermediate transfers its methyl hydrogen atom to the V-O_2 functionality to form H_2CO, H_2O, and the dioxo $K[VO(O)(heida)]_{(aq)}$ compound. In the final step, which completes the catalytic cycle, the dioxo $K[VO(O)(heida)]_{(aq)}$ is reoxidized by $H_2O_{2(aq)}$ to the active $K[VO(O_2)(heida)]_{(aq)}$ peroxo-oxo compound. Thus, this reaction proceeds via a Mars-van Krevelen reaction mechanism[14] since the participating peroxo oxygen in the rate determining step is supplied by the $K[VO(O_2)(heida)]_{(aq)}$ enzyme mimic and not from the $H_2O_{2(aq)}$ oxidant (see Figure 3.1). The proposed reaction

mechanism is supported by density functional theory (DFT) calculations of the energetics of this reaction (to be presented in the following section).

Formic acid is also produced in significant quantities due secondary oxidation of the formaldehyde reaction product by the active $K[VO(O_2)(heida)]_{(aq)}$ enzyme mimic, or by oxidation with excess H_2O_2 or even by facile oxidation of formaldehyde by atmospheric oxygen. The detailed mechanistic steps of HCHO oxidation to HCOOH by the active $K[VO(O_2)(heida)]_{(aq)}$ enzyme mimic, have not been investigated and, thus, will not be further discussed.

Scheme 3.1 Proposed mechanism of partial methanol oxidation to formaldehyde by $K[VO(O_2)(heida)]_{(aq)}$ enzyme mimic in the presence of H_2O_2.

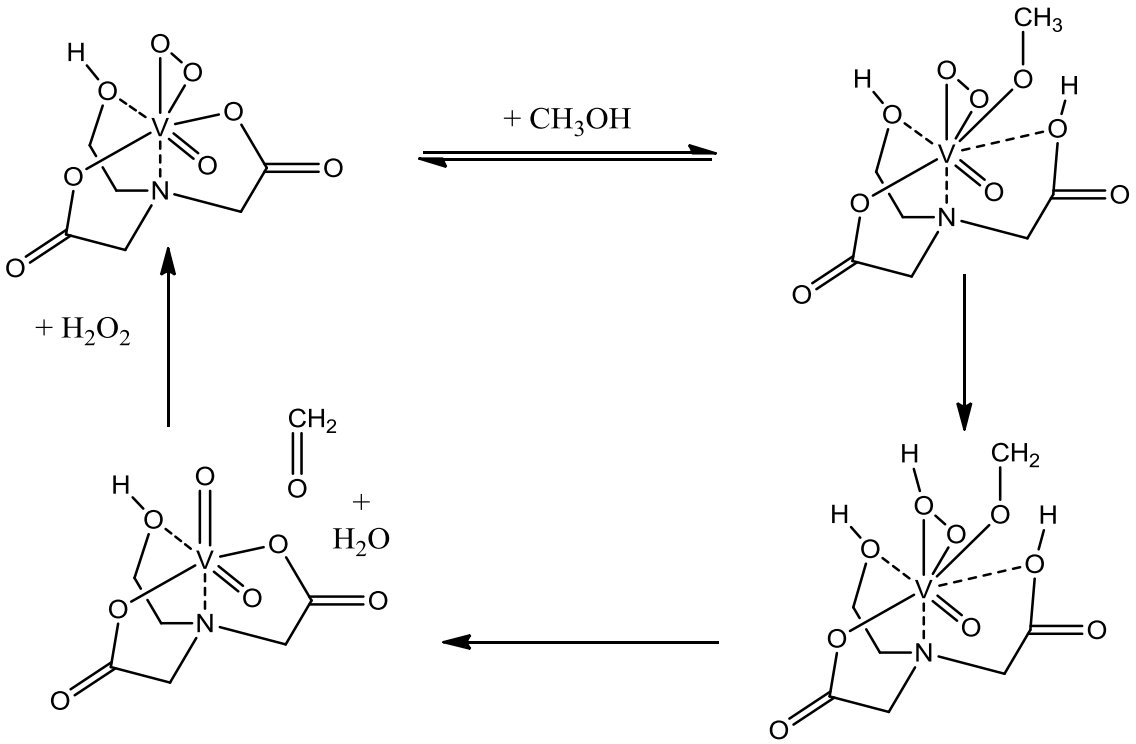

Comparison of Methanol Oxidation in the Vapor Phase by Supported VO_4/SiO_2 and Aqueous Phase by $K[VO(O_2)(heida)]_{(aq)}$ Enzyme Mimic

Vapor phase oxidation of methanol by supported vanadium oxide catalysts (see Scheme 3.2, below) has been extensively investigated and shown to proceed via the Mars-van Krevelen reaction mechanism in which the vanadium oxide catalytic active site, and not gas phase molecular O_2, supplies the oxygen involved in the rate determining step of the oxidation reaction. Dissociative methanol chemisorption occurs at the bridging V-O-Support bond to form the surface V-OCH_3 reaction intermediate and Support-OH species.[15-17] The terminal V=O bond is involved in the rate determining C-H bond breaking step by a hydrogen atom from the methoxy

Scheme 3.2 Oxidation mechanism of methanol to formaldehyde over SiO_2/VO_4

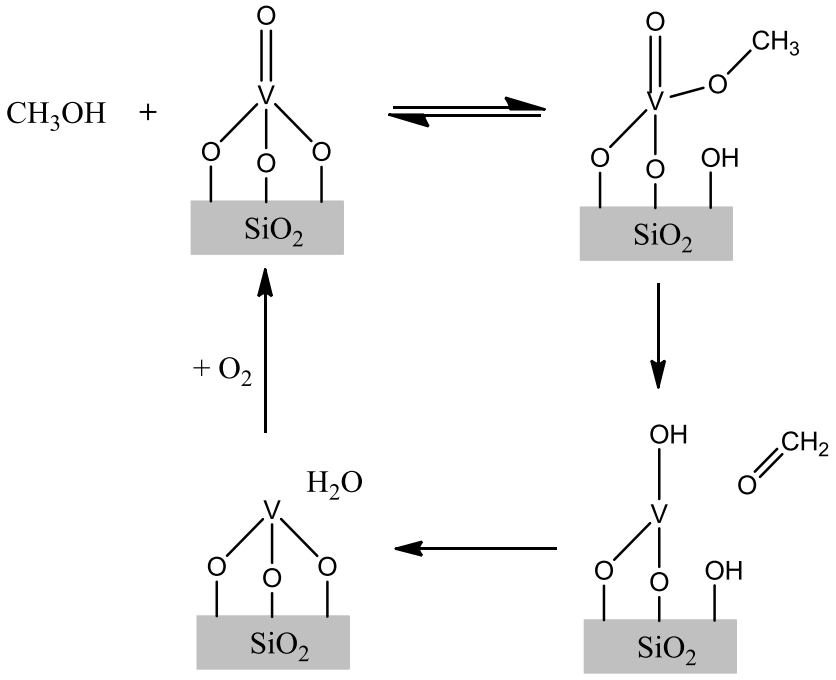

group which leads to the formation of the vapor phase formaldehyde reaction product.[15, 16] The remaining surface V-OH and Support-OH intermediates subsequently recombine to release H_2O. Gas phase molecular O_2 completes the catalytic cycle by reoxidizing the reduced vanadium oxide catalytic active site from V^{+3} back to V^{+5}. The aqueous phase oxidation of methanol by the $K[VO(O_2)(heida)]_{(aq)}$ enzyme mimic catalyst also proceeds via the Mars-van Krevelen reaction mechanism where the vanadium oxide catalytic active site, and not the H_2O_2 oxidant, supplies the oxygen involved in the oxidation reaction. In biocatalysis jargon, this type of mechanism is sometimes also referred to as a ping-pong mechanism.[18] *In situ* Raman and ATR-IR spectroscopy indicate the similarity of the overall mechanism of methanol oxidation by $K[VO(O_2)(heida)]_{(aq)}$ and supported vanadium oxide heterogeneous catalysts. For both catalytic systems, CH_3OH chemisorbs at a bridging V-O-Support/ligand bond to form $V\text{-}OCH_3$ reaction intermediates and both perform oxidation via a Mars-van Krevelen reaction mechanism, but with one critical difference. For $K[VO(O_2)(heida)]_{(aq)}$, the methoxy C-H bond breaking rate determining step is performed by the peroxo $V\text{-}O_2$ group as indicated by the consumption of the peroxo band (see Figure 3.1). For supported VO_4/SiO_2, which does not contain a peroxo $V\text{-}O_2$ group, the C-H bond breaking step is performed by the terminal V=O oxo group.[15, 16] Lastly, reoxidation of the inactive dioxo $K[VO(O)(heida)]_{(aq)}$ to the active $K[VO(O_2)(heida)]_{(aq)}$ peroxo-oxo complex requires H_2O_2 as the oxidant whereas for VO_4/SiO_2 molecular O_2 performs the reoxidation of the reduced surface VO_x site. Thus, methanol oxidation in the vapor and liquid phases exhibits many similarities (Mars-van Krevelen mechanism and bridging V-O-X active site, in which X is either a C ligand or an oxide support cation, for

methanol chemisorption), but also a key fundamental difference in the methoxy C-H bond breaking rate determining step (use of peroxo V-O_2 *vs*. oxo V=O functionalities).

Conclusions

The $K[VO(O_2)(heida)]_{(aq)}$ enzyme mimic and supported vanadium oxide catalysts, such as vanadia supported on silica, differ greatly in the local VO_x molecular structure.[19] $K[VO(O_2)(heida)]_{(aq)}$ contains a peroxo-oxo structure while a $O=VO_3$ trigonal pyramidal structure is present for VO_4/SiO_2. Despite these molecular structural differences, both catalysts share a similar methanol adsorption site (the bridging V-O-X bond and the V-OCH_3 reaction intermediate). The $K[VO(O_2)(heida)]_{(aq)}$ and VO_4/SiO_2 also perform oxidation reactions via a Mars-van Krevelen mechanism where the VO_x catalytic active site relinquishes its active oxygen during the rate determining step and must subsequently be reoxidized to its active fully oxidized form in order to continue the full catalytic cycle. The $K[VO(O_2)(heida)]_{(aq)}$ and supported VO_4/SiO_2, however, differ in the nature of the rate determining step involving the methoxy C-H bond breaking. $K[VO(O_2)(heida)]_{(aq)}$ transfers the methoxy hydrogen atom to the peroxo VO_2 group while supported VO_4/SiO_2 transfers the methoxy hydrogen atom to the oxo V=O group because it does not possess a peroxo functionality. Furthermore, the oxo V=O functionality in the $K[VO(O_2)(heida)]_{(aq)}$ enzyme mimic does not participate in methanol oxidation reflecting the greater reactivity of peroxo VO_2 groups than oxo V=O groups for oxidation reactions.

This is *the first time* experimental evidence has been presented for the catalytic active site, reaction intermediates, rate determining step, and reaction mechanism for an

oxidation reaction by $K[VO(O_2)(heida)]_{(aq)}$ in the presence of H_2O_2. The new fundamental information was provided by time-resolved *in situ* Raman and ATR-IR spectroscopy. The new insights reveal the similarities and differences between methanol oxidation in the vapor phase by supported VO_4/SiO_2 catalysts and $K[VO(O_2)(heida)]_{(aq)}$ enzyme mimics. Although the enzyme mimic and catalyst exhibit many similarities, there is a significant difference in the critical oxidation step. The nature of the oxygen involved in the oxidation reaction is different for both systems: a vanadyl for supported VO_4/SiO_2 and peroxo for the $K[VO(O_2)(heida)]_{(aq)}$ enzyme mimic.

Section 2: Supplemental Density Functional Theory (DFT) Calculations for Methanol Oxidation by $K[VO(O_2)(heida)]_{(aq)}$

Density Functional Theory (DFT) calculations were performed to supplement experimental results. DFT was used to compute the lowest energy pathway for methanol adsorption and for the C-H bond breaking step for methanol oxidation by $K[VO(O_2)(heida)]$. All DFT work was performed in collaboration with Middle East Technical University (METU) in Ankara, Turkey with the gracious help of Ms. Duygu Gerçeker, advised by Professor Işik Önal.

Prior to this study, a few reports in literature included DFT work on the the $K[VO(O_2)(heida)]$ complex, but none of them performed any DFT calculations on methanol oxidation; sulfoxidation and bromide oxidation mechanisms were studied.[3, 4, 20]

Both sulfoxidation and bromide oxidation reactions by $K[VO(O_2)(heida)]$ are typically carried out in a polar aprotic solvent such as acetonitrile which is slightly acidified. Water as a solvent is thought to function as a buffering agent which does not permit protonation of the peroxo group of $K[VO(O_2)(heida)]$. In acetonitrile, protonation of $K[VO(O_2)(heida)]$ is easier because acetonitrile does not possess the same buffering capability as water.

For bromide oxidation to HOBr, it is believed that protonation of $K[VO(O_2)(heida)]$ is required for activity. The protonated peroxo atom is attacked by the incoming bromide, which plucks away an oxygen atom and the associated proton to form the HOBr product.[1, 20] Vanadium haloperoxidases are thought to catalyze halide

oxidation in a similar fashion, but the associated proton is donated by a nearby amino acid.[21-24] In a recent study, DFT was used to investigate the bromide oxidation mechanism by protonated K[VO(O_2)(heida)]. It was found that even though bromide prefers to approach the unprotonated oxygen of the protonated peroxo group, there was no suitable pathway for removal of an –OH group by the bromide. Therefore, it was concluded using DFT that bromide oxidation occurs via nucleophillic attack of the incoming bromide at the protonated oxygen of the protonated peroxo group (See Scheme 3.3 for representation of this bromide attack suggested by the DFT work of Eshtiagh-Hosseini et al.).[20]

Scheme 3.3 Suggested mechanism of bromide attack by the DFT work of Eshtiagh-Hosseini et al.[20]

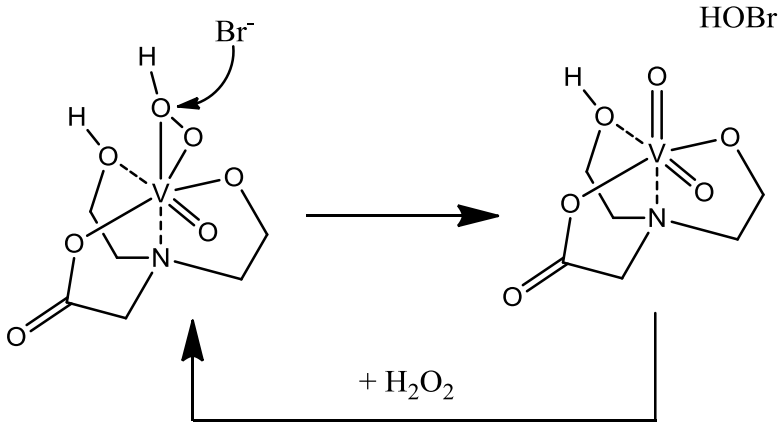

DFT studies have shown that sulfoxidation occurs via thiol or thioether attack at the more electrophilic, unprotonated oxygen atom of the K[VO(O_2)(heida)] protonated peroxo group in acetonitrile solution.[2-4, 25] Vanadium haloperoxidases are also thought to

perform sulfoxidations in the same manner.[25] A schematic of the sulfoxidation mechanism found for K[VO(O_2)(heida)] is shown in Scheme 3.4. [2-4, 25]

Scheme 3.4 Representation of the suggested mechanism for sulfoxidation by K[VO(O_2)(heida)].[2-4, 25]

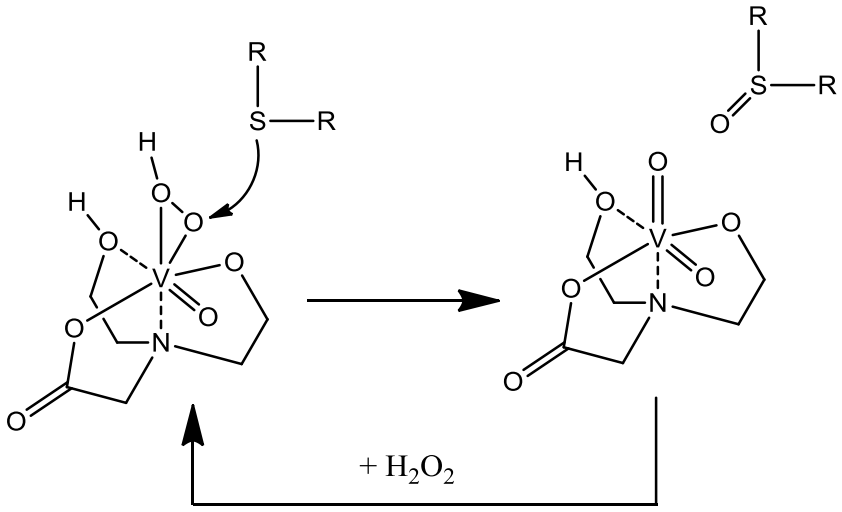

We did not investigate whether or not methanol oxidation by K[VO(O_2)(heida)] occurs in acidified acetonitrile, however we believe that a protonated peroxo group in acetonitrile solution would not be beneficial. This is because during the C-H bond breaking step, an H atom needs to be removed by the unprotonated peroxo group. Still, prior to this study, there has not been any reported DFT work on alcohol oxidation by K[VO(O_2)(heida)]$_{(aq)}$. The DFT performed in this section serves as a complement to the experimental work performed earlier in this Chapter. Here we investigate the energetics of methanol adsorption, and the mechanism for the C-H bond breaking step using DFT. Two mechanistic pathways were investigated and the computational results were compared to the experimental results. The DFT results agree with experimental results

showing that the C-H bond breaking step is most likely performed by the peroxo group and not the oxo group.

Experimental

Density Functional Theory (DFT) Calculations

DFT calculations were performed within the Gaussian 2009 software suite using the functional B3LYP with a 6-31G (d,p) basis set. Gaussian code programming was performed by Ms. Duygu Gerçeker. Water as a solvent was incorporated using the polarizable continuum model (PCM) for all calculations. A single point energy (SPE) calculation was performed to obtain the lowest spin number for the $[VO(O_2)(heida)]^-$ and equilibrium geometry (EG) optimization was performed on the $[VO(O_2)(heida)]^-$ cluster using crystal data for initial bond lengths/bond angles.[1] Solvation energetics of the $[VO(O_2)(heida)]^-$ cluster using the lowest spin number was computed and equilibrium geometry (EG) optimization was also performed on the methanol molecule. An initial starting guess for adsorbed methanol was optimized, and the energy barrier for methanol adsorption was computed.

The C-H bond breaking step was investigated via two reaction coordinate driven computations: via proton transfer to the peroxo group and via proton transfer to the oxo group. Transition state optimization was performed for each reaction pathway, and the activation energy barrier of the C-H bond breaking step was computed for both scenarios.

Results

DFT Study on Methanol Oxidation by K[VO(O$_2$)(heida)]$_{(aq)}$

Single point energy calculations yielded a lowest spin number of 3 for aqueous [VO(O$_2$)(heida)]$^-$. The heat of formation was calculated for both gas phase [VO(O$_2$)(heida)]$^-$ and aqueous phase [VO(O$_2$)(heida)]$^-$ and found to be -1833.05 a.u. and -1833.22 a.u. respectively. The solvation energy in water was computed and found to be -109.85 kcal/mol. The optimized equilibrium geometry (EG) for the [VO(O$_2$)(heida)]$^-$ cluster converged in 20 steps and is shown in Figure 3.6 a. The methanol molecule was also geometry optimized and is shown in Figure 3.6 b.

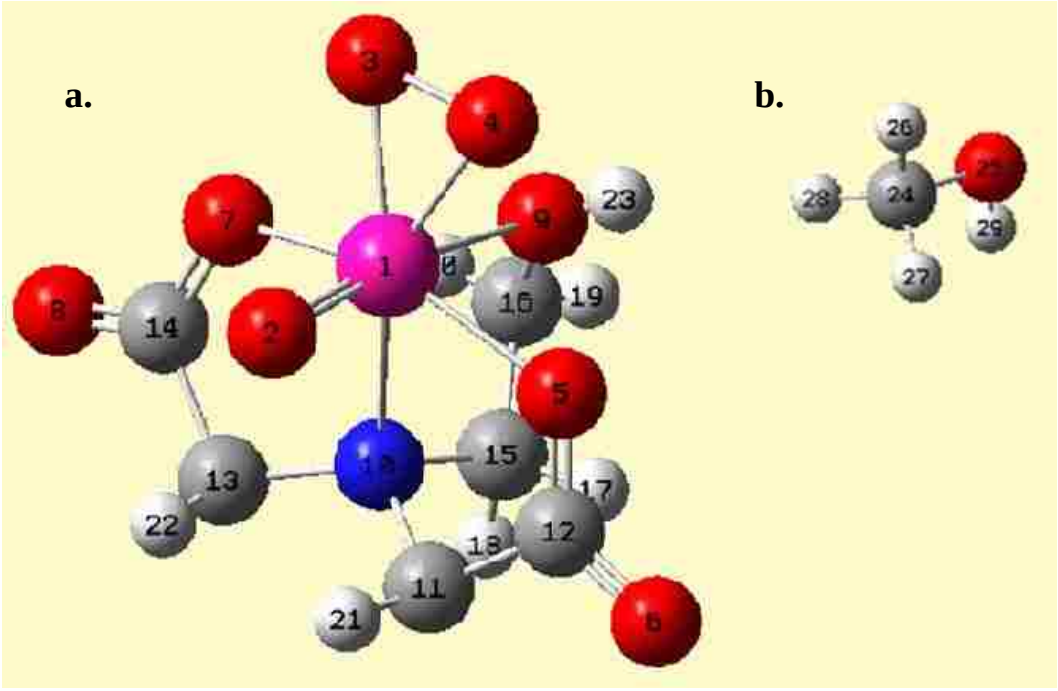

Figure 3.6 a. Ball-and-stick representation of optimized equilibrium geometry structure of aqueous [VO(O$_2$)(heida)]$^-$ cluster with atom labeling, and **b.** optimized geometry structure of methanol with atom labeling.

Next, methanol adsorption was examined via a V-O reaction coordinate driven pathway between the vanadium (V1) and oxygen (O25) atom for methanol. A local minimum was found for non dissociative methanol physisorption at a V1-O25 distance of 2.24 Å. The relative energy for methanol physisorption was calculated to be 3.45 kcal/mol. Further along the coordinate driven pathway dissociative methanol chemisorption was found to occur at V1-O25 distance of 1.82 Å. Simultaneously, the methanol hydroxyl group loses its H atom which breaks the V-O-ligand bond and deposits H29 on O5 with a bond distance of H29-O5 of 0.997 Å. This configuration was found to have a relative energy of -11.61 kcal/mol. This configuration showing methanol chemisorption directly to the vanadium center (V-OCH_3) breaking the V-O-ligand bridging bond and depositing H29 on O5 is shown in Figure 3.7.

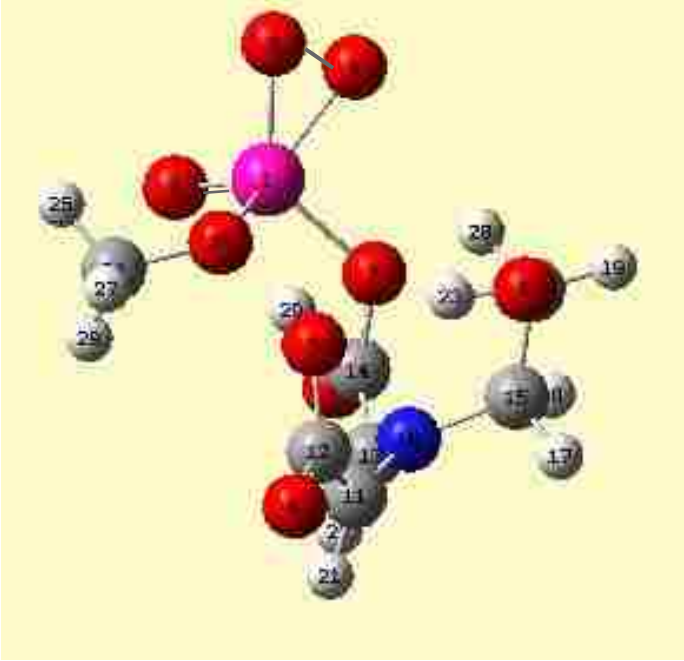

Figure 3.7 Optimized structure of chemisorbed methanol on aqueous $[VO(O_2)(heida)]^-$ cluster with V1-O25: 1.82 Å and H29-O5: 0.997 Å.

Next, the energetics of two possible C-H bond breaking pathways were computed via coordinate driven reaction pathways: abstraction of a methoxy proton by the peroxo O3 or by the oxo O2 to determine the most likely pathway for C-H bond breaking. For proton transfer from the methoxy to the peroxo group at O3, a methoxy rotation step was required prior to C-H abstraction. The rotation step is shown in Figure 3.8 b. H27 transfer to O3 then proceeded with a bonding distance of H27-O3 of 1.253 Å followed by the immediate release of formaldehyde. The activation energy barrier of

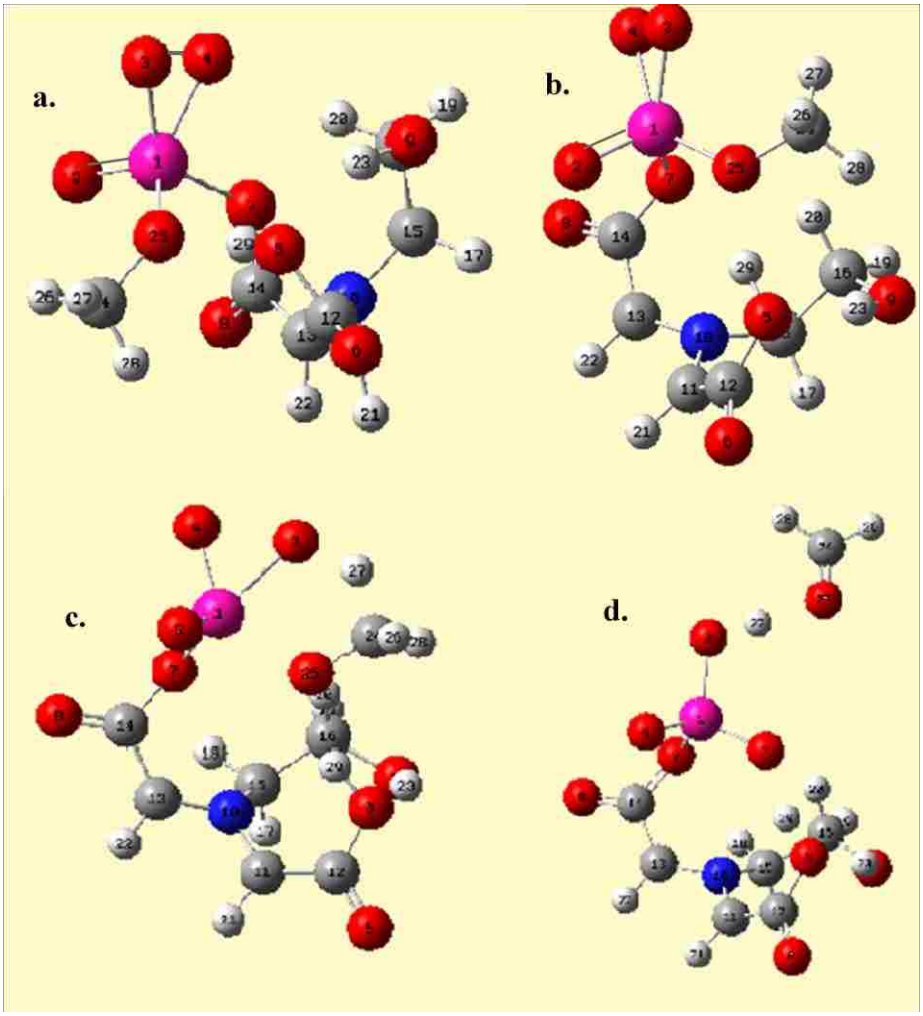

Figure 3.8 Optimized structure of **a.** chemisorbed methanol on aqueous $[VO(O_2)(heida)]^-$ cluster with V1-O25: 1.82 Å and H29-O5: 0.997 Å, **b.** methoxy rotation step, **c.** transition state (TS) showing proton abstraction by peroxo group with H27-O3: 1.253 Å and **d.** final release of formaldehyde product.

proton abstraction by the peroxo group was found to be 17.71 kcal/mol. The optimized structures for rotation, H27 transfer to O3, and subsequent immediate formaldehyde product release are shown in Figure 3.8.

Investigation of the second pathway for C-H bond breaking, abstraction of the proton by the oxo group, met with less success. An upwards rotation of the methoxy for this pathway was not required for this pathway, due to the proximity of H26 to O2. H26 transfer to O2 was initiated and the bonding distance of H26-O2 was found to be 1.14 Å. The activation energy barrier of proton abstraction by the oxo group was found to be 37.31 kcal/mol. Additionally, spontaneous release of formaldehyde was not observed; it simply remained adsorbed. The optimized structures for adsorption and H26 transfer to O2 are shown in Figure 3.9.

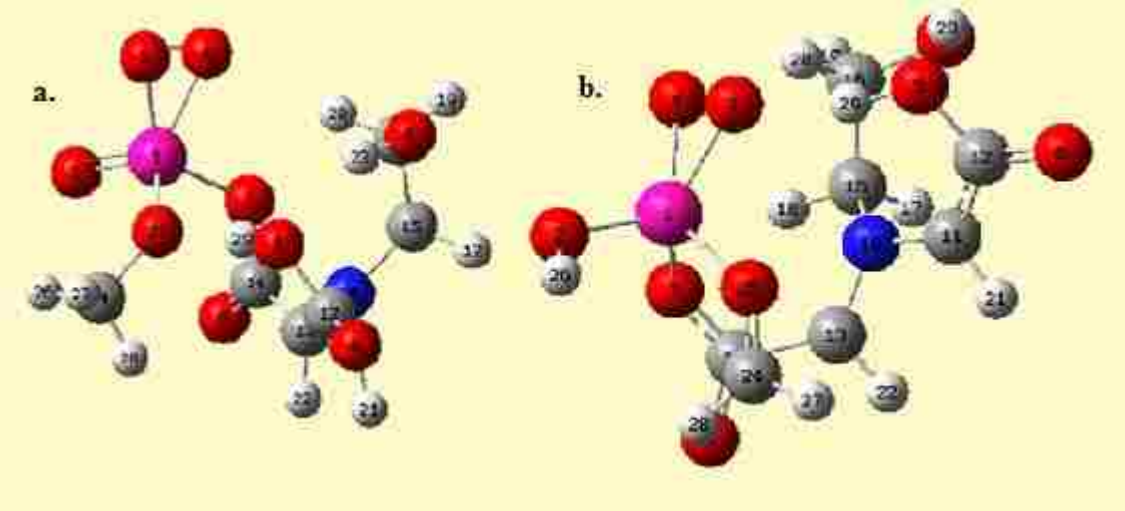

Figure 3.9 Optimized structure of **a.** chemisorbed methanol on aqueous $[VO(O_2)(heida)]^-$ cluster with V1-O25: 1.82 Å and H29-O5: 0.997 Å, **b.** transition state (TS) showing proton abstraction by oxo group with H26-O2: 1.14 Å

The activation energy barrier for H26 abstraction by O2 was found to be significantly higher than the activation barrier for H abstraction by the peroxo group. Figure 3.10 shows the computed relative energy results per equilibrium geometry (EG) optimization step for methanol adsorption, including the local physisorption minimum, which is followed by methanol chemisorption, and the two possible pathways for C-H bond breaking including transition state (TS) energy barriers for H transfer to the oxo and peroxo groups.

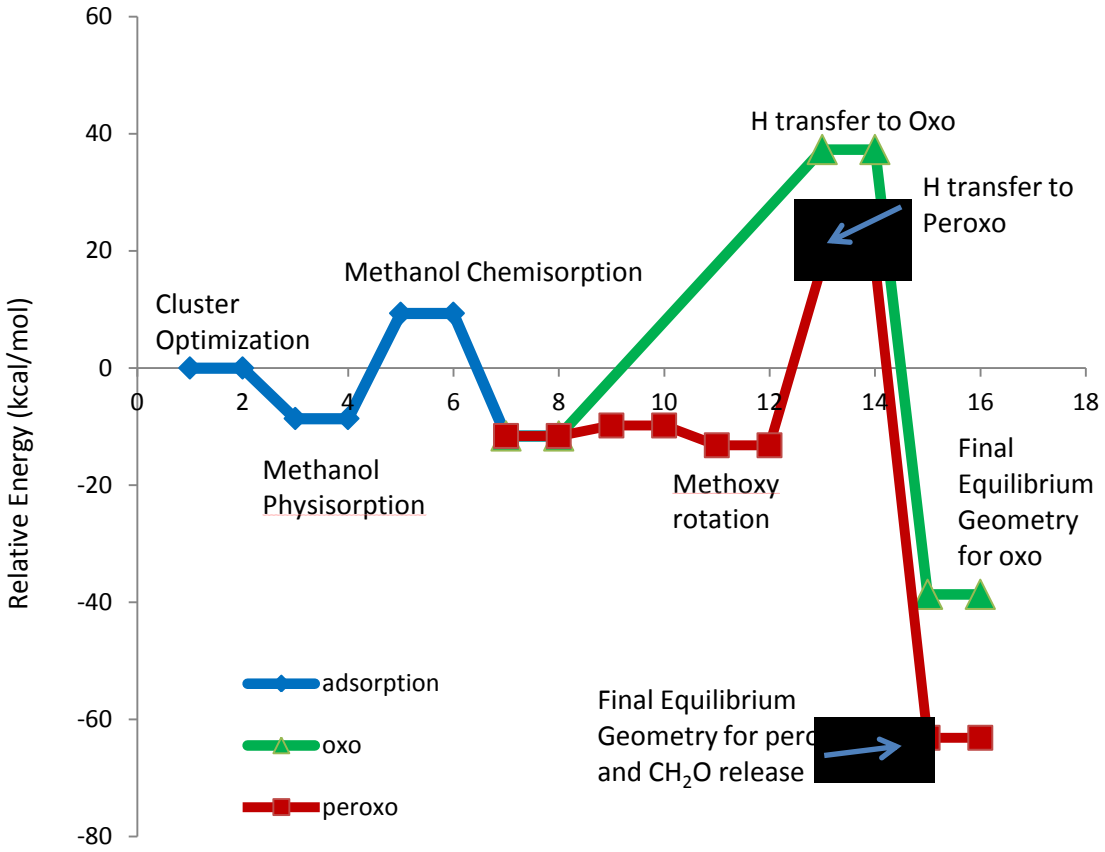

Figure 3.10 Relative energies of computed structures showing adsorption steps (blue), followed by two C-H bond breaking pathways: H abstraction by the peroxo group (red dotted) and H abstraction by the oxo group (green).

Discussion

DFT calculations and experimental results concur that the active site for methanol adsorption is the V-O-ligand bridging bond. Methanol adsorbs directly to the vanadium center forming a V-OCH_3 methoxy group and a ligand-OH hydroxyl group simultaneously. Of the two C-H bond breaking pathways investigated, proton abstraction by the V-O_2 peroxo group was more energetically favorable than proton abstraction by the V=O oxo group. The peroxo C-H bond breaking pathway yielded an activation energy of approximately 18 kcal/mol, while the oxo group C-H bond breaking pathway yielded an activation energy of approximately 37 kcal/mol. Not only is the oxo path unlikely to occur because of its higher activation energy, we were unable to find a suitable path for the release of formaldehyde for the oxo path.

Conclusions

DFT computations are in complete agreement with experimental results for the mechanism of methanol oxidation by $K[VO(O_2)(heida)]_{(aq)}$ (see Scheme 3.1 in Section 1). Experimental results indicate that methanol adsorption occurs by breaking a V-O-ligand bridging bond, and that C-H bond breaking occurs via proton transfer to the V-O_2 peroxo group. DFT results are in agreement. Methanol adsorption, and C-H bond breaking via the V-O_2 peroxo group were calculated to be the lowest energy pathway, and therefore the most likely path for methanol oxidation to formaldehyde by $K[VO(O_2)(heida)]_{(aq)}$. These DFT results provide an additional indication of the similarities and difference between the aqueous enzyme mimic and the heterogeneous catalyst. In the heterogeneous case for VO_4/SiO_2, methanol adsorption also occurs by

breaking a V-O-Si bond to form an adsorbed vanadium methoxy and a silica hydroxyl. DFT studies on VO_4/SiO_2 indicate that C-H bond breaking is performed by the V=O group[16] since VO_4/SiO_2 does not contain a V-O_2 peroxo group.

Section 3: K[VO(O_2)(heida)] Protonation Site for Bromide Oxidation

Bromide oxidation by K[VO(O_2)(heida)] is typically carried out in a polar aprotic solvent such as acetonitrile because it appears that this particular reaction occurs more efficiently in non-aqueous solution. The mechanism for bromide oxidation is completely different than the mechanism for methanol oxidation. For example, bromide may not bind directly to the vanadium atom, instead it appears that oxidation occurs by nucleophilic attack of the incoming halide on the peroxo group of K[VO(O_2)(heida)].[1] The reason why it is believed bromide oxidation does not occur as readily in protic solvents is because K[VO(O_2)(heida)] needs to be protonated in order to oxidize bromide to hypobromous acid.[1] The proposed mechanism for bromide oxidation was shown in the previous section where bromide plucks away the protonated oxygen atom of the peroxo group, yielding HOBr.

As mentioned in the previous section, recent DFT (density functional theory) calculations have proposed that the peroxo functionality, not the oxo group, is protonated in acetonitrile, but not in aqueous solution at normal reaction conditions due to the leveling effect of protic solvents.[3, 4, 26] However, this is only a theoretical result and there have not been any experimental observation of the protonation of the peroxo group in acidified acetonitrile.

In light of the successful structural and mechanistic experiments performed on methanol oxidation by K[VO(O_2)(heida)]$_{(aq)}$ presented in Chapters 2 and 3, the same tools and techniques can be applied to observe the protonation site for K[VO(O_2)(heida)] in acidified acetonitrile solution. Therefore, in order to address the

remaining question in the mechanism for bromide oxidation by K[VO(O_2)(heida)], full characterization of K[VO(O_2)(heida)] by Raman spectroscopy in acetonitrile is presented in this section. A protonated peroxo group should appear as a distorted Raman band, since one side of the group will become lengthened, and the other side shortened.

Experimental

K[VO(O_2)(heida)] was synthesized and crystallized by the method described in Chapter 2.[1] Approximately 0.1 g of K[VO(O_2)(heida)] was added to no less than 3 mL acetonitrile. Next, 0.12 g 18-crown-6 ($C_{12}H_{24}O_6$) was added in order to chelate the potassium ion to facilitate dissolution of the K[VO(O_2)(heida)]. Acidification of the acetonitrile/ K[VO(O_2)(heida)] solution was also achieved by adding a one molar equivalent of perchloric acid ($HClO_4$). The K[VO(O_2)(heida)]/acetonitrile solution was transferred to a screw-top quartz cuvette, and analyzed by Raman spectroscopy, as described in previous sections, this time focusing through the walls of the quartz cuvette. Acetonitrile/perchloric acid/16-crown-8 standards were run to identify background Raman bands.

Results

The Raman spectrum of K[VO(O_2)(heida)] in acetonitrile is presented in Figure 3.11. The Raman spectrum of K[VO(O_2)(heida)] in aqueous solution is also shown in Figure 3.11 for comparison. Acetonitrile exhibits two large Raman bands at 380 cm^{-1} and 924 cm^{-1}. Unfortunately, the 924 cm^{-1} acetonitrile band overlaps the O-O

symmetric stretch of the V-O_2 peroxo group for K[VO(O_2)(heida)] in acetonitrile. The 967 cm^{-1} band, corresponding to the symmetric stretch of the V=O oxo group is seen to be mostly unperturbed in the acetonitrile solvent. It does appear, that the V=O oxo band at 967 cm^{-1} may be slightly red shifted by no more than 3 cm^{-1}. The V-O_2 peroxo symmetric "breathing" vibration, which appears at ~575 cm^{-1} in aqueous solution, is split into a triplicate band for K[VO(O_2)(heida)] in acetonitrile. The V-O_2 breathing mode peak occurs at approximately 585 cm^{-1}, with a shoulder at 575 cm^{-1}, and a second shoulder at 557 cm^{-1}. We are unable to determine if the overtone band at 1150 cm^{-1} has been affected due to the lower signal to noise ratio for K[VO(O_2)(heida)] in acetonitrile.

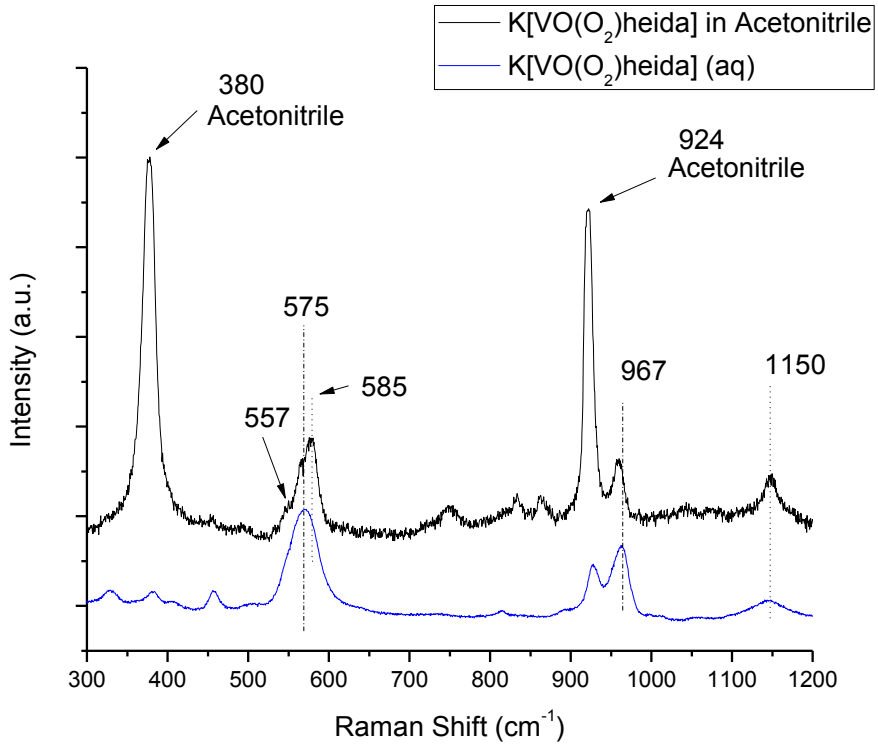

Figure 3.11 Raman spectrum of (blue line) the K[VO(O_2)(heida)]$_{(aq)}$ enzyme mimic in aqueous solution, and (black line) the Raman spectrum of the K[VO(O_2)(heida)] enzyme mimic dissolved in acetonitrile.

Discussion

The Raman spectra of K[VO(O_2)(heida)] in acetonitrile and water clearly indicate that K[VO(O_2)(heida)] is affected by the solvent. The triplicate V-O_2 peroxo breathing mode in acetonitrile indicates that the V-O_2 group has been distorted. A probable explanation for this triplicate Raman band is partial protonation of one of the oxygen atoms of the V-O_2 peroxo group. If one oxygen atom is protonated, one V-O bond becomes lengthened, thereby red shifting its vibration. The other V-O bond becomes shortened, which blue shifts its vibration. It is likely that K[VO(O_2)(heida)] is not fully protonated in acidified acetonitrile, since a shoulder at the original position of 575 cm^{-1} still exists. These results agree with previous DFT work which conclude that protonation of one of the V-O_2 peroxo oxygen atoms is more favorable than protonation of the V=O oxo group.

Conclusions

By comparing the Raman spectra of K[VO(O_2)(heida)] in acetonitrile to that of K[VO(O_2)(heida)] in aqueous solution, the final piece of the bromide oxidation mechanism puzzle has been solved. In acidified, acetonitrile K[VO(O_2)(heida)] is partially protonated at the V-O_2 peroxo group, and not the oxo group. This is indicated by a simultaneous red shift and blue shift from the original position of the V-O_2 group at 575 cm^{-1}. In other words, Raman shows that one side of the peroxo group is protonated, thereby lengthening one V-O bond and shortening the other. The persistence of the original 575 cm^{-1} band indicates that an unprotonated configuration

also exists in acetonitrile. Our findings are in agreement with previous DFT work indicating that the peroxo group, and not the oxo group is protonated in acetonitrile.[4]

References

(1) Colpas, G. J.; Hamstra, B. J.; Kampf, J. W.; Pecoraro, V. L. *J. Am. Chem. Soc.* **1996**, *118*, 3469-3478.

(2) Schneider, C. J. Development of Asymmetric Sulfoxidation Catalysts Based on Functional Models for Vanadium-Dependent Haloperoxidases, University of Michigan, 2009.

(3) Schneider, C. J.; Penner-Hahn, J.; Pecoraro, V. L. *J. Am. Chem. Soc.* **2008**, *130*, 2712-2713.

(4) Schneider, C. J.; Zampella, G.; Greco, C.; Pecoraro, V. L.; De Gioia, L. *Eur. J. Inorg. Chem.* **2007**, *4*, 515-523.

(5) Conte, V.; Di Furia, F.; Modena, G. *J. Org. Chem.* **1988**, *53*, 1665-1669.

(6) Butler, A.; Clague, M. J.; Meister, G. E. *Chem. Rev.* **1994**, *94*, 625-638.

(7) Conte, V.; Floris, B. *Inorg. Chim. Acta* **2010**, *363*, 1935-1946.

(8) Halford, J. O.; Anderson, L. C.; Kissin, G. H. *J. Chem. Phys.* **1937**, *5*, 927-932.

(9) Lebrun, N.; Dhamelincourt, P.; Focsa, C.; Chazallon, B.; Destombes, J. L.; Prevost, D. *J. Raman Spectrosc.* **2003**, *34*, 459-464.

(10) Bartholomew, R. J.; Irish, D. E. *J. Raman Spectrosc.* **1999**, *30*, 325-334.

(11) Burcham, L. J.; Briand, L. E.; Wachs, I. E. *Langmuir* **2001**, *17*, 6164-6174.

(12) Northrop, D. B. *Biochemistry (N. Y.)* **1975**, *14*, 2644-2651.

(13) Swain, C. G.; Stivers, E. C.; Reuwer, J. F.; Schaad, L. J. *J. Am. Chem. Soc.* **1958**, *80*, 5885-5893.

(14) Mars, P.; van Krevelen, D. W. *Spec. Suppl. Chem. Eng. Sci.* **1954**, *3*, 41-57.

(15) Khaliullin, R. Z.; Bell, A. T. *J. Phys. Chem. B* **2002**, *106*, 7832-7838.

(16) Dobler, J.; Pritzsche, M.; Sauer, J. *J. Am. Chem. Soc.* **2005**, *127*, 10861-10868.

(17) Burcham, L. J.; Deo, G.; Gao, X.; Wachs, I. E. *Top. Catal.* **2000**, *11/12*, 85.

(18) Everett, R. R.; Soedjak, H. S.; Butler, A. *J. Biol. Chem.* **1990**, *265*, 15671-15679.

(19) Molinari, J. E.; Wachs, I. E. *J. Am. Chem. Soc.* **2010**, *132*, 12559-12561.

(20) Eshtiagh-Hosseini, H.; Housaindokht, M. R.; Chahkandi, M.; Morsali, A. *Transition Metal Chemistry* **2010**, *35*, 939-947.

(21) Raugei, S.; Carloni, P. *J Phys Chem B* **2006**, *110*, 3747-3758.

(22) Valery M., D. *Tetrahedron* **2003**, *59*, 4701-4720.

(23) Butler, A. *Coordination Chemistry Reviews*, **1999**, *187*, 17-35.

(24) Butler, A.; Tschirret-Guth, R. A.; Simpson, M. T. *ACS Symp. Ser.* **1999**, *711*, 202-215.

(25) ten Brink, H. B.; Tuynman, A.; Dekker, H. L.; Hemrika, W.; Izumi, Y.; Oshiro, T.; Schoemaker, H. E.; Wever, R. *Inorg. Chem.* **1998**, *37*, 6780-6784.

(26) Zampella, G.; Fantucci, P.; Pecoraro, V. L.; De Gioia, L. *J. Am. Chem. Soc.* **2005**, *127*, 953-960.

Chapter 4: Comparison of Methanol Oxidation Kinetics by $K[VO(O_2)heida]_{(aq)}$ Enzyme Mimic Supported Vanadium Oxide Catalysts

In Chapter 3, the mechanism of aqueous oxidation of methanol to formaldehyde by $K[VO(O_2)heida]_{(aq)}$ was shown to be remarkably similar to that of gas phase methanol oxidation by heterogeneous supported VO_4/SiO_2. Both systems perform methanol oxidation via a Mars-van Krevelen mechanism and activate methanol upon chemisorption to surface methoxy with the bridging V-O-ligand bond. The difference between the two systems is found in the surface methoxy C-H bond breaking rate-determining-step. In the case of the $K[VO(O_2)heida]_{(aq)}$ enzyme mimic, C-H bond breaking appears to be performed by the vanadium peroxo group. In the case of the supported VO_4/SiO_2 catalyst, which does not possess a peroxo functionality, the surface methoxy C-H bond breaking is performed by the apical vanadium mono-oxo group.

In the case of methanol oxidation by supported vanadium oxides, the surface methoxy C-H bond breaking step has been shown to be rate-limiting.[1] An interesting finding for supported vanadium oxides is the dependence of the turn over frequency (TOF) on the oxide support, but independence of the apparent activation energy on the oxide support. It has been generally observed that the less electronegative the supporting oxide, the greater the specific activity of the catalyst for methanol oxidation which is reflected in the TOF.[2-5] At 230^{o}C, the redox TOF for methanol to formaldehyde over VO_4/SiO_2 is in the range of 10^{-3} 1/sec, whereas the redox TOF over VO_4/CeO_2 is in the range of 10^{0} 1/sec.[3] However, the apparent activation energy for supported vanadium oxides is approximately 20 to 21 kcal/mol regardless of the oxide support (SiO_2, Al_2O_3, TiO_2, CeO_2, Nb_2O_5, and ZrO_2).[3, 5-7]

There are no reports in literature of kinetic studies for methanol oxidation with hydrogen peroxide by $K[VO(O_2)heida]_{(aq)}$. There are, however, some very interesting reports of aromatic and alcohol compound oxidations by similar vanadium +5 peroxo-oxo compounds which indicate the complexity of the kinetic oxidation reaction by enzyme mimics. For example, at high catalyst concentrations some vanadium peroxo compounds, such as a vanadium tri-isopropoxide compound, have been found to shift from primarily oxidizing the target substrate to decomposing hydrogen peroxide.[8] This has not been investigated for the $K[VO(O_2)heida]_{(aq)}$ enzyme mimic. It has also been noted that in the presence of atmospheric oxygen, some vanadium tri-isopropoxide compounds are able to reduce atmospheric dioxygen to hydrogen peroxide through a radical process, thereby exhibiting oscillatory behavior under certain reaction conditions, but this has not been investigated for $K[VO(O_2)heida]_{(aq)}$.[9] In Chapter 3 of this dissertation, the loss of the peroxo group was observed when methanol oxidation was performed under aerobic conditions without the addition of H_2O_2. It should be noted that under the reaction conditions used throughout this investigation, oscillatory H_2O_2 behavior has not been observed for the $K[VO(O_2)heida]_{(aq)}$ enzyme mimic and the very strong Raman signal for H_2O_2 continuously decreases over the course of the reaction.

These literature reports have shown that identifying the optimal reaction conditions for studying kinetic behavior in similar aqueous enzyme mimic systems is a daunting task. The focus of this dissertation is to provide mechanistic insights into methanol oxidation by the $K[VO(O_2)heida]_{(aq)}$ enzyme mimic rather than to determine the optimal reaction conditions for $K[VO(O_2)heida]_{(aq)}$ or to elucidate its kinetic

behavior (as this type of study is an entire field of research in itself). Still, certain kinetic and reactivity experiments were warranted to support this primary goal. Specifically, an understanding of parameters such as reaction order, and an approximation of the activation energy are integral to fully understanding the mechanism of methanol oxidation by $K[VO(O_2)heida]_{(aq)}$, which is the motivation for this chapter.

The kinetics of aqueous methanol oxidation by $K[VO(O_2)heida]_{(aq)}$ were investigated in order to obtain reaction orders and the activation energy. Additionally, it should be noted that both $K[VO(O_2)heida]$ (peroxo-oxo compound) and K[VO(O)heida] (dioxo compound) contain vanadium in the +5 oxidation state. Supported mono-oxo vanadium oxide catalysts are able to oxidize methanol to formaldehyde and in the process are reduced from +5 to +4. Additionally, the catalytic mechanism for $K[VO(O_2)heida]_{(aq)}$ cycles through the $K[VO(O)heida]_{(aq)}$ dioxo compound. Therefore, the capacity of the dioxo K[VO(O)heida] compound to oxidize methanol was also investigated to see whether or not the dioxo compound contributes to the methanol oxidation mechanism.

Accurate analysis is an additional challenge to performing aqueous phase reactivity studies with labile reaction products such as HCHO. Qualitatively, formaldehyde and formic acid concentration were determined by GC. However, without access to a mass spectrometer designed for handling liquids, there was a need to develop a secondary assay in order to quantify aqueous formaldehyde product concentration. Thus, a quick, chromogenic assay was designed using 4-amino-3-hydrazino-5-mercapto-1,2,4-triazole, a reagent developed by Aldrich Chemical which is

also known as Purpald®.[10] Purpald®, which is colorless, reacts with aldehydes to create a colorless cyclic intermediate. The Purpald®/aldehyde cyclic intermediate then is oxidized by atmospheric oxygen to yield a deep purple compound which can be easily assayed by UV-vis and translated to a formaldehyde concentration by an extinction coefficient. The reaction scheme for this chromogenic technique using Purpald® is shown below in Scheme 4.1, which has been adapted from Hopps et al.[10]

Scheme 2.1 Purpald® assay for formaldehyde developed by Aldrich Chemical, adapted from Hopps et al.[10]

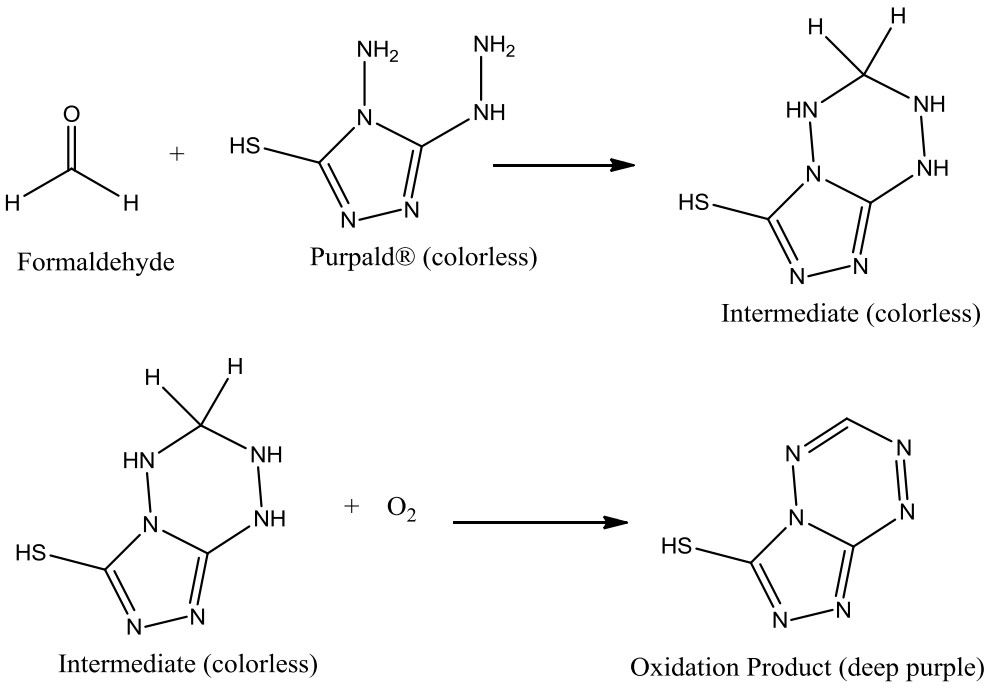

In this section, a Purpald® formaldehyde assay was first developed, and then the kinetics and reactivity of methanol oxidation by $K[VO(O_2)heida]_{(aq)}$ were investigated in order to determine the activation energy for this system, and compare and contrast to

the heterogeneous case of VO_4/SiO_2. With this Purpald® assay, methanol oxidation by $K[VO(O_2)heida]_{(aq)}$ was investigated to determine the reaction orders in both methanol and hydrogen peroxide. Then, the activation energy was determined and compared to that of the heterogeneous supported VO_4/SiO_2 catalyst. The ability for $K[VO(O_2)heida]_{(aq)}$ to perform methanol oxidation at much milder temperatures that VO_4/SiO_2 is due to the presence of the vanadium peroxo group in the enzyme mimic.

Experimental

Formaldehyde Product Concentration Assay Development

Formaldehyde (Sigma Aldrich, reagent grade, 36.5% formaldehyde solution) stock solutions were formulated in deionized water at concentrations between 0.25 mM and 0.05 mM. An alkaline Purpald® reagent solution was freshly prepared daily by dissolving 0.068 g Purpald® in 12 mL of 2N NaOH solution. 200 μL of each formaldehyde solution of known concentration was added to 800 μL of Purpald® reagent solution in a vial and agitated. Additionally, a negative control sample of 200 μL of water was added to 800 μL of Purpald® reagent solution and agitated. Each sample was allowed to rest overnight to allow the full purple color to develop.

Each vial of known formaldehyde concentration was then analyzed by Varian Cary 5E UV-vis spectrophotometer. 100 μL from each vial was added to a 1 cm path length Suprasil quartz cuvette, and diluted with 3 mL of deionized water. The cuvette was placed in the UV-vis sample beam path. Likewise, 100 μL was taken from the negative control sample, placed into a cuvette, and diluted with an additional 3 mL of

deionized water. The negative control cuvette was placed into the rear reference beam of the UV-vis and remained there during the entire sample analysis.

The UV-vis wavelength was set to 546 nm, the absorbance maxima for Purpald®/formaldehyde solutions, and an absorbance reading was taken for each known formaldehyde concentration sample.

Reaction Order in H_2O_2

The reaction order of methanol oxidation with H_2O_2 by $K[VO(O_2)heida]_{(aq)}$ was investigated prior to activation energy experiments, since the reaction order determines the formula used for the activation energy.

To determine the reaction order in H_2O_2, two separate experiments were performed, one with H_2O_2, and one without. This was a short experiment, which was completed before one full turnover was achieved.

Without H_2O_2: Two identical vials were prepared containing 0.2 grams $K[VO(O_2)heida]$ in 20 mL deionized water. One vial was designated as the negative control, the other designated as the positive sample reaction vial. Each vial was placed into a 50^oC hot water bath for approximately 30 minutes before the reagents were added. 200 μL of methanol was added to the reaction vial, and 200 μL of deionized water was added to the negative control vial. Each vial was sampled every 20 minutes, by removing 200 μL from the vial and adding to 800 μL of Purpald® reagent solution, prepared freshly as described above. The Purpald® vials were allowed to rest

overnight, and were analyzed the next day according to the dilution and UV-vis procedure described above.

With H_2O_2: Two identical vials were again prepared containing 0.2 grams K[VO(O_2)heida] in 20 mL deionized water, one the negative control, the other the positive sample reaction vial. Each vial received 100 μL of 30% H_2O_2 and then was placed into the 50^{o}C hot water bath for approximately 30 minutes before the reagents were added. 200 μL of methanol was added to the reaction vial, and 200 μL of deionized water was added to the negative control vial. Each vial was sampled every 20 minutes, and analyzed using the Purpald® technique described above.

Reaction Order in Methanol

To determine the reaction order in methanol, an experiment was performed, with increasing concentrations of methanol.

Four identical vials were prepared containing 0.2 grams K[VO(O_2)heida] in 20 mL deionized water each, one the negative control, the other three labeled as positive sample reaction vials according to the concentration of methanol each was to receive. Each vial received 100 μL of 30% H_2O_2 and then was placed into a 70^{o}C hot water bath for approximately 30 minutes before the reagents were added. 50 μL of methanol was added to one reaction vial, 100 μL to the second, and 200 μL to the third. Each vial was sampled every 20 minutes, and analyzed using the Purpald® technique described above.

Apparent Activation Energy of Methanol Oxidation by K[VO(O$_2$)heida]$_{(aq)}$

Once methanol oxidation by K[VO(O_2)heida]$_{(aq)}$ was determined to be zero-order in H_2O_2 and first-order in methanol, which is in agreement with the Mars-van Krevelen mechanism with an overall rate equation of $r = k_{rds}[CH_3OH]$, the activation energy was able to be determined using the Arrhenius equation. Two separate experiments were performed, one at 50^{o}C, the other at 70^{o}C. Each vial was sampled every 20 minutes, and analyzed using the Purpald® technique described above. Formaldehyde concentration was plotted as a function of time for the 50^{o}C experiment and for the 70^{o}C experiment. A logarithmic plot of the methanol concentration with time yields a slope of $-k_{rds}$. This method was used to determine the apparent rate constant (k_{rds}) from the slope for each experiment. The apparent rate constants at 50^{o}C and 70^{o}C were used to determine the apparent activation energy of the reaction using the Arrhenius equation.

Edge Energy of K[VO(O$_2$)heida]$_{(aq)}$

Since some recent gas-solid oxidation publications have tried to correllate the Edge Energy (E_g) value for supported vanadium oxides to general reactivity trends, we felt that determination of the E_g value for K[VO(O_2)heida]$_{(aq)}$ might be of interest to demonstrate the great difference between the enzyme mimic and supported vanadium oxides. The edge energy was determined by obtaining the UV-vis spectrum from 200-800 nm of aqueous K[VO(O_2)heida] as described in Chapter 2. The spectra were analyzed using the Kubelka-Munk[11] function $F(R_\infty)$ and evaluated for the edge energy

value (Eg) using the method of Davis and Mott[12] for vanadium oxides as further described by Gao for vanadium compounds.[13] R_∞ was evaluated by taking the negative difference between the absorbance of $K[VO(O_2)heida]_{(aq)}$ and the water baseline and taking the antilog (base 10) as shown below in equation 4.1.

$$R_\infty = 10^{\left[-\left(Abs_{sample} - Abs_{baseline}\right)\right]} \tag{4.1}$$

The Kubelka-Munk function was evaluated from R_∞, as shown by equation 4.2

$$F(R_\infty) = \frac{(1 - R_\infty)^2}{2R_\infty} \tag{4.2}$$

and equation 4.3 was plotted as a function of hν, the incident photon energy in eV.

$$y = \left[F(R_\infty) \cdot h\nu\right]^2 \tag{4.3}$$

Capacity of K[VO(O)heida] Dioxo to Perform Methanol Oxidation

The dioxo compound K[VO(O)heida] was synthesized similarly to the method described in Chapter 2. 1.5 mmol of KVO_3 was dissolved in 40 mL of deionized water, filtered, and chelated to 1.5 mmol of the heida ligand. No H_2O_2 was added. The yellow solution was divided evenly into two vials and placed in the 50°C hot water bath for approximately 30 minutes before any reagents were added. 200 μL of methanol was added to the reaction vial, and 200 μL of deionized water was added to the negative

control vial. Each vial was sampled every 20 minutes, and analyzed using the Purpald® technique described above.

Results

Formaldehyde Product Concentration Assay

The UV-vis absorbance of each Purpald®-derivatized formaldehyde sample was plotted against its formaldehyde concentration to provide a calibration curve (Figure 4.1). Using the Beer-Lambert law, a linear trend line reveals an extinction coefficient, which is specific for this assay procedure, of ε = 8333.8 (1/M). This extinction coefficient was used to determine formaldehyde concentrations in each reaction batch in subsequent experiments.

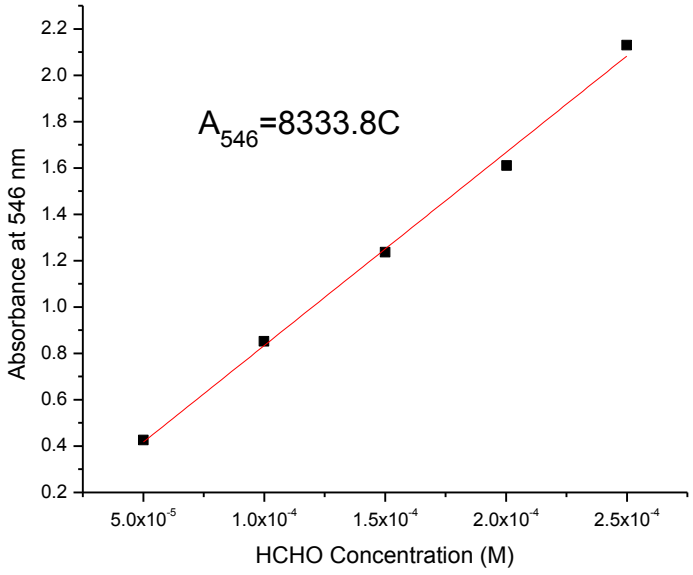

Figure 4.1 Absorbance at 546 nm of known concentration formaldehyde solutions. Used for formaldehyde assay development.

Reaction Orders

The rate of methanol oxidation by $K[VO(O_2)heida]_{(aq)}$ is shown in in Figure 4.2 and is initially unaffected by the concentration of H_2O_2, indicating that the reaction is zero-order in H_2O_2. This experiment was carried out over a period of two hours, which is shorter than the time required to achieve one turnover. It should be noted that this relatively low oxidation rate is not uncommon since other homogenous vanadium peroxo compounds (in aqueous and non-aqueous media) typically require several hours to achieve one turnover at mild temperatures.

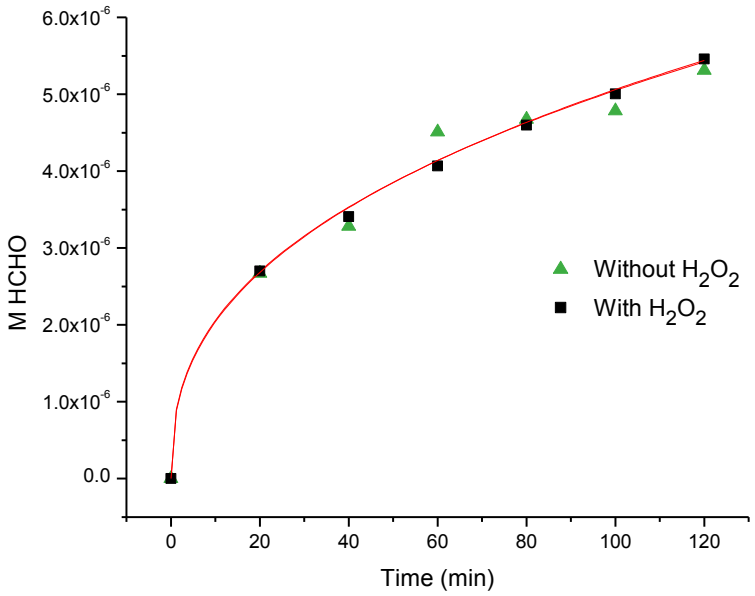

Figure 4.2 Formaldehyde product concentration with time, both with and without the addition of H_2O_2.

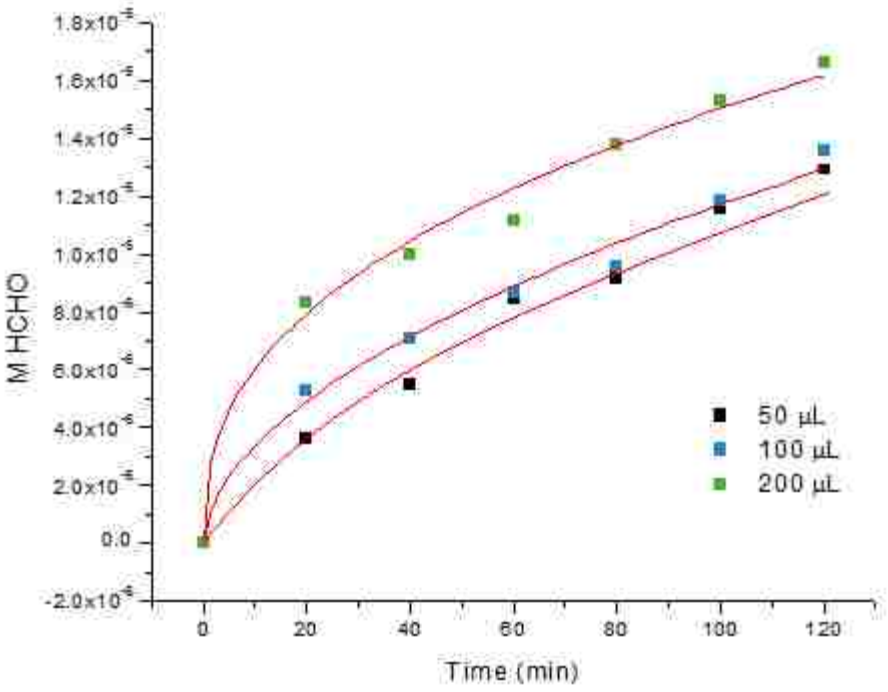

Figure 4.3 Formaldehyde product concentration with time, starting with different initial volumes of methanol, 50, 100, or 200 µL.

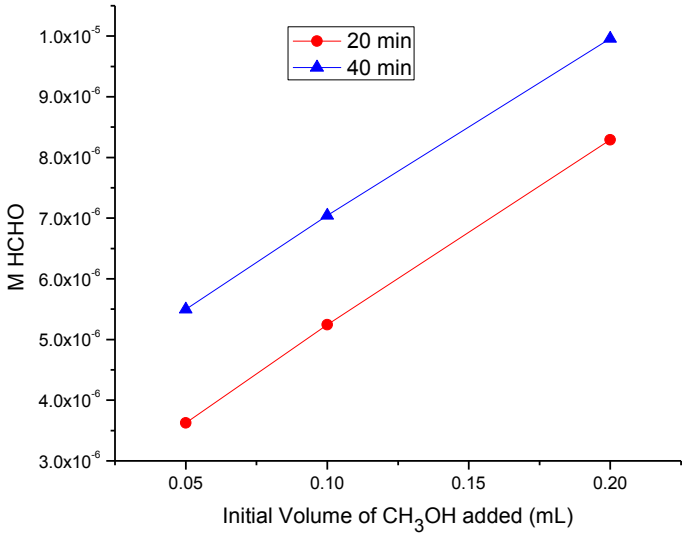

Figure 4.4 Formaldehyde product concentration versus initial volume of methanol added at two distinct time points.

The rate of methanol oxidation by $H_2O_{2(aq)}$ and $K[(VO)O_2heida]_{(aq)}$ is dependent on the aqueous concentration of methanol as shown in Figure 4.3. As the initial concentration of methanol is increased, the reaction proceeds faster. The concentration of formaldehyde produced as a function of initial quantity of methanol added to the reaction vessel is plotted at two different time points, 20 mins, and 40 mins, are presented in Figure 4.4. The data are linear with the starting methanol concentration indicating that the reaction order is first-order in aqueous methanol concentration.

Apparent Activation Energy of Methanol Oxidation by $K[VO(O_2)heida]_{(aq)}$

The oxidation of methanol by $H_2O_{2(aq)}$ and $K[VO(O_2)heida]_{(aq)}$ was determined to be zero-order in $H_2O_{2(aq)}$ and first-order in $CH_3OH_{(aq)}$ for an overall reaction order of one with a rate equation of $r=k_{rds}[CH_3OH]$. The method of determining activation energy was selected based on this finding and the formaldehyde product concentration as a function of time for at two different reaction temperatures, 50°C and 70°C, are presented in Figure 4.5.

The data for each temperature experiment were plotted as a logarithmic function of the methanol concentration with time to obtain k_{rds}. A plot of $\ln[CH_3OH]$ versus time for each temperature is shown in Figure 4.6, which yields $slope = -k_{rds}$. The apparent rate constant for 50°C was found by this method to be $k_{rds50}= 9x10^{-8}$ min^{-1}, and the apparent rate constant for 70°C was found to be $k_{rds70}= 5x10^{-7}$ min^{-1}.

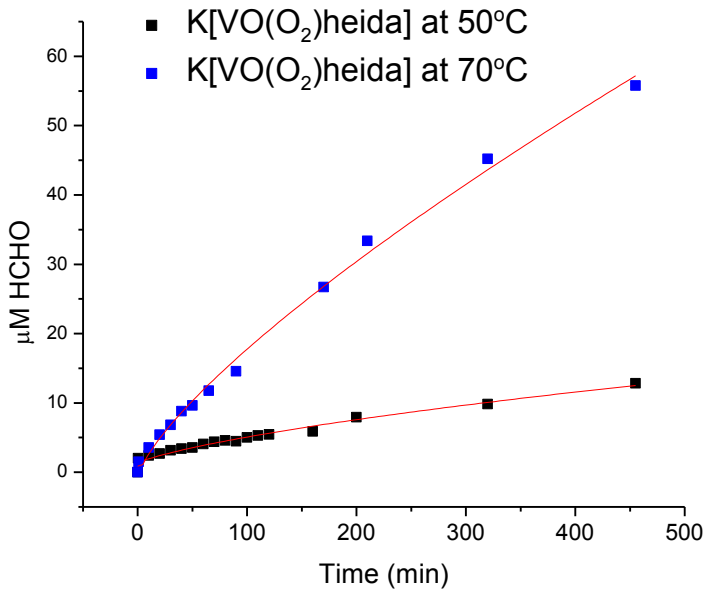

Figure 4.5 Formaldehyde product concentration with time at 50°C and 70°C.

To determine the apparent activation energy (E_{app}) for methanol oxidation by K[VO(O_2)heida]$_{(aq)}$, the following first-order kinetic equation was used.

$$\ln\left(\frac{k_{rds70}}{k_{rds50}}\right) = \frac{E_{app}}{R}\left(\frac{1}{T_{50}} - \frac{1}{T_{70}}\right) \tag{4.4}$$

Plugging in the apparent rate constant for each temperature, the absolute reaction temperature, and the gas constant (R)

$$\ln\left(\frac{5\times10^{-7}}{9\times10^{-8}}\right) = \frac{E_{app}}{8.3145}\left(\frac{1}{323.15} - \frac{1}{343.15}\right) \tag{4.5}$$

yields an apparent activation energy of E_{app} = 79 kJ/mol or 19 kcal/mol for methanol oxidation by $H_2O_{2(aq)}$ and K[VO(O_2)heida]$_{(aq)}$.

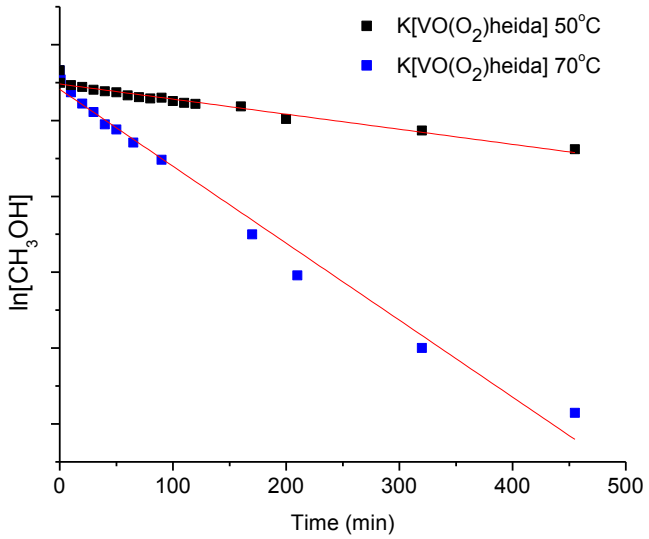

Figure 4.6 Log plot of decreasing methanol concentration with time for different reaction temperatures, 50°C, and 70°C.

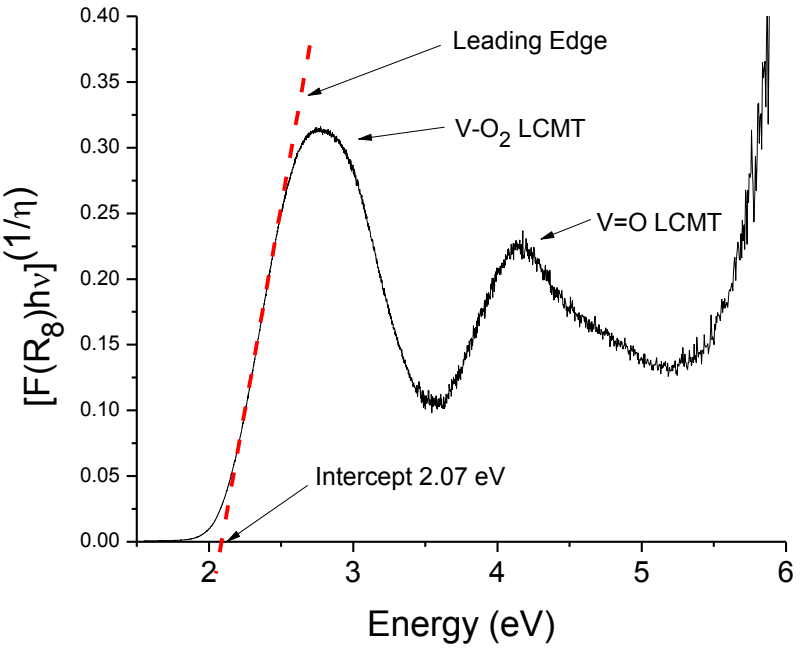

Figure 4.7 Kubelka-Munk transform of the UV-vis absorbance spectrum of $K[VO(O_2)heida]_{(aq)}$. Determination of the E_g value is demonstrated by the red dotted line which extrapolates the leading linear edge of the vanadium peroxo LCMT to the abscissa.

Edge Energy of K[VO(O_2)heida]$_{(aq)}$

The UV-vis Kubelka-Munk plot vs. hν is given in Figure 4.7. Two ligand to metal charge transition (LMCT) bands are present in the Kubelka-Munk transformed absorbance spectrum of K[VO(O_2)heida]$_{(aq)}$: one for the V=O oxo group at 300 nm (4.14 eV); and one for the V-O_2 peroxo group at 470 nm (2.64 eV). The edge energy (E_g) was found to be 2.07 eV, determined by extrapolating the leading linear edge for the V-O_2 peroxo LCMT and is reflected by the red line in Figure 4.7.

Capacity of K[VO(O)heida]$_{(aq)}$ Dioxo to Perform Methanol Oxidation

The dioxo compound K[VO(O)heida]$_{(aq)}$ was not found to oxidize methanol at any significant rate in the absence of $H_2O_{2(aq)}$. In the presesence of $H_2O_{2(aq)}$, the oxidation of the dioxo K[VO(O)heida] to the active peroxo-oxo K[VO(O_2)heida] was found to be nearly instantaneous. Therefore, we have concluded that the dioxo compound K[VO(O)heida] does not contribute to methanol oxidation activity.

Discussion

Formaldehyde Product Concentration Assay

The plot of absorbance versus concentration for known formaldehyde concentrations was linear. A linear trend line indicates that formaldehyde concentrations in a reaction solution are able to be determined by the above Purpald® dilution procedure and dividing the absorbance at 546 nm by the extinction coefficient ε = 8333.8 (1/M).

Purpald® does not react with methanol or hydrogen peroxide, therefore, this assay is unaffected by the reaction substrates. However, a major disadvantage of this assay is that Purpald® does not react with formic acid. In Chapter 3, we reported that formaldehyde is not the only oxidation product produced by methanol oxidation by $K[VO(O_2)heida]_{(aq)}$; formic acid is also produced. Since this Purpald® assay is only able to quantify formaldehyde product concentration and not formic acid concentration, it cannot be used to quantify absolute reactivity and turn over frequency for comparison to the heterogeneous case of VO_4/SiO_2. However, this Purpald® assay can be used for determination of reactivity properties by $K[VO(O_2)heida]_{(aq)}$ where reaction scenarios involving methanol oxidation by the same system under similar conditions are compared to each other, so that the formic acid contribution can be minimized as a variable. For example, when determining the activation energy of methanol oxidation by $K[VO(O_2)heida]_{(aq)}$, two reaction scenarios are compared to each other; two experiments with identical experimental reaction conditions with the exception of one parameter, the reaction temperature.

Reaction Order

Methanol oxidation by $K[VO(O_2)heida]_{(aq)}$ has been shown in Chapter 3 to take place via a Mars van-Krevelen mechanism. Mars van-Krevelen is inherently zero-order in the oxidant/re-oxidant, and first order in the substrate, indicating that it is first- order overall.[14] Methanol oxidation by $K[VO(O_2)heida]_{(aq)}$ is seen in Figure 4.2 to be unaffected by H_2O_2 concentration, which makes the reaction zero-order in H_2O_2. The K[VO(O)heida] dioxo compound was not found to contribute to formaldehyde

production. Since conversion of the dioxo K[VO(O)heida] to the peroxo-oxo K[VO(O_2)heida] is almost instantaneous, the contribution of the dioxo component is negligible for methanol oxidation.

The linear dependence of formaldehyde production on the concentration of methanol (shown in Figure 4.4) demonstrates that methanol oxidation by $H_2O_{2(aq)}$ and K[VO(O_2)heida]$_{(aq)}$ is first-order in methanol. This is consistent with Mars van-Krevelen kinetics. Therefore, the rate expression can be represented by equation 4.6 below where k_{rds} is the temperature dependent apparent rate constant for the rate-determining-step.

$$r = k_{rds}[CH_3OH] \tag{4.6}$$

Apparent Activation Energy of Methanol Oxidation by K[VO(O_2)heida]$_{(aq)}$

For gas phase methanol over supported vanadium oxides, E_{app} is approximately 21 kcal/mol, regardless of the oxide support (SiO_2, Al_2O_3, TiO_2, CeO_2, Nb_2O_5, and ZrO_2).[3, 5-7] It is important to note that the apparent activation energy (E_{app}) is the sum of the true activation energy (E_{act}) plus the heat of adsorption (ΔH_{ads}) as seen below in equation 4.7.

$$E_{app} = E_{act} + \Delta H_{ads} \tag{4.7}$$

When activation energy experiments, such as those for VO_4/SiO_2, are performed at steady state in a plug flow reactor prior to catalytic active site saturation by the methanol substrate, E_{app} contains a ΔH_{ads} component. Temperature programmed desorption (TPD) experiments on VO_4/SiO_2 have revealed that ΔH_{ads} is approximately

-13.3 kcal/mol,[4] which makes Eact approximately 34.4 kcal/mol for the C-H bond breaking step for methanol oxidation by VO_4/SiO_2.[3, 4]

Aqueous methanol oxidation by $K[VO(O_2)heida]_{(aq)}$ was performed as a batch reaction, therefore at steady state, the V sites for methanol adsorption are saturated with surface V-OCH_3 species. In this case where all adsorption sites are saturated, the ΔH_{ads} contribution is zero. Therefore, $E_{app} = E_{act}$ for methanol oxidation by $K[VO(O_2)heida]_{(aq)}$ at steady state in a batch reactor. For liquid phase methanol oxidation by $K[VO(O_2)heida]_{(aq)}$ E_{act} is equal to 19 kcal/mol.

In Chapter 3, the activation energy for proton transfer from the V-methoxy to the peroxo group was computed using density functional theory (DFT). DFT results indicated that the activation barrier for this C-H bond breaking step was approximately 18 kcal/mol. This agrees with experimental results. Thus, comparable energy barriers for the C-H bond breaking step by the V-peroxo group were found by both theory and experiment.

Although the reaction is fairly slow, why is $K[VO(O_2)heida]$ able to perform one-electron oxidations at all at 50°C, whereas vanadium oxides such as VO_4/SiO_2 are unable to produce any formaldehyde until reaction temperatures approach 230°C? The ability of $K[VO(O_2)heida]_{(aq)}$ to perform methanol oxidation at mild temperatures and the inability of VO_4/SiO_2 to perform methanol oxidation at mild temperatures is not explained by the E_{app}, however, it is explained by E_{act}. We believe the answer is that $K[VO(O_2)heida]_{(aq)}$ possesses a vanadium peroxo group which drops E_{act} to 19 kcal/mol, whereas VO_4/SiO_2 does not contain a vanadium peroxo group and therefore possesses an E_{act} of 34.4 kcal/mol.

In the field of heterogeneous catalysis, researchers sometimes try to correlate reactivity with the Edge Energy. The Edge Energy (E_g) reflects the difference in energy between the lowest unoccupied molecular orbital (LUMO) and the highest occupied molecular orbital (HOMO). Gao *et al*. have shown that, for heterogeneous vanadium oxide catalysts, the E_g value decreases as domain size (i.e. extent of vanadia polymerization) increases.[15] In a recent publication, Tian *et al*. expressed that although the E_g value typically decreases as the redox TOF increases, there is no link between the surface metal oxide domain size and redox TOFs.[16] This referenced publication states that the correlation of lower E_g value to redox TOF is related to another factor not addressed in that publication such as the support effect.[16] In other words, the E_g value for heterogeneous vanadium oxide catalysts is not affected by domain size, but by the electronegativity of the oxide support ligand (SiO_2, Al_2O_3, TiO_2, CeO_2, Nb_2O_5, or ZrO_2). Therefore, any link between the E_g value and TOF is a reflection of the support effect.

A publication in the same vein regarding the support (ligand) effect by Conte *et al*. points out that a vanadium peroxo compound with a lower E_g performs 1-electron oxidations more efficiently than vanadium peroxo compounds with high E_g values.[17] The E_g value for $K[VO(O_2)heida]_{(aq)}$ is 2.07 eV and is significantly lower than purely isolated site dehydrated 1% VO_4/SiO_2 which has an E_g value of 3.60 eV[13] However, this lower energy is due solely to the presence of the vanadium peroxo group. Without the contribution of the peroxo group, the V=O LMCT energy would fall above 3 eV. Therefore, it is not a fair comparison to equate the E_g value for $K[VO(O_2)heida]_{(aq)}$ to

the E_g value for VO_4/SiO_2, since the respective E_g values are determined by two totally different chemical groups.

The goal of this part of the discussion is to separate two factors which affect the E_g value: the support/ligand effect, and functional/oxidizing group effect. For $K[VO(O_2)heida]_{(aq)}$ the HOMO occurs at a significantly lower energy when it is determined by a peroxo group, instead of an oxo group. For solid supported vanadium oxides, if the LUMO is determined by the vanadium metal d-orbital, and the HOMO is determined by the π-orbital of the axial mono oxo group, then the E_g value will only change by degree of electronegativity provided by the oxide support (within the limits of what the oxo group will permit). For $K[VO(O_2)heida]$, we have the additional factor of the peroxo group. If, for $K[VO(O_2)heida]$, the LUMO is still determined by the vanadium d-orbital, but now the HOMO is determined by the π-orbital of the peroxo group, the E_g value cannot be expected to fall within the same range as that of a solid supported vanadium oxide catalyst. The E_g value may still change in response to the degree of electronegativity provided by the ligand support, as suggested by Conte et *al.*[17], but this time within the limits of what a peroxo group may permit. It is important in future studies to only equate the E_g values of vanadia compounds with the same chemical groups.

Conclusions

Methanol oxidation by $K[VO(O_2)heida]_{(aq)}$ has been shown to be first-order in methanol and zero-order in H_2O_2, making the overall reaction order first-order. This is consistent with Mars-van Krevelen kinetics. This is similar to methanol oxidation by

the heterogeneous catalyst VO_4/SiO_2. Gas phase methanol oxidation by VO_4/SiO_2 also follows a Mars-van Krevelen mechanism and is first-order in methanol and zero-order in O_2 for an overall reaction order of 1.

The E_{act} for liquid phase methanol oxidation by $K[VO(O_2)heida]_{(aq)}$ was found experimentally to be 19 kcal/mol which is in agreement with the activation energy barrier calculated by DFT methods of 17.71 kcal/mol (see Chapter 3). The E_{app} for gas phase methanol oxidation by supported VO_4/SiO_2 is approximately 34.4 kcal/mol.[3-7] This indicates why $K[VO(O_2)heida]_{(aq)}$ is able to perform methanol oxidation at low temperatures, but VO_4/SiO_2 is unable to produce any formaldehyde until temperatures approaching 230^{o}C.

References

(1) Wong, G. S.; Concepcion, M. R.; Vohs, J. M. *J Phys Chem B* **2002**, *106*, 6451-6455.

(2) Wachs, I. E.; Deo, G.; Juskelis, M. V.; Weckhuysen, B. M. In *Methanol oxidation over supported vanadium oxide catalysts: New fundamental insights about oxidation reactions over metal oxide catalysts from transient and steady state kinetics;* Studies in Surface Science and Catalysis; Elsevier: Vol. Volume 109, pp 305-314.

(3) Deo, G.; Wachs, I. E. *Journal of Catalysis* **1994**, *146*, 323-334.

(4) Burcham, L. J.; Briand, L. E.; Wachs, I. E. *Langmuir* **2001**, *17*, 6164-6174.

(5) Feng, T.; Vohs, J. M. *Journal of Catalysis* **2002**, *208*, 301-309.

(6) Wachs, I. E.; Deo, G.; Vuurman, M. A.; Hu, H.; Kim, D. S.; Jehng, J. -. *J Mol Catal. A: Chem.* **1993**, *82*, 443.

(7) Oyama, S. T.; Radhakrishnan, R.; Seman, M.; Kondo, J. N.; Domen, K.; Asakura, K. *J Phys Chem B* **2003**, *107*, 1845-1852.

(8) Bonchio, M.; Conte, V.; Di Furia, F.; Modena, G.; Moro, S.; Eckert, H. *Inorg. Chem.* **1994**, *33*, 1631.

(9) Bonchio, M.; Bortolini, O.; Carraro, M.; Conte, V.; Primon, S. *J. Inorg. Biochem* **2000**, *80*, 191.

(10) Hopps, H. B. *Aldrichimica Acta* **2000**, *33*, 28-30.

(11) Kubelka, P.; Munk, R. *Z. Tech. Phys.* **1931**, *12*.

(12) Davis, E. A.; Mott, N. F. *Philos. Mag.* **1970**, *22*, 903-922.

(13) Gao, X.; Wachs, I. E. *J. Phys. Chem. B* **2000**, *104*, 1261-1268.

(14) Mars, P.; van Krevelen, D. W. *Spec. Suppl. Chem. Eng. Sci.* **1954**, *3*, 41-57.

(15) Gao, X.; Jehng, J.; Wachs, I. E. *Journal of Catalysis* **2002**, *209*, 43-50.

(16) Tian, H.; Ross, E. I.; Wachs, I. E. *J. Phys. Chem. B* **2006**, *110*, 9593-9600.

(17) Conte, V.; Di Furia, F.; Moro, S. *Journal of Molecular Catalysis A: Chemical* **1995**, *104*, 159-169.

Chapter 5: Vanadium Haloperoxidases

In light of the successful experiments using the vanadium haloperoxidase mimic K[VO(O_2)(heida)], the final step in bridging the gap between heterogeneous catalysis and biocatalysis is studying the vanadium haloperoxidase family of enzymes. As discussed first in Chapter 1, vanadium haloperoxidases (VHPOs) are a family of enzymes characterized by their vanadate-dependent active site. They are named for their ability to catalyze the two-electron oxidation of halide ions (Cl^-, Br^-, or I^-) in the presence of hydrogen peroxide to produce hypohalous acids (HOCl, HOBr, or HOI).[1]

$$H^+ + X^- + H_2O_2 \rightarrow HOX + H_2O \qquad (5.1)$$

There is no known form of vanadium fluoroperoxidase simply because VHPOs are not strong enough to oxidize fluoride, but the other three forms of vanadium haloperoxidases can be extracted from many types of algae and terrestrial fungus. The chloroperoxidase form can be extracted from fungus such as *Curvularia inaequalis*, the bromoperoxidase form of the enzyme can be extracted from brown and red algae such as *Corallina officinalis* and *Ascophyllum nodosum*, and the iodoperoxidase enzyme can be found in green algae such as *Acrosiphonia sonderi*.[2-4] The molecular mass and number of amino acid residues for each type of VHPO varies from species to species. However, on average, the molecular mass of a vanadium haloperoxidase monomer is approximately 73.4 kDa. The bromo- and chloro- forms of vanadium haloperoxidase have nearly identical active site geometries including the amino acid residues present in the coordination sphere around the vanadium oxide cofactor.[5-7] Figure 5.1 is a ribbon

type diagram of the monomeric vanadium chloroperoxidase structure from the fungus *Curvularia inaequalis* as published by Butler et al.[2]

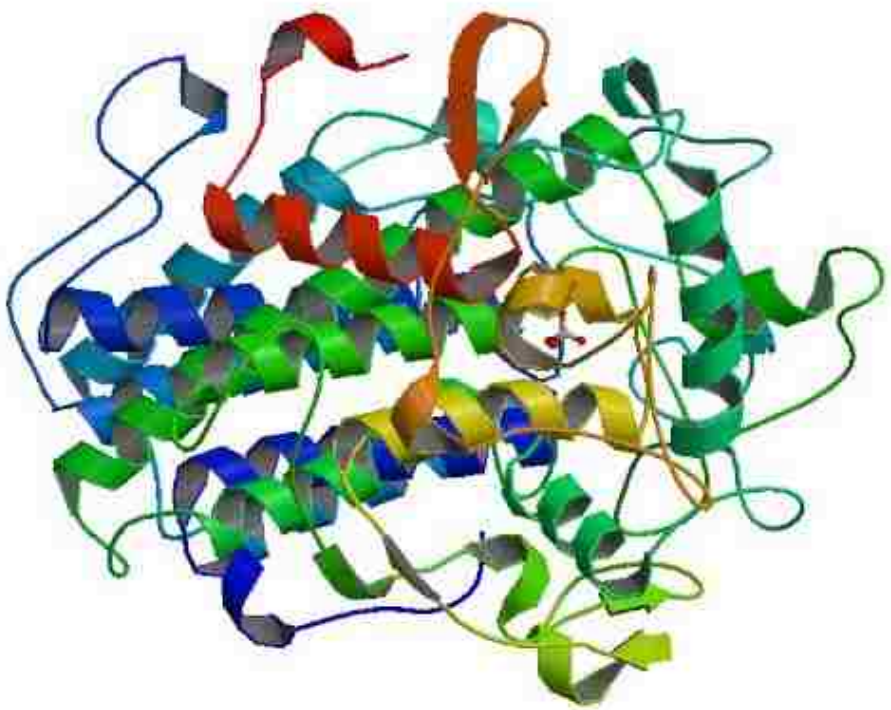

Figure 5.1 Ribbon structure of vanadium chloroperoxidase monomer from the fungus *Curvularia inaequalis.*[2]

Recombinant vanadium chloroperoxidase (VCPO) from fungal species such as *Curvularia inaequalis*, can be expressed as the apoenzyme in *Saccharomyces cerevisiae* or *E. Coli*, and dialyzed against orthovanadate solution to form the holoenzyme.[8] Affinity of the vanadate cofactor for the native form of VCPO from *Curvularia inaequalis* is around K_d = 140 nM at pH 8.[9] Vanadium bromoperoxidases (VBPO) from seaweed species such as *Corallina officinalis* are typically present as dodecamers with slight differences in each protein chain, and are therefore more easily obtained by extraction and isolation from the seaweed.[10] The apoenzyme for VBPO has a higher

affinity for vanadate with K_d values ranging from 35 to 55 nM for the native form near pH 8.[11, 12]

Despite differences in amino acid sequence, the vanadate cofactor and amino acid coordination sphere around the vanadium cofactor in each species of vanadium haloperoxidase enzyme is highly conserved with little variation in the active site residues between different VHPO species.[7]

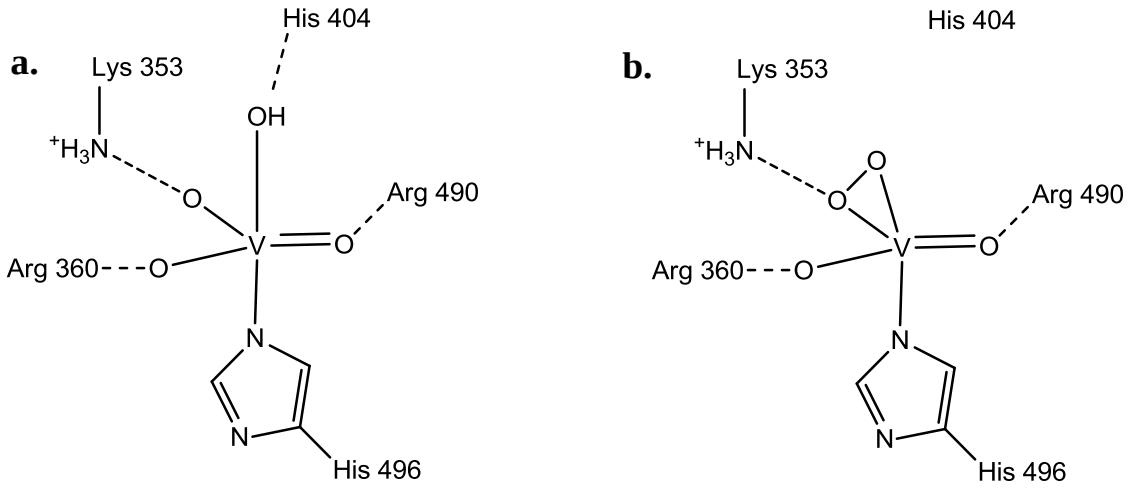

Figure 5.2 Vanadium chloroperoxidase vanadium cofactor in **a.** the native form and **b.** in the active form once exposed to hydrogen peroxide.

As seen in Figure 5.2 a, the native form of the vanadium active site for VCPO exists in a trigonal bi-pyramidal coordination. In Figure 5.2, the amino acid residues which are displayed in the area around the vanadium active site are labeled with the corresponding number where the residues are located in the chloroperoxidase enzyme peptide chain. The corresponding residues for the bromoperoxidase enzymes are nearly super imposable, as seen in Chapter 1, Figure 1.1. There is little variation in the amino

acid residues surrounding the vanadate cofactor between the chloroperoxidase and the bromoperoxidase enzymes.[7] The chloroperoxidase equatorial V-O bonds possess an average bond length of approximately 1.65 Å, and the bromoperoxidase equatorial V-O bonds possess an average bond length of 1.6 Å.[12] At this bond length, it can be suggested that the equatorial V-O bonds are considered "short bonds" that have double bond resonance structures. Additionally, ^{51}V MAS NMR spectroscopy and DFT agree that the native form the vanadate cofactor possesses two oxo bonds in the equatorial plane, a hydroxo in the apical position, and also probably an additional hydroxyl in the third equatorial position.[7, 13, 14] The vanadate entity is bound covalently at the basal position to a histidine residue for both VCPO and VBPO. The apical V-O bond possesses a bond length of 1.93 Å for the VCPO, and about 1.8 Å for the VBPO, indicating that the apical group is most likely a hydroxide.[12] In the native form, the vanadate cofactor is negatively charged, but is balanced by hydrogen bonding.[12] The apical hydroxide is hydrogen bound to the nucleophilic imidazole component of the histidine 404 residue in the chloroperoxidase enzyme and of the histidine 418 residue in the bromoperoxidase enzyme. The apical hydroxide may also experience hydrogen bonding with two water molecules in aqueous environments, which are not shown in Figure 5.2. The VCPO equatorial oxygen atoms experience hydrogen bonding to the lysine, arginine and serine residues in the sphere around the active vanadate moiety.[7] The degree of hydrogen bonding to the remaining amino acid residues in Figure 5.2 is debated in other publications.[15, 16] It has been suggested that the hydrogen bond between the apical hydroxide and the histidine 404/418 residue for chloro/bromo peroxidase is able to make the hydroxide more nucleophilic, contributing to the activity of the

enzyme. When vanadium haloperoxidases are exposed to hydrogen peroxide, the apical oxygen becomes deprotonated by the histidine 404/418 and a water molecule dissociates from the active site.[3, 15, 17] The vanadate cofactor converts to the active peroxo-oxo structure seen in Figure 5.2 b, similar in central structure to the peroxo-oxo form of the K[$VO(O_2)$(heida)] mimic compound. Affinity of the VCPO apoenzyme for the activated peroxo-oxo form of the vanadate cofactor was found to be approximately 200 fold stronger than the affinity of the native form of the vanadate cofactor.[18]

Site directed mutagenesis studies were also performed on the amino acid residues surrounding the vanadate cofactor for vanadium chloroperoxidase, histidine 496, lysine 353, arginine 360, and arginine 490. It was found that when the His-496 residue is mutated to an alanine, the enzyme completely loses its activity since the covalent bond to the vanadate is removed. The vanadate was found to dissociate from the protein scaffold. When the remaining three mutated residues were changed to alanine residues, the enzyme lost its ability to oxidize chloride, but it retained the ability to oxidize bromide. This study has shown that the His-496 residue is essential to enzyme activity.[8]

A directed evolution study by Hasan et al. identified a vanadium chloroperoxidase mutant which exhibited a 100-fold increase in halide oxidization activity at pH 8. In this experiment the proline 395 residue was changed to an aspartic acid residue, the leucine 241 was changed to a valine residue, and the threonine 343, was changed to an alanine residue. It has also been suggested that the lysine 353 and

the phenylalanine 397 residues are essential for biocatalytic activity and that these residues could be fine-tuned to obtain a more active enzyme.[16]

The proposed minimal reaction scheme for the oxidation of a halide to the hypohalous acid in the presence of hydrogen peroxide by vanadium chloroperoxidase is shown in Figure 5.3. The active vanadium site is shown coordinated to the three oxygen atoms in the equatorial position (v1, v2, and v3), the apical hydroxyl (v4), and the N atom from the basal histidine residue. The peroxide functionality is formed in step C. Halide oxidation occurs via nucleophilic attack of the incoming halide on the peroxo group as seen in step D. The hypohalous acid is released and the enzyme returns to its native form in steps E and F.[8] This proposed mechanism for halide oxidation by K[VO(O_2)(heida)].

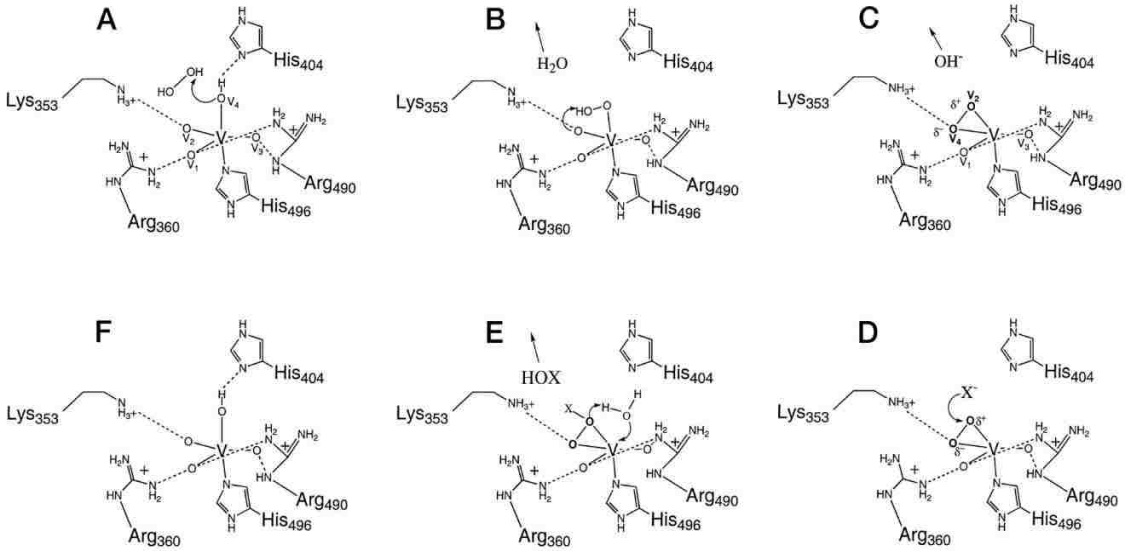

Figure 5.3 Proposed minimal reaction scheme for the oxidation of a halide catalyzed by vanadium chloroperoxidase adapted from Hemrika et al.[8]

It has been suggested that, instead of occurring via nucleophilic attack of the halide directly on the peroxo group, that the halide first coordinates to the vanadium center, and then interacts with the peroxo group.[19] This has been investigated using EXAFS (Extended X-ray Absorption Fine Structure), where a solution of vanadium chloroperoxidase and NaCl was examined for evidence of a V-Cl bond.[20] No evidence of a V-Cl bond was seen using EXAFS, however this experiment was performed using the native form of VCPO, without any added hydrogen peroxide to form the active peroxo structure. Therefore, this experiment was not able to determine whether or not a V-Cl bond exists. EXAFS on VCPO with both H_2O_2 and NaCl would have proven to be difficult, according to a personal conversation with Professor Ron Wever from University of Amsterdam, because any excess H_2O_2 in the sample would react with halides present resulting in a burst of singlet oxygen. This causes foaming in the sample and makes EXAFS analysis difficult (We encountered this foaming phenomenon in our experiments as well). H_2O_2 disproportionation by VHPOs has been shown to only occur if halides are present; it is not catalase activity.[21, 22] Therefore, this recent EXAFS study is only able to confirm the order of several steps in the mechanism of halide oxidation by VCPO: formation of the peroxo group must occur first, before interaction with the incoming halide. The halide does not first coordinate to the vanadium in the native form before it interacts with hydrogen peroxide to form the vanadium peroxo group. This study, however, is not able to indicate if halide coordination directly to the vanadium center may occur after the formation of the active form vanadium peroxo group.[20]

The mechanism for sulfoxidation has not been investigated directly (only indirectly through DFT studies on $K[VO(O_2)(heida)]$[23-25]) but reactivity and selectivity for asymmetric sulfoxidation by VCPO and VBPO have been investigated.[1, 26-28] The mechanism for the VHPO catalyzed oxidation of methanol has not been investigated, but the mechanism is expected to be similar to the mechanism for the oxidation of methanol to formaldehyde by $K[VO(O_2)(heida)]_{(aq)}$ (see Chapter 3).

In addition to the above mentioned ^{51}V MAS NMR, EXAFS/XANES, and X-ray crystallography studies, EPR and UV-vis studies have been performed on VBPO and VCPO. EPR studies were of limited value, since vanadium in the +5 oxidation state is not paramagnetic and therefore, not observable by EPR spectroscopy.[9] EPR did, however, indicate that the VBPO vanadate cofactor is not reduced to the +4 oxidation state during catalytic turnover.[9] This is not surprising, since the peroxo-oxo active form of the enzyme and the dioxo native form are both V^{+5}. UV-vis spectroscopy also indicated no presence of V^{+4}. Additionally, the UV-vis spectrum reveals a band at 315 nm for the native dioxo form of the VCPO enzyme, which does not appear to be present for the apoenzyme without the vanadate cofactor.[18] The band at 315 nm was found to disappear when VCPO was converted to the active peroxo-oxo form when exposed to H_2O_2.[18]

In this Chapter, we have taken the first steps towards characterization of the vanadate cofactor of VHPOs by Raman and ATR-IR spectroscopy. However, we have only scratched the surface of the capabilities of these techniques for enzyme characterization. Raman spectroscopy has been called the "Sleeping Giant in Structural

Biology,"[29] however, Raman characterization of the VHPO enzymes has proven to be more challenging than previously thought. Here we report on the challenges we faced in characterizing VCPO and VBPO by Raman and ATR-IR spectroscopy.

Experimental

Vanadium Chloroperoxidase and Bromoperoxidase

With the gracious help of our collaborators, Prof. Polenova's group at University of Delaware, Ms. Minyue Li and Ms. Jenna Yehl, vanadium chloroperoxidase was produced recombinantly from *E. coli* using the expression[16] and purification[8] procedures published by the Wever group at University of Amsterdam. Vanadium chloroperoxidase (VCPO) from the fungus *Curvularia inaequalis* was chosen specifically for recombinant production because this form of VCPO is a monomer in its active form. VCPO was expressed as the apoenzyme, without the vanadate cofactor, and vanadium was incorporated by adding K_3VO_4 to the apoenzyme after purification. VCPO was formulated in 25mM Tris-acetate, pH 8.1. VCPO enzymatic activity was assayed using the standard monochlorodimedon (MCD) UV-vis absorbance method published by Hemrika et al.[8]

VBPO which has been extracted from *Corallina officinalis* was obtained from Sigma Aldrich as a lyophilized powder with 2-(N-morpholino)ethanesulfonic acid buffer salts (MES). Extraction of VBPO from the seaweed *Corallina officinalis* is often complicated by the presence of phycoerythrin, which is a major component of the photosynthesis system of *C. officinalis.* Phycoerythrin tends to co-purify with VBPO

and if present in the final sample, will cause fluorescence in the Raman spectrum, among other interference bands. In order to attempt to minimize the presence of intact phycoerythrin in the VBPO sample, VBPO was first heat treated for two hours in a hot water bath at 70^{o}C according to the procedure published by Zhang et al, since phycoerythrin is found to denature at 40-45^{o}C.[30] VBPO, which is a very hardy enzyme, is stable at 70^{o}C.[31] Both VCPO and VBPO were activated by adding approximately 0.5 μmol H_2O_2 per mg of enzyme, converting the enzyme from the native form to the active form. Isotpopic $H_2{}^{18}O_2$ (90 atom % was purchased from ICON Isotopes) was also used to aid in the identification of Raman bands. If foaming due to H_2O_2 disproportionation was observed, the sample was allowed to settle for 1-2 minutes before performing spectroscopy experiments.

UV-vis Spectroscopy

Transmission UV-vis spectroscopy was used to identify the native and active peroxo form of VBPO and VCPO. Results were compared against current literature to ensure the integrity of the samples.[18] Active and Native VHPO was examined using a Varian Cary 5E UV-vis spectrophotometer. First, the corresponding buffer blank baseline spectrum was prepared over the range of 200-800 nm under ambient conditions, and the spectrum of each aqueous catalyst sample was collected from 200-800 nm under ambient conditions. If needed, the UV-vis spectra were analyzed using the Kubelka-Munk function $F(R_\infty)$ in order to aid in better visualization of broad bands, however this was not typically needed, since VHPOs produce rather strong UV-vis bands.[32]

Raman Spectroscopy

Raman spectra of VBPO and VCPO were collected with a Horiba-Jobin Yvon LabRam-HR spectrometer equipped with a confocal microscope, 2400/900 grooves/mm gratings, and a notch filter. Three laser excitations were used to experimentally determine the ideal wavelength for use with VHPOs. The visible laser excitation at 532 nm (green) was supplied by a Yag doubled diode pumped laser (20 mW), the visible laser excitation at 442 nm (blue) and 325 nm (UV) were supplied by a He-Cd laser. The scattered photons were directed and focused onto a single-stage monochromator and measured with a UV-sensitive liquid nitrogen-cooled CCD detector (Horiba-Jobin Yvon CCD-3000V). For the collection of enzyme spectra, a single droplet was placed on a glass or CaF_2 slide and left for about one minute, to permit enzyme migration to the exterior of the droplet via a coffee ring effect. The laser was focused near the edge of the droplet, but just slightly below the droplet surface in order to accommodate droplet spreading. MES and 25 mM Tris-acetate buffer blanks were also investigated by Raman spectroscopy using each laser in order to identify interfering buffer bands.

ATR-IR Spectroscopy

The ATR-IR spectra for VCPO and VBPO were recorded using a Thermo Nicolet 8700 IR spectrometer equipped with a liquid nitrogen cooled DTGS detector and Harrick Horizon ATR attachment on a zinc selenide crystal. The spectrum was collected in the 400-4000 cm^{-1} range with 72 scans, and the corresponding MES or Tris-acetate buffer blank spectrum was background subtracted.

Results

UV-vis Spectroscopy

Native form and active form VBPO was examined by UV-vis spectroscopy and compared to the UV-vis results for VCPO published by Renirie et al.[18] UV-vis results are shown in Figure 5.4 and our results are in agreement. Native VBPO exhibits a band at 270 nm which is probably due to absorbance by aromatic amino acids, and a broad band between 300 and 350 nm most likely indicating V^{+5}. This is in agreement with findings for VCPO.[18] When VBPO is converted to the active form by adding H_2O_2, the band at 270 nm decreases and red-shifts slightly to 280 nm, and the V^{+5} band red shifts to approximately 350 nm. There is no indication of a V-peroxo band at 470 nm as there

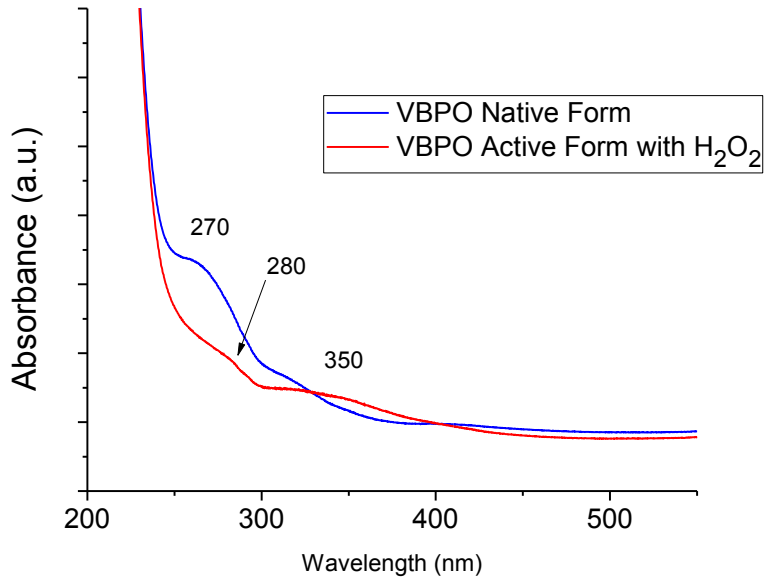

Figure 5.4 UV-vis spectra for native and active form VBPO showing the native form band at 270 nm which decreases and the 350 nm band which increases when VBPO is activated by H_2O_2.

was for K[VO(O_2)(heida)]. We thought it was interesting that no V-peroxo band was observed at 470 nm, so we became suspicious of potential differences in the vanadium cofactor between the crystal form (which indicates a V-peroxo by X-ray crystallography) and the free aqueous form. If the X-ray crystallography indicates the active form possesses a V-peroxo group, is it possible that in the aqueous form it is actually converted to a V-hydroperoxo (V-O-O-H)? In order to test this suspicion, we suspended native and active form VBPO in 25% glycerol buffer in order to closer simulate the crystal form of the enzyme. The UV-vis spectra for native and active VBPO in 25% glycerol is shown in Figure 5.5. However, active form VBPO in 25% glycerol, exhibits no band at 470 nm. The broad 350 nm band appears in the same position.

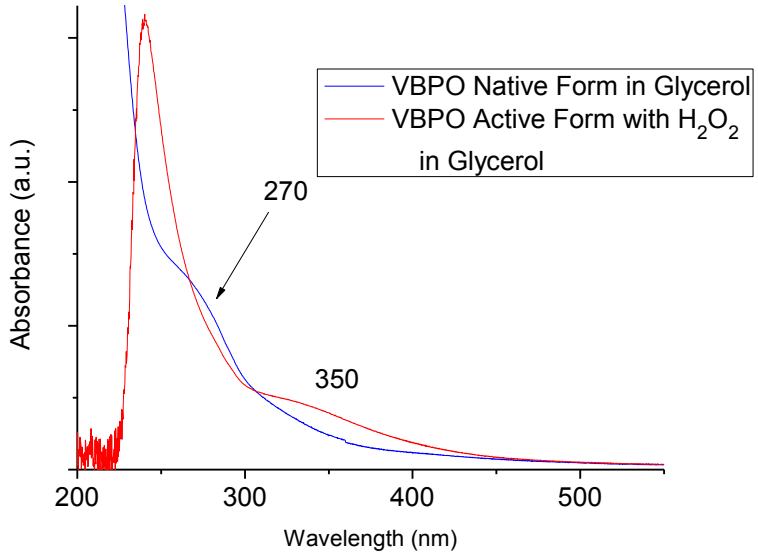

Figure 5.5 UV-vis spectra for native and active form VBPO in 25% glycerol conditions to simulate crystal form conditions. The 350 nm band is still present, and no band is observed at 470 nm for active form VBPO in 25% glycerol.

Raman Spectroscopy

Enzyme work has proven to be the most difficult part of this dissertation. Recombinant production of VCPO by *E. coli*, unfortunately yields low titers, so we only had approximately 1.4 mg of VCPO to work with at a total volume of about 1 mL, for a very low concentration sample of 1.4 mg/mL. For Raman spectroscopy, it is beneficial to have a very concentrated sample. The more concentrated the sample, the better the signal to noise ratio. The vanadate cofactor of VCPO in the native form which is present as a vanadium dioxo structure was expected to exhibit Raman bands similar in position to those of the K[VO(O)(heida)] dioxo compound (broad band at ~920 cm^{-1} in both Raman and ATR-IR spectroscopy). Likewise, VCPO in the active peroxo-oxo form was expected to exhibit bands similar to the peroxo-oxo K[$VO(O_2)$(heida)] mimic (peroxo breathing mode at ~575 cm^{-1}, O-O stretching at ~932 cm^{-1}, and V=O stretching at ~967 cm^{-1}) since X-ray crystallography data indicated VCPO and K[$VO(O_2)$(heida)] possess the same V-O bond lengths.[5, 23] However, our first attempt at Raman spectroscopy with the 1.4 mg/mL sample yielded spectra from all 3 laser wavelengths (532, 442, and 325) with a significant amount of noise. None of the expected Raman bands were observable. Additionally, the overall signal was too weak to interpret. The Raman spectrum for VBPO, despite heat treatment to denature the phycoerythrin still exhibited a great deal of fluorescence using both the 532 and 442 nm Raman lasers. The 325 nm laser did not cause fluorescence in the sample, however the signal was dominated by Raman bands corresponding to the MES buffer. Thus, we proceeded with the VCPO enzyme only.

We were able to concentrate our VCPO sample approximately 3-fold, with the help of Ms. Rachael Barton advised by Professor Berger's at Lehigh University, using a 10 kDa centrifugal filter (Millipore), increasing the sample concentration to approximately 4.2 mg/mL. The more concentrated sample of VCPO was examined again by Raman spectroscopy using all three lasers. The more concentrated sample of VCPO yielded a signal significantly stronger than that of the first, more dilute sample. However, none of the expected Raman bands were observable for neither the native form of VCPO, nor that active form of VCPO. Even though, the signal was significantly stronger for the more concentrated sample, the signal to noise ratio was still too low to allow us to interpret the spectra. The Raman spectra for VCPO in the native and active form using the 325 nm UV laser are shown, for demonstration purposes only, in Figure 5.6. Additionally, the Raman spectrum for active form VCPO

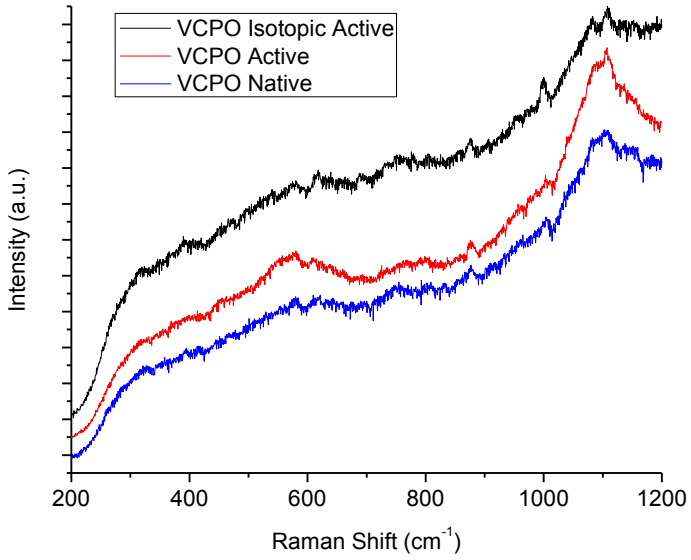

Figure 5.6 Raman spectra using the 325 nm laser for VCPO in the native and active form, along with isotopic active form VCPO using $H_2{}^{18}O_2$. No resonance Raman enhancement was observed. The spectra were unfortunately too weak to interpret.

using isotopic $H_2{}^{18}O_2$ is included in Figure 5.6. We had hoped, by using the 325 nm laser, we would observe some degree of resonant enhancement from the vanadate cofactor electronic transition observed by UV-vis spectroscopy between 300 and 350 nm.[18] Unfortunately, we were not able to observe any enhancement.

The Raman spectra for the active form of VCPO and the isotopic active form of VCPO (using $H_2{}^{18}O_2$) using the 532 nm laser are also shown in Figure 5.7 for demonstration purposes only. The native form spectrum is not shown in Figure 5.7 for brevity, because it did not yield any information. In Figure 5.7, a broad set of bands is observed between 400 and 450 cm^{-1} which correspond to the Tris Acetate buffer. Unfortunately, the rest of the spectra are unable to be interpreted because of the weak signal. No real observable difference can be seen between the active form of VCPO

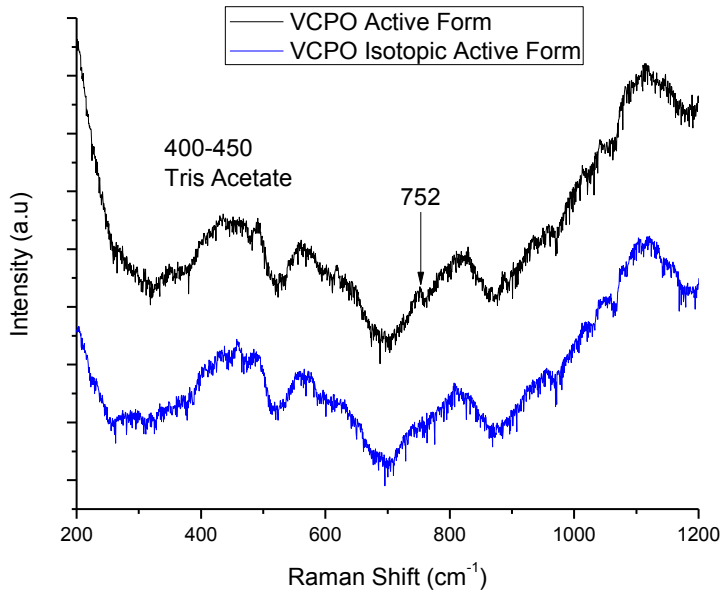

Figure 5.7 Raman spectra using the 532 nm laser for VCPO in the active form and the isotopic active form of VCPO using $H_2{}^{18}O_2$. The spectra were unfortunately too weak to interpret, and no significant difference between the two spectra can be observed.

and the isotopic active form of VCPO, with the exception of an ambiguous band at 752 cm^{-1}.

ATR-IR Spectroscopy

VCPO was examined by and ATR-IR spectroscopy, similar to the characterization performed on the K[$VO(O_2)$(heida)] mimic, and the results are shown in Figure 5.8. A large band is present at 883 cm^{-1} for the active form of VCPO, but not for the native form. This 883 cm^{-1} band is not due to H_2O_2, as the H_2O_2 would occur at 878 cm^{-1} as a very small band. The 883 cm^{-1} band observed in ATR-IR spectrum certainly warrants further characterization.

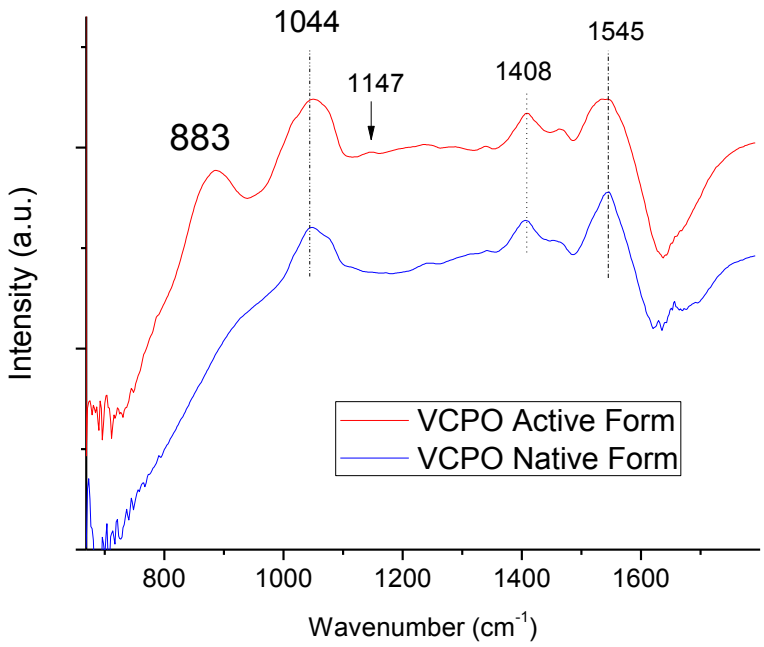

Figure 5.8 ATR-IR spectra for VCPO in the native form and the active form of VCPO using H_2O_2. A large band is observed at 883 cm^{-1} for the active form of VCPO.

Discussion

Although we were not able to gain any information from Raman experiments on VCPO and VBPO, we remain optimistic that a more concentrated sample yielded a stronger signal to noise ratio. Unfortunately, we were limited by the low titer yielded by the *E. coli* expression method for VCPO. If multiple batches of recombinant VCPO can be pooled and concentrated, we are optimistic that a better quality Raman signal can be obtained. Citing a personal conversation with Professor Ron Wever from the University of Amsterdam, the maximum obtainable concentration of VCPO is about 100 mg/mL, but over 80 mg/mL is not advisable because of the risk of aggregate formation. Therefore, we remain optimistic that Raman studies on a more concentrated sample would yield better results since we have only been able to try a concentration of up to 4.2 mg/mL. Additionally, the weak Raman spectra for VCPO were consistent. This is a good indication that the enzyme sample is not being altered by the Raman laser.

It appears that ATR-IR could be a better method for characterizing VCPO. A large broad band is observable at 883 cm^{-1} for the VCPO active form. This is band is not present in the native form. Additionally, the prominence of this 883 cm^{-1} band indicates that it must be an asymmetric vibration, since ATR-IR is more sensitive to asymmetric vibrations, and Raman is more sensitive to symmetric vibrations. It is possible that an asymmetric stretch of a vanadium hydroperoxo group would appear much stronger as an in the ATR-IR spectrum. VCPO requires further characterization by ATR-IR spectroscopy to determine the origin on the 883 cm^{-1} band.

UV-vis remains a reliable source for indicating the oxidation state of VCPO and VBPO. No reduced vanadium (V^{+4}/V^{+3}) was observed, only a broad V^{+5} band is present between 300 and 400 nm. We however, did not observe a vanadium-peroxo band at 470 nm as we had expected. Formulating the enzyme in a 25% glycerol buffer in order to simulate crystal structure conditions did not indicate any change in the V^{+5} band between 300 and 400 nm, nor did it reveal a vanadium-peroxo band at 470. This does not indicate any discrepancy between the crystal form of the enzyme and the free aqueous form.

Conclusions

We have merely scratched the surface here in regards to VCPO and VBPO characterization. Although we were not able to extract any clear information at present from the Raman spectrum, the increasing signal to noise ratio observed with an increase in concentration is promising for future work. Since VCPO can be produced recombinantly as several separate batches, pooled, and concentrated, we are confident that Raman spectroscopy will be able to yield detailed information about the nature of the active site for VCPO. The Raman lasers do not appear to change the enzyme signal indicating that VCPO is stable enough to withstand Raman laser irradiation.

ATR-IR experiments have shown the potential of this technique for characterizing enzymes. The presence of the 883 cm^{-1} band for active VCPO warrants further investigation. We expect that this band is an asymmetric stretch, however we cannot currently say which chemical group is responsible for this vibration. Future

isotopic H_2O_2 experiments would indicate whether or not this band is associated with an asymmetric V-hydroperoxo vibration.

References

(1) Butler, A. *Coordination Chemistry Reviews,* **1999**, *187*, 17-35.

(2) Butler, A.; Walker, J. V. *Chem. Rev.* **1993**, *93*, 1937-1944.

(3) Schijndel, J. W. P. M.; Barnett, P.; Roelse, J.; Vollenbroek, E. G. M.; Wever, R. *European Journal of Biochemistry* **1994**, *225*, 151-157.

(4) Mehrtens, G. *Polar Biology* **1994**, *14*, 351.

(5) Messerschmidt, A.; Wever, R. *Proceedings of the National Academy of Sciences* **1996**, *93*, 392-396.

(6) Weyand, M.; Hecht, H. J.; Kieb, M.; Liaud, M. F.; Vilter, H.; Schomburg, D. *Journal of Molecular Biology,* **1999**, *293*, 595-611.

(7) Pooransingh-Margolis, N.; Renirie, R.; Hasan, Z.; Wever, R.; Vega, A. J.; Polenova, T. *J. Am. Chem. Soc.* **2006**, *128*, 5190-5208.

(8) Hemrika, W.; Renirie, R.; Macedo-Ribeiro, S.; Messerschmidt, A.; Wever, R. *J. Biol. Chem.* **1999**, *274*, 23820-23827.

(9) Van Schijndel, J. W. P. M.; Vollenbroek, E. G. M.; Wever, R. *Biochim. Biophys. Acta* **1993**, *1161*, 249-256.

(10) Isupov, M. N.; Dalby, A. R.; Brindley, A. A.; Izumi, Y.; Tanabe, T.; Murshudov, G. N.; Littlechild, J. A. *J. Mol. Biol.* **2000**, *299*, 1035-1049.

(11) Tromp, M. G.; Olafsson, G. Krenn, B. E.; Wever, R. *Biochim. Biophys. Acta* **1990**, *1040*, 192-198.

(12) Wever, R.; Hemrika, W. In *Vanadium Haloperoxidases;* Messerschmidt, A., Huber, R., Poulos, T. and Wieghardt, K., Eds.; Handbook of Metalloproteins; Wiley: Chichester, 2001; pp 1417-1428.

(13) Zampella, G.; Kravitz, J. Y.; Webster, C. E.; Fantucci, P.; Michael, B.; Carlson, H. A.; Pecoraro, V. L.; De Gioia, L. *Inorg. Chem.* **2004**, *43*, 4127-4136.

(14) Kravitz, J. Y.; Pecoraro, V. L.; Carlson, H. A. *Journal of Chemical Theory and Computation* **2005**, *1*, 1265-1274.

(15) Zampella, G.; Fantucci, P.; Pecoraro, V. L.; De Gioia, L. *J. Am. Chem. Soc.* **2005**, *127*, 953-960.

(16) Hasan, Z.; Renirie, R.; Kerkman, R.; Ruijssenaars, H. J.; Hartog, A. F.; Wever, R. *J. Biol. Chem.* **2006**, *281*, 9738-9744.

(17) de Boer, E.; Wever, R. *J. Biol. Chem.* **1988**, *263*, 12326.

(18) Renirie, R.; Hemrika, W.; Piersma, S. R.; Wever, R. *Biochemistry (N. Y.)* **2000**, *39*, 1133-1141.

(19) Butler, A.; Clague, M. J.; Meister, G. E. *Chem. Rev.* **1994**, *94*, 625-638.

(20) Renirie, R.; Charnock, J. M.; Garner, C. D.; Wever, R. *J. Inorg. Biochem.* **2010**, *104*, 657-664.

(21) Everett, R. R.; Butler, A. *Inorg. Chem.* **1989**, *28*, 393-395.

(22) Everett, R. R.; Soedjak, H. S.; Butler, A. *J. Biol. Chem.* **1990**, *265*, 15671-15679.

(23) Schneider, C. J. Development of Asymmetric Sulfoxidation Catalysts Based on Functional Models for Vanadium-Dependent Haloperoxidases, University of Michigan, 2009.

(24) Schneider, C. J.; Zampella, G.; Greco, C.; Pecoraro, V. L.; De Gioia, L. *Eur. J. Inorg. Chem.* **2007**, *4*, 515-523.

(25) Schneider, C. J.; Penner-Hahn, J.; Pecoraro, V. L. *J. Am. Chem. Soc.* **2008**, *130*, 2712-2713.

(26) Valery M., D. *Tetrahedron* **2003**, *59*, 4701-4720.

(27) ten Brink, H. B.; Tuynman, A.; Dekker, H. L.; Hemrika, W.; Izumi, Y.; Oshiro, T.; Schoemaker, H. E.; Wever, R. *Inorg. Chem.* **1998**, *37*, 6780-6784.

(28) Andersson, M.; Willetts, A.; Allenmark, S. *J. Org. Chem.* **1997**, *62*, 8455-8458.

(29) Carey, P. R. *J. Biol. Chem.* **1999**, *274*, 26625-26628.

(30) Bennett, A.; Siegelman, H. **1975**.

(31) Zhang, B.; Cao, X.; Cheng, X.; Wu, P.; Xiao, T.; Zhang, W. *Biotechnol. Lett.* **2011**, *33*, 545-548.

(32) Kubelka, P.; Munk, R. *Z. Tech. Phys.* **1931**, *12*.

Chapter 6: Conclusions and Future Directions

The work included in this dissertation has made a significant contribution towards bridging the gap between heterogeneous catalysis and biocatalysis. A great deal was already known about gas phase methanol oxidation by solid VO_4/SiO_2, but essentially nothing was known about aqueous phase methanol oxidation by $K[VO(O_2)(heida)]_{(aq)}$. We were presented with a unique opportunity to utilize the techniques traditionally used in the field of heterogeneous catalysis, Raman, ATR-IR, and UV-vis, to begin bridging the gap from heterogeneous catalysis to biocatalysis through biocatalysis mimics.

Prior to embarking on our study of $K[VO(O_2)(heida)]_{(aq)}$ we developed our techniques for analyzing vanadium-containing clusters by Raman spectroscopy using vanadium-containing Keggins. These studies using tungstophosphoric acid (TPA) and molybdophosphoric acid (MPA) resulted in two publications,[1, 2] and permitted us to develop the techniques and proceed with the characterization of $K[VO(O_2)(heida)]_{(aq)}$.

Raman spectroscopy proved to be a valuable tool in the characterization of $K[VO(O_2)(heida)]_{(aq)}$. We were able to identify the Raman bands associated with the vanadium-peroxo group using isotopic $H_2{}^{18}O_2$ during synthesis. Raman characterization of the isotopic $K[VO(^{18}O_2)(heida)]_{(aq)}$ revealed the symmetric breathing mode (575 cm^{-1}) and overtone (1150 cm^{-1}), and the symmetric O-O stretch (932 cm^{-1}) for the vanadium-peroxo group. Incubation with $H_2{}^{18}O$ resulted in the exchange of the

oxygen atom of the V=O vanadium-oxo group. Raman characterization permitted the identification of the V=O oxo stretch at 967 cm^{-1}.

Comparison of the unique peroxo-oxo structure of $K[VO(O_2)(heida)]_{(aq)}$ to VO_4/SiO_2 resulted in a publication highlighting the structural differences between the two catalysts.[3] The vanadium peroxo-oxo structure, previously dubbed the vanadium "umbrella structure" was found to only be present in biocatalyst and biocatalyst mimic systems such as $K[VO(O_2)(heida)]_{(aq)}$. VO_4/SiO_2 at low coverage is present as a trigonal pyramid structure with one V=O oxo group and no peroxo group. This study finally settled the long debate over the existence of the umbrella structure for supported vanadium oxide heterogeneous catalysts.

Considering the significant difference in structure between $K[VO(O_2)(heida)]_{(aq)}$ and VO_4/SiO_2, we moved forward to determine whether or not the methanol oxidation mechanism for each system was the same or different. *In situ* ATR-IR studies during methanol oxidation by $K[VO(O_2)(heida)]_{(aq)}$ indicated that methanol adsorption happens by breaking the V-O-ligand bond. This is the same as methanol adsorption for VO_4/SiO_2. In the case of VO_4/SiO_2, methanol adsorption occurs by breaking the V-O-Si bond.

Raman spectroscopy during methanol oxidation by $K[VO(O_2)(heida)]_{(aq)}$ in the presence of H_2O_2 indicated that methanol is not adsorbing on the vanadium peroxo group. Raman spectroscopy during methanol oxidation by $K[VO(O_2)(heida)]_{(aq)}$ without the presence of H_2O_2 indicated that the peroxo group was lost during the course

of the reaction when a reoxidant was not present. This means that the rate determining step, the C-H bond breaking of the methoxy, is performed by the peroxo group. An oxygen atom is lost from the peroxo group with the release of the water byproduct. In order to continue the full catalytic cycle, $K[VO(O_2)(heida)]_{(aq)}$ must be reoxidized to regenerate the vanadium-peroxo group. This is similar to VO_4/SiO_2. This overall type of mechanism where the catalyst loses an oxygen atom and must be reoxidized in order to continue the catalytic cycle is called the Mars-van Krevelen mechanism.[4] Methanol oxidation by both $K[VO(O_2)(heida)]_{(aq)}$ and VO_4/SiO_2 proceeds via the Mars-van Krevelen mechanism.

There is, however, one major difference between the two systems: the C-H bond breaking step. For $K[VO(O_2)(heida)]_{(aq)}$ the C-H bond breaking is performed by the vanadium-peroxo group. VO_4/SiO_2 does not contain a vanadium-peroxo group, therefore C-H bond breaking is performed by the V=O oxo group.

Density functional theory (DFT) provided a complement to these experimental results. DFT calculations have shown that methanol adsorption on $K[VO(O_2)(heida)]_{(aq)}$ is favorable when it occurs at the V-O-ligand bridging bond. DFT has also agrees with experiment on the C-H bond breaking step. It was found to be more energetically favorable when the proton from the vanadium methoxy is transferred to the vanadium peroxo group than if it were transferred to the vanadium oxo group. Therefore, DFT indicates that the C-H bond breaking step is performed by the vanadium-peroxo group, followed by the release of the formaldehyde product.

Kinetic experiments revealed methanol oxidation by $K[VO(O_2)(heida)]_{(aq)}$ is first order in methanol and zero order in H_2O_2, making the overall reaction first order. This is consistent with Mars-van Krevelen kinetics where the reaction is first order in the substrate and zero order in the reoxidant for an overall first order reaction. The activation energy (E_{act}) for methanol oxidation by $K[VO(O_2)(heida)]_{(aq)}$ was found experimentally to be 19 kcal/mol. Since, this experiment was performed in a batch reactor where the V sites for methanol adsorption were completely saturated, the heat of adsorption ΔH_{ads} approaches zero. Therefore the apparent activation energy (E_{app}) is equal to E_{act} for steady state methanol oxidation by $K[VO(O_2)(heida)]_{(aq)}$ in a batch reactor. The activation energy for C-H bond breaking by the vanadium-peroxo group was also calculated by DFT to be approximately 17 kcal/mol, which indicates that theory and experimental results concur.

E_{app} for VO_4/SiO_2 and VO_4 supported on other oxide supports has been found to be approximately 21 kcal/mol regardless of the support. However, the E_{app} for VO_x/MO_x is composed of the actual activation energy for the C-H bond breaking step (E_{act}) plus a heat of adsorption term (ΔH_{ads}). Subtracting ΔH_{ads} = -13.4 kcal/mol, yields an actual activation energy of E_{act} = 34.4 kcal/mol for methanol oxidation by VO_4/SiO_2.[5-9] This difference in activation energy between methanol oxidation by VO_4/SiO_2 and $K[VO(O_2)(heida)]_{(aq)}$ indicates why $K[VO(O_2)(heida)]_{(aq)}$ is able to perform methanol oxidation at low temperatures, and VO_4/SiO_2 is not able to produce any formaldehyde until temperatures approaching 230^{o}C.

The enzyme studies on VCPO and VBPO were by far the most difficult portion of the research work included in this dissertation. Although we did not have as much success studying the full enzymes as we did with $K[VO(O_2)(heida)]_{(aq)}$ we are optimistic about the potential of the characterization systems in our laboratory. We believe that a more concentrated sample of VCPO would be easily characterized by Raman and ATR-IR spectroscopy.

Considering the great success we had in studying $K[VO(O_2)(heida)]_{(aq)}$, future work on other enzyme mimics would certainly be valuable. During my research work, I became interested in iron enzymes, especially the cytochrome P family of enzymes. Cytochrome P450 oxidase (CYP450) is a class of enzymes found abundantly in the

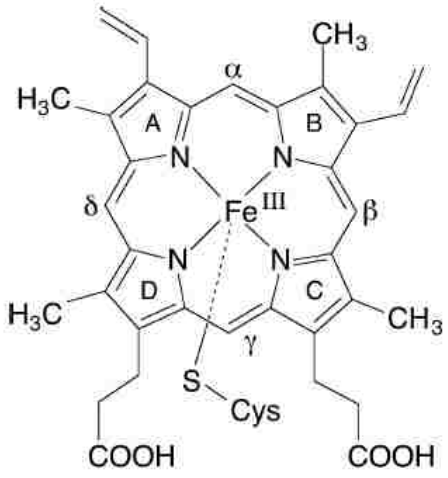

Figure 6.1 Detailed view of heme group Fe^{+3} protoporphyrin IX with linking cysteine ligand. Adapted from Meunier et al.[13]

human body. CYP450 enzymes are responsible for oxidation metabolism of endogenous and exogenous compounds in the liver and they functions in the synthesis of hormones and sterols. CYP450s are the most important selective metabolic oxidation enzymes in the body, in fact, 75% of all drugs currently on the market are metabolized by CYP450s.[10] CYP450s are broken down into families, subfamilies, and polypeptide numbers for classification purposes. For example CYP450 2D6 identifies the enzyme as belonging to the CYP450 family number two, subfamily D, with a polypeptide number six which specifies the parent gene. All CYP450 enzymes contain a heme cofactor. The heme cofactor is a Fe^{+3} protoporphyrin IX prosthetic group, which is linked to the sulfur atom of a cysteine amino acid ligand. This Fe^{+3} cofactor is present in the resting state of all CYP450 enzymes.[11-13] The Fe^{+3} cofactor and linking cysteine residue pictured in Figure 6.1 are identical in all forms of CYP450.[13] In order to become activated, the Fe^{+3} cofactor is oxidized to Fe^{+5} either by NADPH as a coenzyme for electron transfer, or by using hydrogen peroxide.

CYP450s are able to catalyze a variety of stereoselective reactions such as the hydroxylation of C-H bonds, epoxidations of olefins, and aromatic oxidations. They are also able to catalyze the hydroxylation of an unactivated C-H bond at room temperature using hydrogen peroxide. This is a valuable reaction for the production of fine chemicals and pharmaceuticals which require stereoselectivity and can be sensitive to high processing temperatures during production.[13] The oxidation of alkanes to the alcohol via the CYP450 hydrogen peroxide shunt is shown in Figure 6.2.

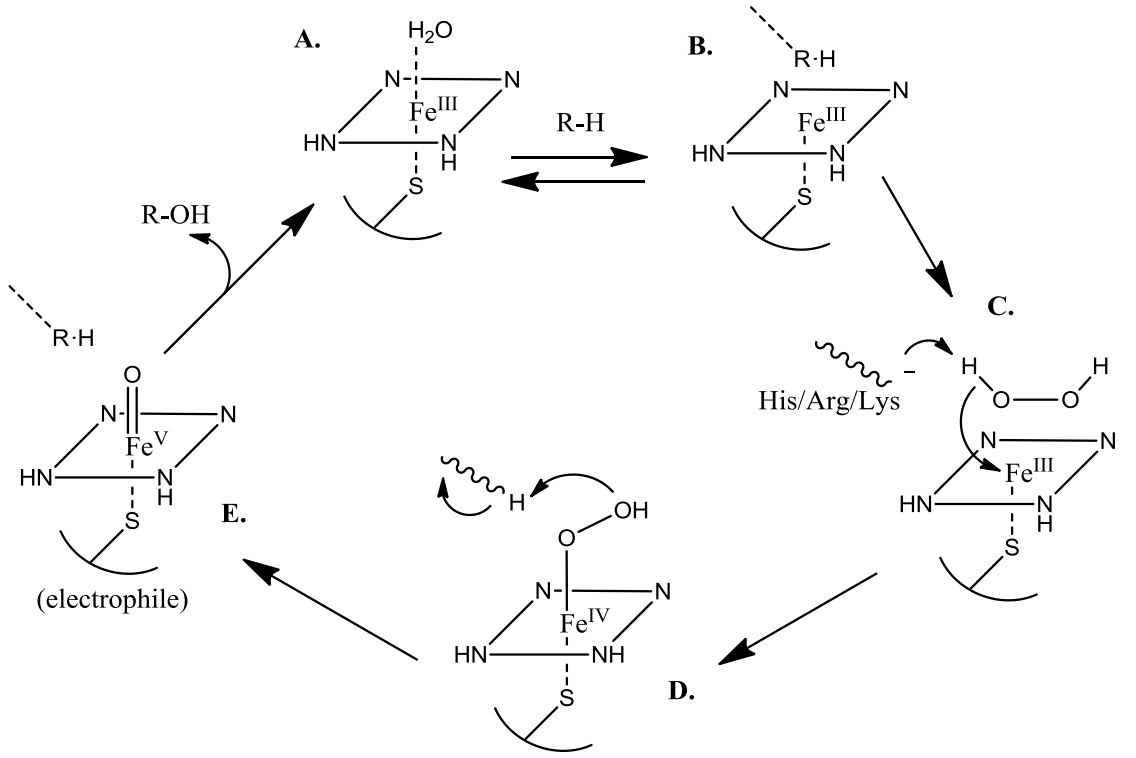

Figure 6.2 Oxidation of an alkane to the alcohol, adapted from Meunier et al.[13] **A.** Resting state of CYP450, **B.** alkane adsorption in adjacent amino acid pocket, **C.** and **D.** activation using hydrogen peroxo, and **E.** fully activated Fe ^{V} and subsequent hydroxylation of adsorbed alkane.

The CYP450 enzyme is first present in the Fe (III) resting state in step A in Figure 6.2. The alkane is able to adsorb onto the surrounding amino acid pocket in step B. In order to hydroxylate the alkane, the heme cofactor of the CYP450 must be activated to Fe (V). The activation mechanism via the hydrogen peroxide shunt can be seen in steps C through E. Step E is then followed by alkane hydroxylation and the return of the heme cofactor to the Fe (III) resting state. It is unclear exactly how the alkane hydroxylation proceeds, and exactly how the alkane interacts with the Fe (V) heme cofactor.

CYP450s are of particular interest to chemists because there are currently no other alkane hydroxylation methods involving essentially one step at mild temperatures.

C-H bond transformation in one step has been called a "holy grail."[14] This is why mimic compounds designed to properly mimic the structure and function or the CYP450 family of enzymes are of great desirability. The first CYP450 enzyme mimics consisted of simple iron porphyrins linked to a thiolate or nitrogen base ligand, however many of these simple ligands permitted aggregation of the porphyrins and oxidation of the associated ligand.[15] Other CYP450 mimic compounds were developed which consisted of a "picnic basket" type ligand which serves to form a rigid cavity in which the intended substrate is permitted to enter.[15] It was found that a manganese porphyrin form of this particular "picnic basket" CYP450 was found to perform steroselective epoxidation reactions.[15] Cyclodextrin "supramolecular" porphyrin CYP450 enzyme mimic compounds have also been synthesized specifically to better mimic the amino acid pocket that is present around the heme cofactor in the CYP450 enzymes. The cyclodextrin-porphyrin enzyme mimics were found to catalyze stereoselective epoxidations of substrates that bind specifically within the cyclodextrin ring such as hexane.[15]

Although many different kinds of iron porphyrin CYP450 and manganese substituted enzyme mimics have been developed and examined for their capability to perform selective oxidation reactions, there have been no *in situ* spectroscopic investigations on the oxidative mechanism for CYP450 mimics under reaction conditions. There have been no reports using ATR-IR to investigate the substrate adsorption site and reactive intermedieates. There have been no Raman studies clearly

investigating the evolution of the iron-hydroperoxo and iron-oxo intermediate structures under reaction conditions.

Considering the versatility of the CYP450 family of enzymes, it would certainly be interesting to explore some CYP450 mimic compounds. CYP450 mimics could be examined in the same fashion as $K[VO(O_2)(heida)]_{(aq)}$ by Raman and ATR-IR spectroscopy in order to visualize the active site, and the role of the Fe=O bond in the activated form. With these studies, we have deomonstrated the potential of *in situ* Raman and ATR-IR spectroscopy for the study of enzyme mimics under reaction conditions. CYP450 mimic research would continue to extend our novel work bridging the gap between heterogeneous and biocatalysis.

References

(1) Molinari, J. E.; Nakka, L.; Kim, T.; Wachs, I. E. *ACS Catal.* **2011**, *1*, 1536-1548.

(2) Nakka, L.; Molinari, J. E.; Wachs, I. E. *J. Am. Chem. Soc.* **2009**, *131*, 15544-15554.

(3) Molinari, J. E.; Wachs, I. E. *J. Am. Chem. Soc.* **2010**, *132*, 12559-12561.

(4) Mars, P.; van Krevelen, D. W. *Spec. Suppl. Chem. Eng. Sci.* **1954**, *3*, 41-57.

(5) Feng, T.; Vohs, J. M. *Journal of Catalysis* **2002**, *208*, 301-309.

(6) Burcham, L. J.; Briand, L. E.; Wachs, I. E. *Langmuir* **2001**, *17*, 6164-6174.

(7) Deo, G.; Wachs, I. E. *Journal of Catalysis* **1994**, *146*, 323-334.

(8) Wachs, I. E.; Deo, G.; Vuurman, M. A.; Hu, H.; Kim, D. S.; Jehng, J. -. *J Mol Catal. A: Chem.* **1993**, *82*, 443.

(9) Oyama, S. T.; Radhakrishnan, R.; Seman, M.; Kondo, J. N.; Domen, K.; Asakura, K. *J Phys Chem B* **2003**, *107*, 1845-1852.

(10) Guengerich, F. P. *Chemical Research in Toxicology* **2008**, *21*, 70-83.

(11) Rowland, P.; Blaney, F. E. :. S., M.G.; Jones, J. J.; Leydon, V. R.; Oxbrow, A. K.; Lewis, C. J.; Tennant, M. G.; Modi, S.; Eggleston, D. S.; Chenery, R. J.; Bridges, A. M. *J. Biol. Chem.* **2006**, *281*, 7614-7622.

(12) Thomas, G. In *Medicinal Chemistry: An Introduction;* John Wiley & Sons: West Sussex, England, 2007; .

(13) Meunier, B.; de Visser, S. P.; Shaik, S. *Chemical Reviews* **2004**, *104*, 3947-3980.

(14) Arndtsen, B. A.; Bergman, R. G.; Mobley, T. A.; Peterson, T. H. *Acc. Chem. Res.* **1995**, *28*, 154-162.

(15) Feiters, M. C.; Rowan, A. E.; Nolte, R. J. M. *Chem. Soc. Rev.* **2000**, *29*, 375-384.

Vitae

Julie Elizabeth Molinari was born April 4, 1983 in Passaic, New Jersey to parents Chris and Lauren Molinari, grandparents Betty and George Duff, and Joan and Ignatius Molinari. After receiving her B.S. in Chemical Engineering from Lehigh University in 2005, Julie was employed at Laureate BioPharmaceutical Services, a small biopharmaceutical company in Princeton, NJ. In 2007, Julie returned to graduate school at Lehigh and joined the research group of Professor Israel E. Wachs. Julie will be graduating with her Ph.D. in Chemical Engineering from Lehigh University on May 21, 2012, and she intends to return to the pharmaceutical industry.

Publications:

Molinari, J. E.; Nakka, L.; Kim, T.; Wachs, I. E. The Dynamic Surface Structures and Reactivity of Vanadium-containing Molybdophosphoric Acid ($H_{3+x}PMo_{12-x}V_xO_{40}$) Keggin Catalysts during Methanol Oxidation and Dehydration *ACS Catal*., **2011**, 1, 1536.

Molinari, J. E.; Wachs, I. E. Presence of Surface Vanadium Peroxo-oxo Umbrella Structures in Supported Vanadium Oxide Catalysts: Fact or Fiction? *J. Am. Chem. Soc*., **2010**, *132*, 12559.

Nakka, L.; Molinari, J. E.; Wachs, I. E. Surface and Bulk Aspects of Mixed Oxide Catalytic Nanoparticles: Oxidation and Dehydration of CH_3OH by Polyoxometallates *J. Am. Chem. Soc.* **2009**, *131*, 15544.

Awards and Honors:

1st Place - Catalysis Society of Metropolitan New York, Spring Symposium 2011 - Graduate Student Poster Competition

2nd Place – Catalysis Club of Philadelphia, Spring Symposium 2010 – Graduate Student Poster Competition

3rd Place – 7th International Symposium on the Chemistry and Biological Chemistry of Vanadium (Toyama, Japan) - Outstanding Poster Awards for Young Scientists

Leonard A. Wenzel Award, For Outstanding Qualifying Examination Performance, September 2008, Lehigh University

Presentations:

Bridging the Gap between Heterogeneous and Enzyme Catalysis: *In Situ* Spectroscopic Study of Vanadium Haloperoxidase Enzyme Functional Mimics- *Invited Student Speaker Catalysis Society of Metropolitan New York, October 2011 Meeting*

Bridging the Gap between Heterogeneous and Enzyme Catalysis: *In Situ* Spectroscopic Study of Vanadium Haloperoxidase Enzyme Functional Mimics- *Oral Presentation- VII International Symposium on Group Five Elements, Riccione, Italy, May 2011*

Bridging the Gap between Heterogeneous and Enzyme Catalysis: *In Situ* Spectroscopic Study of Vanadium Haloperoxidase Enzyme Functional Mimics- *Invited Student Speaker Catalysis Club of Philadelphia, February 2011 Meeting*